

**DEVELOPMENT OF HIGH-TEMPERATURE LEAD-FREE
SOLDER FOR SEMICONDUCTOR CHIP ATTACHMENT**

ASHRAFUL HAQUE

**FACULTY OF ENGINEERING
UNIVERSITY OF MALAYA
KUALA LUMPUR**

2011

**DEVELOPMENT OF HIGH-TEMPERATURE LEAD-FREE
SOLDER FOR SEMICONDUCTOR CHIP ATTACHMENT**

ASHRAFUL HAQUE

**DISSERTATION SUBMITTED IN FULFILMENT
OF THE REQUIREMENTS
FOR THE DEGREE OF MASTER OF ENGINEERING SCIENCE**

**FACULTY OF ENGINEERING
UNIVERSITY OF MALAYA
KUALA LUMPUR**

2011

ORIGINAL LITERARY WORK DECLARATION

Name of the candidate: **Ashraful Haque** (Passport No. **Q0864594**)

Registration/Matric No: ~~XXXXXXXXXX~~

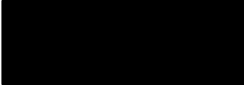
Name of the Degree: **Master of Engineering Science**

Title of Project Paper/ Research Report/ Dissertation / Thesis (“this work”):
Development of High-Temperature Lead-Free Solder for Semiconductor Chip Attachment

Field of Study: **Microelectronics Packaging**

I do solemnly and sincerely declare that:

- (1) I am the sole writer /author of this work;
- (2) This work is original;
- (3) Any use of any work in which copyright exists was done by way of fair dealings and any expert or extract from, or reference to or reproduction of any copyright work has been disclosed expressly and sufficiently and the title of the Work and its authorship has been acknowledged in this Work;
- (4) I do not have any actual knowledge nor do I ought reasonably to know that the making of this work constitutes an infringement of any copyright work;
- (5) I, hereby assign all and every rights in the copyrights to this Work to the University of Malaya (UM), who henceforth shall be owner of the copyright in this Work and that any reproduction or use in any form or by any means whatsoever is prohibited without the written consent of UM having been first had and obtained actual knowledge;
- (6) I am fully aware that if in the course of making this Work I have infringed any copyright whether internationally or otherwise, I may be subject to legal action or any other action as may be determined by UM.

Candidate’s Signature: ...

Date: 03 October 2011

Subscribed and solemnly declared before,

Witness’s Signature: 

Date: 03 October 2011

Name: Assoc. Prof. Dr. Saidur Rahman

ASSOC. PROF. DR. SAIDUR RAHMAN
Department of Mechanical Engineering
Faculty of Engineering
University of Malaya
50603 Kuala Lumpur
Malaysia

ABSTRACT

Lead (Pb)-free electronic product is a catchphrase of consumer and different regulators worldwide which turns in to an obligatory for the electronic industries to remove Pb from semiconductor assembly for the reason that it is highly toxic, harmful for human health and environment. Alternative as well as drop-in-replacement of high-Pb solder used for Si die attachment in power device packaging is the bottleneck for the Pb-free electronic product. Operating temperature of such power devices is less than 250°C. In this study, two Bi-based, two Zn-Al-based alloys and one SAC-Cu epoxy solder were studied for Si die attachment on Cu lead-frame as a high-temperature Pb-free solder. Except SAC-Cu-epoxy solder, the other alloys were used in wire form to attach Ti/Ni/Ag metallized Si die on Cu lead-frame. Die attach was performed in automatic machine in a forming gas environment at temperature ranging from 370°C to 400°C. Interfacial reactions between lead-frame/solder and Si die/solder interfaces, bulk microstructure and die attach properties such as wetting, void, and die shear strength were investigated using optical, scanning electron microscope (SEM), energy dispersive x-ray (EDX) and electron probe microanalyzer (EPMA). Reliability tests such as autoclave (AC), temperature cycling (TC), high-temperature operating life (HTOL), high-temperature storage life (HTSL) were conducted for some selected solders. Die attach properties and reliability test results were compared with the standard Pb-5Sn soldered samples. Out of these Pb-free solders, void and wetting problem were encountered in Bi-based soldered samples to an extent which was not within acceptable limit. Moreover, for this solder, die displacement was observed during wire bonding process due to solder re-melt. Therefore, Bi-based alloys were not found suitable for high-temperature Pb-free solder. Among the Zn-Al-based alloys, Zn-Al-Ge solder was also associated with void problem which was not within acceptable limit. Average die

shear strength of Zn-Al-Ge solder was found 22.3 MPa for die attach samples at 390°C which is close to the maximum operating temperature (400°C) of Si die. Due to void and small operating temperature window for die attachment, this solder is not suitable for Si die attachment. Zn-Al-Mg-Ga solder wetted well on Cu lead-frame, covered entire die area and flowed in all directions under the Si die. Cumulative void was found less than 10% for die attach temperature of 380°C and 390°C. Average die shear strength varies from 21.8 MPa to 29.4 MPa with the corresponding die attach temperature of 370°C and 400°C. Reliability test results of Zn-Al-Mg-Ga soldered samples were also found satisfactory. Die attach properties and reliability tests of SAC-Cu epoxy soldered samples was also found within acceptable limit. However, creak was found in intermetallic compound layers at lead-frame/solder interface for Zn-Al-Mg-Ga soldered samples and at bulk for SAC-Cu epoxy soldered samples after 1000 thermal cycles and high-temperature operating life test which may affect on reliability during long term use.

ABSTRAK

Plumbum (Pb)-free produk elektronik adalah kata-kata hikmah pengguna dan pengawal selia yang berbeza di seluruh dunia yang bertukar menjadi wajib bagi industri elektronik untuk menghapuskan Pb dari pemasangan semikonduktor atas sebab-sebab bahawa ia adalah sangat toksik yang berbahaya untuk kesihatan manusia dan alam sekitar. Alternatif serta drop-in-penggantian pateri-Pb tinggi yang digunakan untuk lampiran Si die dalam bungkusan peranti kuasa adalah hambatan untuk produk elektronik Pb bebas. Suhu operasi peranti kuasa itu adalah kurang daripada 250°C. Dalam kajian ini, dua Bi-based, dua Zn-Al-based alloys dan satu SAC-Cu epoxy pateri dikaji untuk lampiran Si die di Cu lead-frame sebagai pateri bebas Pb-suhu tinggi. Kecuali SAC-Cu-epoxy pateri, paduan lain telah digunakan dalam bentuk dawai untuk melampirkan Ti/Ni/Ag metallized Si die pada Cu lead-frame. Lampiran die dilakukan dalam mesin automatik dalam persekitaran gas yang membentuk pada suhu antara 370°C untuk 400°C. Tindak balas antara muka antara lead-frame/solder dan Si die/pateri antara muka, mikrostruktur besar dan hartanah lampiran die seperti kebasahan, tidak sah, dan die kekuatan ricih disiasat menggunakan optik, imbasan mikroskop elektron (SEM), serakan tenaga x-ray (EDX) dan elektron kuar microanalyzer (EPMA). Kebolehpercayaan ujian seperti autoklaf (AC), suhu berbasikal (TC), suhu tinggi jangka hayat operasi (HTOL), penyimpanan hidup suhu tinggi (HTSL) telah dijalankan untuk beberapa solders yang dipilih. Hartanah lampirkan die dan keputusan ujian kebolehpercayaan berbanding dengan sampel dipateri Pb-5Sn standard. Daripada solders bebas Pb ini, tidak sah dan masalah kebasahan ditemui dalam sampel dipateri berasaskan Bi-based yang tidak berada dalam had yang boleh diterima. Selain itu, untuk pateri ini, die anjakan diperhatikan semasa proses ikatan dawai kerana pateri semula cair. Oleh itu, aloi berasaskan Bi-tidak didapati sesuai untuk suhu tinggi pateri bebas Pb. Antara Zn-Al-

based alloy, Zn-Al-Ge pateri juga dikaitkan dengan masalah tidak sah yang tidak berada dalam had yang boleh diterima. Die purata kekuatan ricih Zn-Al-Ge pateri ditemui 22.3 MPa untuk sampel lampiran die pada 390°C yang dekat dengan suhu operasi maksimum (400°C) Si die. Oleh kerana tidak sah dan suhu operasi kecil tettingkap untuk lampiran die, pateri ini tidak sesuai untuk lampiran Si die. Zn-Al-Mg-Ga pateri basah pada Cu lead-frame, die kawasan seluruh dilindungi dan mengalir dalam segala arahan di bawah Si die. Tidak sah Kumulatif didapati kurang daripada 10% untuk die lampirkan suhu 380°C dan 390°C. Kekuatan ricih die purata berbeza daripada 21.8 MPa hingga 29.4 MPa sama dengan suhu lampiran die 370°C dan 400°C. Kebolehpercayaan keputusan ujian sampel dipateri Zn-Al-Mg-Ga juga didapati memuaskan. Hartanah Lampiran Die dan ujian kebolehpercayaan SAC-Cu epoxy sampel dipateri juga dijumpai dalam had yang boleh diterima. Walau bagaimanapun, berderak ditemui di lapisan kompaun intermetallic pada antara muka lead-frame/solder untuk sampel dipateri Zn-Al-Mg-Ga dan pada sebahagian besar SAC-Cu epoxy sampel dipateri selepas 1000 habakitaran dan ujian kehidupan operasi suhu tinggi yang boleh menjejaskan kebolehpercayaan semasa penggunaan jangka panjang.

ACKNOWLEDGEMENTS

I would like to mention with gratitude to Almighty Allah's continual kindness without which no work would reach its goal. I am very much grateful to my supervisors Prof. Dr. A.S.M.A. Haseeb and Prof. Dr. Musjuki Hj Hassan for their continuous guidance, constant support, supervision, inspiration, advice, infinite patience and enthusiastic encouragement throughout this research work.

I gratefully acknowledge ON Semiconductor, 70450 Seremban, Malaysia, for financial support, providing lead-free solder materials, permission for using production machineries and their labs. Special thanks to Mr. Shutesh Krishnan and Mr. Y. S. Won, ON Semiconductor, Package Innovation & Development Center, ON Semiconductor for their continuous guidance and inspiration. I also gratefully acknowledge different research grants of University of Malaya, such as IPPP (PS073/2009B), Science fund (13-02-03-3072), FRGS fund (FP013/2010B) and UMRG fund (RG068/09AET) for their financial support to my research.

Special thanks to the authority of Bangladesh Atomic Energy Commission, Dhaka, Bangladesh for providing me an opportunity for getting higher degree in Malaysia. I wish to thank to all members in the Energy Lab for their enthusiastic support.

Finally, I express my profound and heartfelt gratitude to my parents, parents-in-law, my wife Shiuly, my son Wasi and my daughter Ariba for their encouragement, support, devotion and patience throughout my study.

TABLE OF CONTENTS

ORIGINAL LITERARY WORK DECLARATION	ii
ABSTRACT	iii
ABSTRAK	v
ACKNOWLEDGEMENTS	vii
TABLE OF CONTENTS	viii
LIST OF FIGURES	xii
LIST OF TABLES	xvii
LIST OF ABBREVIATIONS	xviii
CHAPTER 1 INTRODUCTION	1
1.1 Background and Problem Statement	1
1.2 Research Objectives.....	5
1.3 Outline of the Dissertation.....	5
CHAPTER 2 LITERATURE REVIEW	7
2.1 Introduction.....	7
2.2 Power Semiconductor Package.....	7
2.3 Die Attachment	9
2.4 Requirements of High-Temperature Solder.....	12
2.5 High-Temperature Pb-Free Solder for Die Attach	13
2.6 Reliability of Die Attach Joint.....	16
CHAPTER 3 METHODOLOGY	19
3.1 Introduction.....	19
3.2 Preliminary Assessment of High-Temperature Pb-Free Solders.....	19
3.2.1 Melting behavior and microstructure analysis of solder	19
3.2.2 Si die attachment	21
3.2.2(a) Die attach using Bi-Ag-Cu/ Bi-Ag-Cu-In solder	22

3.2.2(b) Die attach using Zn-Al-Ge solder	23
3.2.2(c) Die attach using Zn-Al-Mg-Ga solder	23
3.2.2(d) Die attach using SAC-Cu-epoxy solder	25
3.2.3 Investigation of bulk and interfacial microstructure	26
3.2.4 Wetting on Cu lead-frame	26
3.2.5 Void analysis	27
3.2.6 Die shear strength test	27
3.3 Package Reliability Performance Test of Potential High-Temperature Pb-Free Solders	27
3.3.1 Sample preparation for reliability test	27
3.3.2 Preconditioning	29
3.3.3 Autoclave test	29
3.3.4 Temperature cycling test	30
3.3.5 High-temperature operating life test.....	31
3.3.6 High-temperature storage life test	31
3.4 Failure Mode Analysis.....	31
CHAPTER 4 RESULTS AND DISCUSSION.....	32
4.1 Introduction.....	32
4.2 Die Attachment Using Bi-Based Alloys.....	32
4.2.1 Bi-Ag-Cu solder	32
4.2.1(a) Microstructure and melting behavior of Bi-Ag-Cu solder wire.....	32
4.2.1(b) Microstructure of die attach joint.....	34
4.2.1(c) Wetting and void analysis of Bi-Ag-Cu soldered samples	35
4.2.1(d) Summary	36
4.2.2 Bi-Ag-Cu-In solder.....	36
4.2.2(a) Microstructure and melting behavior of Bi-Ag-Cu-In solder wire.....	36
4.2.2(b) Microstructure of die attach joint.....	38
4.2.2(c) Wetting and void analysis of Bi-Ag-Cu-In soldered samples.....	39

4.2.2(d) Observation during wire bonding operation	41
4.2.2(e) Summary	42
4.3 Die Attachment Using Zn-Al-Based Alloys.....	42
4.3.1 Zn-Al-Ge solder	42
4.3.1(a) Microstructure and melting behavior of Zn-Al-Ge solder wire.....	42
4.3.1(b) Microstructural characterization of Zn-Al-Ge solder on Cu lead-frame	44
4.3.1(c) Wetting and void analysis of Zn-Al-Ge soldered samples.....	49
4.3.1(d) Die shear strength of Zn-Al-Ge soldered samples	52
4.3.1(e) Summary	55
4.3.2 Zn-Al-Mg-Ga solder.....	56
4.3.2(a) Introduction	56
4.3.2(b) Microstructure and melting behavior of Zn-Al-Mg-Ga solder wire.....	56
4.3.2(c) Microstructural characterization of Zn-Al-Mg-Ga solder on Cu lead-frame.....	58
4.3.2(d) Wetting and void analysis of Zn-Al-Mg-Ga soldered samples on Cu lead-frame.....	65
4.3.2(e) Die shear strength of Zn-Al-Mg-Ga soldered samples on Cu lead-frame	67
4.3.2(f) Microstructural characterization of Zn-Al-Mg-Ga solder on Ni metallized Cu lead-frame	71
4.3.2(g) Wetting and void analysis of Zn-Al-Mg-Ga soldered samples on Ni metallized Cu lead-frame	73
4.3.2(h) Die shear strength of Zn-Al-Mg-Ga soldered samples on Ni metallized Cu lead-frame	75
4.3.2(i) Reliability tests.....	78
4.3.2(j) Summary	84
4.4 SAC-Cu-Epoxy Solder	84
4.4.1 Microstructure characterization of SAC-Cu-epoxy solder.....	84
4.4.2 Die shear strength test	87

4.4.3 Reliability tests	87
4.4.3(a) Autoclave test.....	87
4.4.3(b) Temperature cycling test.....	88
4.4.3(c) Scanning acoustic microscopy test.....	88
4.4.4 Summary	89
4.5 Summary Overall.....	90
CHAPTER 5 CONCLUSIONS AND FUTURE WORK.....	91
5.1 Conclusions.....	91
5.2 Future Work.....	93
APPENDIX-A DIE SHEAR STRENGTH DATA	94
APPENDIX-B PUBLICATIONS.....	95
REFERENCES.....	96

LIST OF FIGURES

Figure 2.1 Inside of power module used in pumps.....	8
Figure 2.2 The electronic packaging hierarchy.....	10
Figure 2.3 Schematic view of Si die attachment.....	10
Figure 2.4 The schematic of how Pb from solder materials affects the human beings.	14
Figure 3.1 Inside of the DSC machine.....	20
Figure 3.2 Si die attach machine with solder wire as feed.....	21
Figure 3.3 Optical images of the die attach samples using: a) Zn-Al-Mg-Ga solder at 380°C; b) standard Pb-5Sn solder.	24
Figure 3.4 Schematic view of the die attach area of lead-frame.....	24
Figure 3.5 Optical images of the die attach samples using: a) & b) Zn-Al-Mg-Ga solder on bare & Ni metallized Cu lead-frame respectively, and c) standard Pb-5Sn solder on bare Cu lead-frame.	24
Figure 3.6 Reflow profile for SAC-Cu epoxy.....	25
Figure 3.7 Wire bonding machine.....	28
Figure 3.8 Wire bonding diagram.	28
Figure 3.9 Optical images of the encapsulated package: a) front view; b) back side view; and c) side view.....	28
Figure 4.1 SEM micrograph of Bi-Ag-Cu solder wire.	33
Figure 4.2 DSC curve of Bi-Ag-Cu solder wire.	33
Figure 4.3 SEM micrograph of die attach sample with Bi-Ag-Cu solder at 350°C: a) cross-section of the joint; b) Si die/solder interface at higher magnification.	34
Figure 4.4 Contact angle of Bi-Ag-Cu solder on Cu lead-frame: a) at 350°C; b) at 450°C.....	35
Figure 4.5 Voids in the die attach samples with Bi-Ag-Cu solder on Cu lead-frame: a), b) & c) at 350°C; and d), e) & f) at 450°C.	36
Figure 4.6 SEM image of Bi-Ag-Cu-In solder wire.	37
Figure 4.7 DSC curve of Bi-Ag-Cu-In solder wire.....	37

Figure 4.8 Optical and SEM micrographs of die attach sample with Bi-Ag-Cu-In solder at 350°C: a) optical micrograph of the cross-section; b) SEM micrograph of Si die/solder interface at higher magnification; c) SEM micrograph of lead-frame/solder interface at higher magnification.	38
Figure 4.9 Contact angle of Bi-Ag-Cu-In solder on Cu lead-frame: a) at 350°C; b) at 450°C; and c) at 350°C with scrubbing.	40
Figure 4.10 Voids in the die attach samples with Bi-Ag-Cu-In solder on Cu lead-frame at 350°C: a), b) & c) without scrubbing; and d) & e) with scrubbing.	41
Figure 4.11 Optical image of the die attach sample with Bi-Ag-Cu-In solder on Cu lead-frame at 350°C with scrubbing.	41
Figure 4.12 SEM image of Zn-Al-Ge solder wire.	43
Figure 4.13 DSC curve of Zn-Al-Ge solder wire.	43
Figure 4.14 Zn-Al binary phase diagram.	44
Figure 4.15 SEM images of die attach sample at 390°C with Zn-Al-Ge solder on Cu lead-frame: a) cross-section of the solder joint; b) SEM image at higher magnification.	45
Figure 4.16 Interfacial reactions of the die attach sample on Cu lead-frame at 390°C with Zn-Al-Ge solder at: a) Si die/solder interface; b) lead-frame/solder interface.	46
Figure 4.17 EPMA elemental mapping of the solder joint at 370°C with Zn-Al-Ge solder: (a) SEM image of the mapping region; and element maps of (b) Zn; (c) Cu; (d) Ge; and (e) Al.	48
Figure 4.18 AL-Ge binary phase diagram.	49
Figure 4.19 Ge-Zn binary phase diagram.	49
Figure 4.20 Back scan SAM images of die attach samples: a) Standard Pb-5Sn solder wire was used, and Zn-Al-Ge solder wire was used at b) 370°C, c) 380°C, & d) 390°C.	50
Figure 4.21 Cumulative void % of die attach samples calculated from back scanning images.	51
Figure 4.22 Comparison of wetting diameter of Zn-Al-Ge soldered samples with standard Pb-5Sn soldered samples.	51
Figure 4.23 Comparison of die shear strength of Zn-Al-Ge soldered samples at different die attach temperatures with standard Pb-5Sn soldered samples.	52
Figure 4.24 SEM/Optical images of the die sheared surface: a) Zn-Al-Ge soldered sample at 380°C; b) & c) SEM image at higher magnification; d) standard Pb-5Sn soldered sample.	53

Figure 4.25 EDX elemental mapping of the sheared surface of the soldered sample with Zn-Al-Ge solder: (a) SEM image of the mapping region; and element maps of (b) Si; (c) Ni; (d) Ti; (e) Zn; (f) Al; (g) Ge; and (h) Cu.	54
Figure 4.26 Failure mechanism of Zn-Al-Ge soldered samples during die shear.	55
Figure 4.27 SEM image of Zn-Al-Mg-Ga solder wire.	57
Figure 4.28 DSC curve of Zn-Al-Mg-Ga solder wire.....	58
Figure 4.29 SEM micrograph of the die attach sample at 390°C using 2000 nm Ag thickness at the die back: a) cross-section of the joint; b) IMC layers at solder/lead-frame interface; c) bulk solder micrograph at higher magnification d) IMC layers at Si die/solder interface.	59
Figure 4.30 Ag-Zn binary phase diagram.	60
Figure 4.31 SEM image at the Si die/solder interface of the die attach sample on Cu lead-frame at 390°C with Zn-Al-Mg-Ga solder using 200 nm Ag thickness at the die back.	61
Figure 4.32 Typical SEM micrograph of the die attach sample at 380°C using 200 nm Ag thickness at the die back: a) cross-section of the joint; b) SEM image at higher magnification.....	62
Figure 4.33 Al-Ga binary phase diagram.....	63
Figure 4.34 Ga-Zn binary phase diagram.	63
Figure 4.35 Effect of die attach temperature on thickness of IMCs layers at Si die/solder interface with Zn-Al-Mg-Ga solder: (a) 370°C, (b) 380°C, (c) 390°C and (d) 400°C.	64
Figure 4.36 Effect of die attach temperature on thickness of IMCs layers at lead-frame/solder interface with Zn-Al-Mg-Ga solder: (a) 370°C, (b) 380°C, (c) 390°C and (d) 400°C.	64
Figure 4.37 Total IMC layer thicknesses with respect to die attach temperature.....	64
Figure 4.38 Element mapping of the die attach joint at 390°C on bare Cu lead-frame: (a) SEM image of the mapping region and element maps of (b) Zn; (c) Al; (d) Mg; (e) Ga; (f) Cu; (g) Si; (h) Ag and (i) Ni.....	65
Figure 4.39 SAM images of the die attach samples using back scanning method: a) standard Pb-Sn soldered sample; and Zn-Al-Mg-Ga soldered samples at b) 370°C; c) 380°C; d) 390°C; e) 400°C.....	66
Figure 4.40 Comparison of cumulative voids of Zn-Al-Mg-Ga soldered samples at different die attach temperatures with standard Pb-5Sn soldered samples.....	67
Figure 4.41 Comparison of die shear strength of Zn-Al-Mg-Ga soldered samples at different die attach temperatures with standard Pb-5Sn soldered samples.....	68

Figure 4.42 SEM/Optical images of the die sheared surface: a) Zn-Al-Mg-Ga soldered sample; b) SEM image at higher magnification; c) standard Pb-5Sn soldered sample.....	69
Figure 4.43 EDX elemental mapping of the sheared surface of the soldered sample with Zn-Al-Mg-Ga solder: (a) SEM image of the mapping region; and element maps of (b) Si; (c) Ti; (d) Ni; (e) Ag; (f) Zn; (g) Al; and (h) Cu.	70
Figure 4.44 Failure mechanism of Zn-Al-Mg-Ga soldered samples during die shear....	71
Figure 4.45 Typical microstructure of the die attached joint on Ni metallized Cu lead-frame. (a) cross-section of the joint; (b) SEM image at higher magnification.	71
Figure 4.46 Element mapping of the die attached joint on Ni metallized Cu lead-frame. (a) SEM image of the mapping region and element maps of (b) Zn; (c) Al; (d) Mg; (e) Ga; (f) Si; (g) Cu; (h) Ni and (i) C.....	73
Figure 4.47 Back scanning images of the die attach samples: a) using standard Pb-5Sn solder; and using Zn-Al-Mg-Ga solder at 380°C on b) bare Cu lead-frame; and c) Ni metallized Cu lead-frame.....	74
Figure 4.48 Comparison of cumulative voids of Zn-Al-Mg-Ga soldered samples on different lead-frames with standard Pb-5Sn soldered samples.	74
Figure 4.49 Optical images representing wetting angle: a) standard Pb-5Sn solder; and Zn-Al-Mg-Ga solder on b) bare Cu lead-frame; c) Ni metallized Cu lead-frame.	75
Figure 4.50 Comparison of die shear strength of Zn-Al-Mg-Ga soldered samples on different lead-frame conditions with standard Pb-5Sn soldered samples.	75
Figure 4.51 EDX elemental mapping of the sheared surface of the soldered sample with Zn-Al-Mg-Ga solder on Ni metallized Cu lead-frame: (a) SEM image of the mapping region; and element maps of (b) Ni; (c) Si; (d) Zn; (e) Cu; (f) Al.....	77
Figure 4.52 Optical images of die shared samples with: a) standard Pb-5Sn solder; and Zn-Al-Mg-Ga solder b) on bare Cu lead-frame; c) on Ni metallized Cu lead-frame; d) backside of the die with solder lifted from Ni metallized Cu lead-frame.	77
Figure 4.53 SEM micrograph of molded die attach sample soldered with Zn-Al-Mg-Ga solder after AC test with PC.....	78
Figure 4.54 Deviation of output voltage after completion of TC test with PC.....	79
Figure 4.55 SEM micrograph of TC test samples soldered with Zn-Al-Mg-Ga solder: a) & b) after 1000 TC without PC; c) & d) after 1000 TC with PC test.	80
Figure 4.56 SEM micrograph of standard Pb-5Sn soldered sample after TC 1000 cycles with PC.....	80

Figure 4.57 SEM micrograph of HTOL test samples soldered with Zn-Al-Mg-Ga solder after 1008 hours of operation.	81
Figure 4.58 Optical images of die attach samples aged at 175°C for: a) 48 hours; b) 168 hours; and c) 1008 hours.	82
Figure 4.59 SEM micrograph of die attach sample with SAC-Cu epoxy: a) cross-section of the die attach sample; and b) SEM image at higher magnification.	85
Figure 4.60 Optical image of the die attach sample with SAC-Cu epoxy: a) at lower magnification; and b) at higher magnification.	86
Figure 4.61 SEM micrograph of molded die attach sample soldered with SAC-Cu-epoxy after autoclave test without preconditioning: a) cross-section of the sample; and b) SEM image at higher magnification.	87
Figure 4.62 SEM micrographs of molded die attach samples soldered with SAC-Cu-epoxy after 1000 temperature cycle test: a) without preconditioning; and b) with preconditioning.	88
Figure 4.63 SAM images of molded die attach samples soldered with SAC-Cu epoxy: a) fresh samples; b) after AC test; and c) after 1000 TC test.	89

LIST OF TABLES

Table 2.1 Usage of current high-temperature solders and their requirements	13
Table 2.2 Typical High-Temperature Solders.....	16
Table 4.1 EDX analysis results of the bulk microstructure of die attach sample using Bi-Ag-Cu-In solder.....	39
Table 4.2 EDX analysis results of the bulk microstructure of die attach sample using Zn-Al-Ge solder.	45
Table 4.3 EDX analysis results of IMC layers at lead-frame/solder interface using Zn-Al-Ge solder on bare Cu lead-frame.	47
Table 4.4 EDX analysis results of bulk microstructure of die attach sample using Zn-Al-Mg-Ga solder on bare Cu lead-frame with 2000 nm Ag thickness at the die back.	60
Table 4.5 EDX analysis results of IMC layers at Si die/solder interface using Zn-Al-Mg-Ga solder with 2000 nm Ag thickness at the die back.....	60
Table 4.6 EDX analysis results of bulk microstructure of die attach sample using Zn-Al-Mg-Ga on bare Cu lead-frame with 200 nm Ag thickness at the die back.	62
Table 4.7 EDX analysis results of bulk microstructure of die attach sample using Zn-Al-Mg-Ga solder on Ni metallized Cu lead-frame.....	72
Table 4.8 EDX analysis results of Ni layer on Cu lead-frame.....	72
Table 4.9 Shear failure mode of die attach samples using standard Pb-5Sn and Zn-Al-Mg-Ga solder.	76
Table 4.10 Effect of ageing time and storage temperature on IMC thicknesses at lead-frame/solder interface.....	82
Table 4.11 SAM test result of Zn-Al-Mg-Ga soldered samples before and after PC.....	83

LIST OF ABBREVIATIONS

AC	Autoclave
ASIC	Application-Specific Integrated Circuit
BLT	Bond Line Thickness
CTE	Coefficients of Thermal Expansion
DBC	Direct Bond Copper
DSC	Differential Scanning Calorimetric
EDX	Energy Dispersive X-Ray
EPMA	Electron Probe Micro Analyzer
HTOL	High-Temperature Operating Life
HTSL	High-Temperature Storage Life
IGBT	Insulated Gate Bipolar Transistor
IMC	Intermetallic Compound
JEIDA	Japan Electronic Industry Development Association
LED	Light Emitted Diode
MOSFET	Metal Oxide Semiconductor Field Effect Transistor
NEMI	National Electronics Manufacturing Initiative
PC	Preconditioning
RoHS	Restriction of Hazardous Substances
SAC	Sn-Ag-Cu
SAM	Scanning Acoustic Microscopy
SEM	Scanning Electron Microscope
TC	Temperature Cycling
WEEE	Waste Electrical and Electronic Equipment

CHAPTER 1 INTRODUCTION

1.1 Background and Problem Statement

Lead-tin (Pb-Sn) alloy is an ideal material for soldering electrical contacts because it melts easily, has excellent wettability, high ductility, low Young's modulus, maintains a reliable connection even after multiple reflow processes, and is relatively inexpensive. High-Pb solder such as Pb-5 mass% Sn (melting point: 314-310°C) or Pb-10Sn (melting point: 302-275°C) is required for temperature-hierarchical bonding in power device packages in which first soldering is performed at a temperature of about 330°C and in which second bonding is then performed by use of a low-melting point solder without melting the first soldered portion (U.S. patent No. US 6563225, 2003). Currently about 150 tons/year of high-Pb solders are being used for semiconductor chip (die) attach applications of which most of it as solder wire, ribbon or perform (Tschudin, et al., 2002). However, obligation imposed by different regulations such as Restriction of Hazardous Substances (RoHS) and Waste Electrical and Electronic Equipment (WEEE) and based on their recent appreciation of the negative impact of Pb to the human health and environment due to its toxicity has encouraged great effort to develop Pb-free solders (Directive 2002/95/EC of the European Parliament, 2003). Alternative as well as drop-in-replacement of high-Pb solder currently using in semiconductor industries has not been found yet (Anderson, 2007; Jang, et al., 2004; Kim, et al., 2003; Suganuma, 2001; Tu, et al., 2003). RoHS therefore, exempts the use of high melting temperature type solders (i.e. Pb based alloys containing 85% by weight or more Pb) up to December 2014 as there no alternative alloys are available having similar melting point, ductility and high electrical conductivity (*RoHS Regulations (UK) Government Guidance Notes*, 2011). Such properties ensure fewer defects during manufacturing and high reliability throughout the life of the component, thereby also resulting in fewer

components going into the waste stream. High-Pb solder therefore still being used together with mid-temperature Pb-free solder such as Sn-Ag-Cu (SAC), and this hinders the recycling of consumer electronic products (Kim, et al., 2009; Suganuma, et al., 2009). Ever increasing pressure from regulators and consumer to remove Pb from the semiconductor assembly, electronic industries are looking for high-temperature Pb-free solders for attaching die to the lead-frame. As a result, high-temperature Pb-free solder has become an important production factor for the semiconductor industry (Tschudin, et al., 2002). The semiconductor die attachment is predominantly done in sophisticated, fully automated production lines. Therefore, the properties of the Pb-free solder materials should be within acceptable limits of the present production conditions such that it avoids major capital expenses. For that reason, the industry is looking for drop-in replacement of the high-Pb solder which will minimize the financial impacts as well as better opportunity to successfully market the product.

Si is commonly used as semiconductor wafer material in many conventional electronic devices. Operating temperature of these devices is less than 250°C (Baliga, 1989). Semiconductor devices for ultra-high temperature applications (> 350°C) in automotive, down-hole oil and gas industries for well logging, aircraft, space exploration, nuclear environment and radars, conventional die attach materials and Si wafer cannot meet their stringent requirements (Chin, et al., 2010). For these devices, silicon carbide (SiC) has been identified as one of the potential semiconductor wafers for the future generation power devices. Ultra-high temperature die attach materials for SiC dies have been reported, namely off-eutectic gold-based (Johnson, et al., 2007), bismuth-based (Yamada et al., 2006), liquid-based (Mannan & Clode, 2004) and silver-based material (Chuang & Lee, 2002; Zhang & Guo-Quan, 2002). In this study, Si die is used and replacement of high-Pb solder is investigated.

Unlike mid-temperature Pb-free solder such as SAC, limited numbers of Pb-free solders have been proposed for high-temperature solder applications, such as, Au-(Sn/Si/Ge), Bi-(Ag), Zn-Sn, and Zn-Al-(Cu/Ga/Mg-Ga)-based alloys (Jang, et al., 2004; Kim, et al., 2009; Kim, et al., 2008; Lalena, et al., 2002; Rettenmayr, et al., 2002; Shimizu, et al., 1999; Song, et al., 2001; Japan patent No. 2004-237375, 2004; Tsai, et al., 2005). Each of the solder has pro and cons as a high-temperature Pb-free solder. Out of these alloy systems, Au-based alloys are expensive, forms a massive intermetallic compound (IMC), and their brittle nature (Ishikawa, et al., 2004; Matijasevic, et al., 1990; Song, et al., 2001; Takao & Aoyama, 2005; Tsai, et al., 2006; Tsai, et al., 2005).

Bi-based alloys have been suggested as a replacement of high-lead solders by different researchers. Unfortunately, the wetting on copper, which is a popular metallization type, is very limited. Wetting on silver lead-frame have been shown good with low wetting angle and intermetallics (Thomas, 2007). Void rate and thermal cycle test results of the samples on nickel plated lead-frame have been shown slightly better results than the standard Pb-based solder (Tschudin, et al., 2002). However, Bismuth (Bi)-based solders are very brittle, difficult to produce in foil or wire form, and have relatively lower thermal/electrical conductivities than those of currently used solders such as Pb-5Sn and Au-20Sn (Lalena, et al., 2002; Song, et al. 2006).

Zn-based alloys can be a good choice for high-temperature Pb-free solder because of suitable melting range, inexpensive, and good thermal/electrical conductivities (Japan patent No. 2006-320913, 2006; Rettenmayr, et al., 2002; Shimizu, et al., 1999). Zn-Sn has no intermetallic compound in the whole range of composition of its eutectic binary phase diagram (SGTE Alloy Phase Diagrams, 2004). It has excellent ductility at room temperature, excellent mechanical properties, electrical properties, and oxidation

resistance even in high temperature high-humidity conditions (Lee, et al., 2005; Lee, et al., 2007). On the other hand, the main problem of Zn-Sn alloy as a high-temperature solder is that it forms liquid at its eutectic temperature of 199°C (Suganuma, et al., 2009). Zn-Al has a long history of use as a high-temperature solder for aluminum alloys mainly for structural purposes (Çay & Can, 2005; Gervais, et al., 1985). Literature on Zn-Al-based alloys used in electronics as a high-temperature solder is very limited. Among these, Zn-4Al-1Cu has been suggested for ultra-high-temperature soldering due to its high melting point (Kang, et al., 2009; Takaku, et al., 2008). Zn-4Al-3Mg-3Ga alloy has proper melting range but it has been reported that it could not be formed into wire which is essential for drop-in-replacement of high-Pb solder (Shimizu, et al., 1999). It also has been reported that excluding Mg and reducing the amount of Ga content, Zn-6Al-1Ga alloy could be extruded in to wire form but unexpected embrittlement of the wire was observed within 24 hours after extrusion due to Ga segregation (Rettenmayr, et al., 2002).

Therefore, further study is necessary on Bi-based and Zn-Al-based alloys for the development of a suitable high-temperature Pb-free die attach material which should not have above limitations. Beside these, SAC-Cu-epoxy solder is also analyzed as a high-temperature die attach material as per interest of some electronic industries.

1.2 Research Objectives

This research is undertaken to explore potential high-temperature Pb-free solder solution for Si die attachment.

The specific objectives of this research are as follows:

1. to investigate the wettability of Bi-Ag-Cu, Bi-Ag-Cu-In, Zn-Al-Ge, Zn-Al-Mg-Ga and SAC-Cu-epoxy solders as high-temperature (melting temperature $> 260^{\circ}\text{C}$ & process temperature $< 400^{\circ}\text{C}$) Pb-free solders on Cu lead-frame;
2. to analyze interfacial reactions via microstructural study at lead-frame/solder and Si die/solder joints;
3. to evaluate die attach performance of the above mentioned high-temperature Pb-free solders with the analysis of die attach void and shear strength;
4. to investigate package reliability performance of the potential high-temperature Pb-free solders;

The main tasks to achieve the aforementioned objectives were as follows:

- i. Die attachment on Cu lead-frame with Bi-based, Zn-Al-based and SAC-Cu-epoxy solders using conventional automatic die attach machine;
- ii. Fabrication of electronic package for reliability performance test;

1.3 Outline of the Dissertation

Chapter 1 introduces the background of this research work and brief outline of the proposed high-temperature Pb-free solder materials. Chapter 2 describes background information on application of high-temperature solders and its requirements. Literature

review on high-temperature Pb-free die attach material are also describes in this chapter. Chapter 3 describes the detailed methods and standards used for evaluating high-temperature Pb-free die attach materials. Chapter 4 illustrates the obtained results from this research work. Microstructure of solder wire and die attach joint, interfacial reactions between Si die/solder and lead-frame/solder interfaces, wetting on Cu lead-frame, die attach void, die shear strength and package reliability performance at accelerated conditions are discussed in this chapter. Chapter 5 discusses conclusions from this work and proposes several recommendations for future work.

CHAPTER 2 LITERATURE REVIEW

2.1 Introduction

This chapter presents background information that will provide a better understanding of the research done in this dissertation. This chapter is split into the following sub topics:

- Power Semiconductor Package
- Die Attachment
- Requirements of High-Temperature Solder
- High-Temperature Pb-Free Solder for Die Attach
- Reliability of Die Attach Joint

2.2 Power Semiconductor Package

Power semiconductors are used in a wide-range of commercial and industrial applications, which require switching of high current or voltage, such as the following (Mazda, 1997):

1. Power supplies
2. Electrical machine control
3. Heating and lighting
4. Automotive electronics
5. Electrochemical processing

Typical life cycle requirements for power devices range from 10 years (pumps) to more than 30 years (locomotive traction) (Coquery, et al., 2003). IGBTs (Insulated Gate Bipolar Transistors) and MOSFETs (Metal Oxide Semiconductor Field Effect

Transistors) are the most common power semiconductor switching devices for high power and high frequency respectively. These power semiconductor devices are often packaged in multi-chip packaging systems (Figure 2.1). The large amount of power dissipated by the devices (as high as megawatts for IGBTs and kilowatts for power MOSFETs) creates a large amount of heat, even if the device has a high level of device efficiency. This power dissipation results in a temperature increase when the devices are on and a decrease when the devices are off. Such power cycling is one of the main causes of failure in the packaging system.

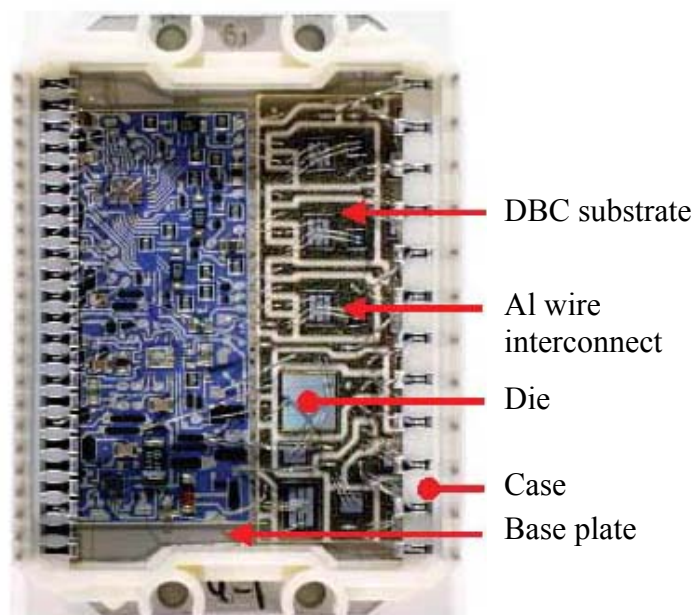


Figure 2.1 Inside of power module used in pumps.
(Zheng, 2005)

The reliability of a power module depends largely on its package structure (Shammas, 2003). The package (Figure 2.1) has to provide a convenient method for electrical current to flow to and from the device, and give mechanical support to the device, while enabling heat generated by the devices to be conducted away to the ambient. Typically, power modules consist of several layers including the die, die attach, Direct Bond Copper (DBC) substrate, substrate attach and a copper base plate (or heat spreader). The

layers are designed to be thin and large in area in order to dissipate heat efficiently. DBC substrates, for example, consist of a thermally conductive ceramic (usually Al_2O_3 or AlN) layer with the thickness of around 0.635mm sandwiched between two copper layers with the thickness around 0.3mm. To complete the packages, large diameter (125~375 μm) gold or aluminium wires are used to interconnect the die, substrate, and terminals. The heat spreader (or base plate) is often attached to a heat sink through thermal grease to dissipate the heat.

During application, packages experience temperature fluctuations introduced by the switching operation. Different layers in the package have different coefficients of thermal expansion (CTE), so they will expand/contract at different rates in response to this fluctuation. The different expansions generate thermal stress in the modules, especially in the solder attach and wire bonds. In fact, thermal stress induced die attach fatigue cracking has been reported as a major failure mechanism for power MOSFETs. It is critical that the die attach is able to sustain the thermo-mechanical stress generated by power on/off operation over intended life span of the module.

2.3 Die Attachment

There are several levels in electronic packaging system (Figure 2.2). Die attachment is the first level of packaging systems. It is a process of affixing Si die to a lead-frame or other substrate with adhesive, conductive adhesive or solder. Schematic view of Si die attachment is shown in Figure 2.3. Various elements are involved in a power device packages, but this thesis focuses on the development of high-temperature Pb-free solder for Si die attachment. Conventional solder alloys used in die attach usually are in the melting range of 275-345°C (liquidus), either to resist subsequent reflow during surface mounting, or, in the case of power devices, to allow higher device operating temperatures without joint failure. The die attach material should have specific

characteristics to ensure that the package is mechanically reliable and thermally efficient at the operating temperature (Muralidharan & Tieg, 2006). These characteristics include good adhesion on conventional part surfaces

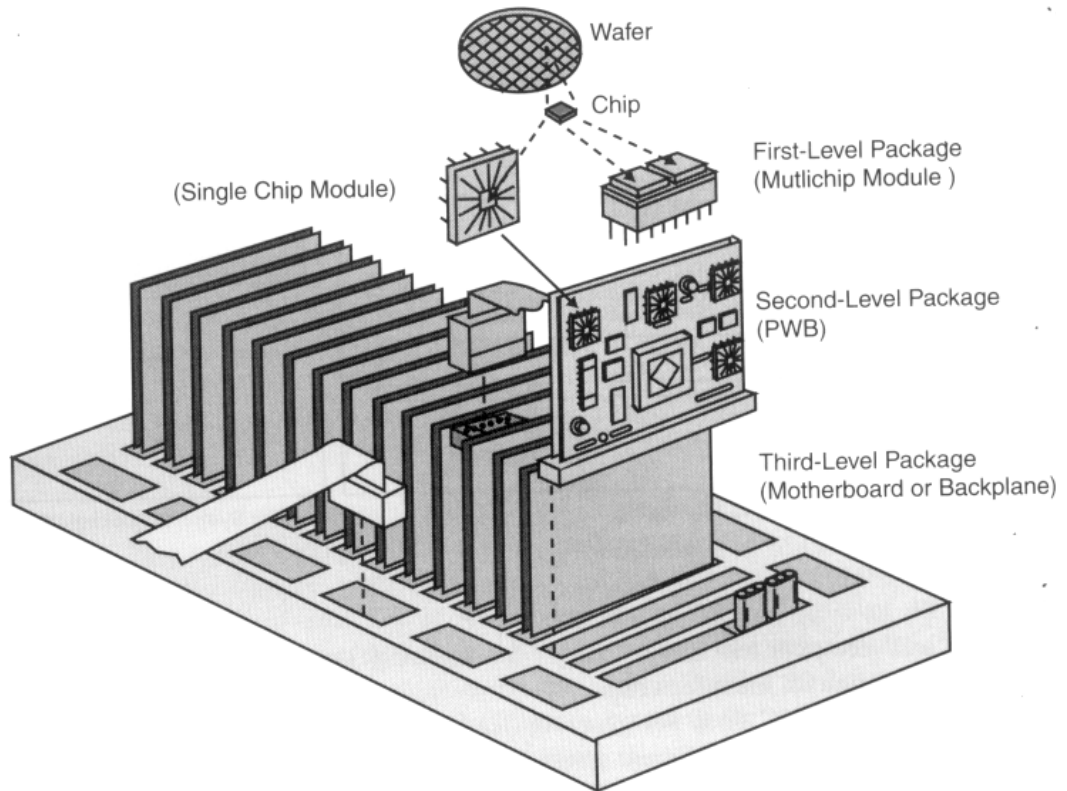


Figure 2.2 The electronic packaging hierarchy. (Tummala, 2001).

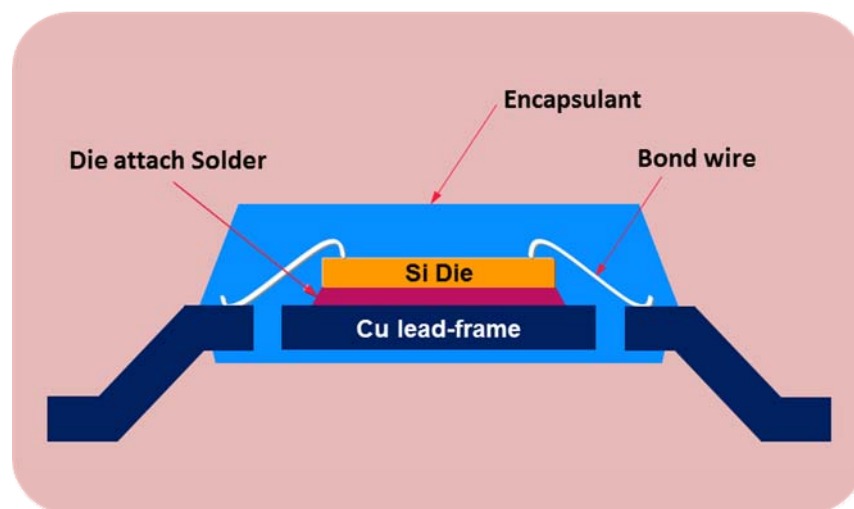


Figure 2.3 Schematic view of Si die attachment.

(die and lead-frame), good resistance against thermal fatigue, low electrical resistance and high thermal conductivity for carrying current and high heat dissipation, CTE that matches with both lead-frame and die, good wetting on lead-frame, low void rate on the die-attach layer, the ability to be processed at appropriate temperature with conventional die attach machine, and maintain stability at operating temperature throughout the package life (Coppola, et al., 2007; Kayali, et al., 1996). Among these characteristics, CTE of die, solder and lead-frame plays a vital rule for the stability and reliability of die attachment in thermal cyclic loading condition. Due to mismatch of CTE, thermomechanical stress is developed and concentrated at the interface between Si die and solder and the interface between solder and lead-frame. A correlation known as Coffin-Manson relation has been developed to relate the number of thermal cycles a die attachment can withstand before failure to the properties of the system (Tuhus & Bjorneklett, 1993).

This correlation is

$$N_f \propto \gamma^m \left(\frac{2 \times t}{L \times \Delta CTE \times \Delta T} \right) \quad (1)$$

where

γ = shear strain for failure

m = constant dependent on the material

L = diagonal length of the die

t = die attach material thickness

The presence of voids in the die attach joint can significantly reduce the number of thermal cycles before failure (Kayali, et al., 1996). Since voids are not good thermal conductor and number of void increases during thermal cycle, they cause localized

heating and increase stress concentration which leads premature die delamination. Moreover, it has been shown that humidity accelerates the aging process of the die-attach material (Rusanen & Lenkkeri, 1995). To minimize these effects, the CTE of Si die, die attach material and lead-frame should be matched as closely as possible, the die-attach material should have a high shear strain before failure, and the presence of voids in the die-attach material should be avoided.

2.4 Requirements of High-Temperature Solder

High-temperature solders not only used in die-attach process but also widely used in various types of applications such as assembling optical components, automobile circuit boards, circuit modules for step soldering, etc. Some of the typical high-temperature solder applications with their major requirements are summarized in Table 2.1. Since each application has its own specific requirement, a single high-temperature solder cannot cover all of the applications. For example, for internal joining of passive/active components such as die attachments, flip chip joints, and resistors/capacitors 90–95 wt.% lead solder have been used. On the other hand, gold-based alloys are used as main solder for assembling optical components because those devices require flux-free solder. Typical requirements for high-temperature solder (Suganuma, et al., 2009) are given below:

- Melting temperature in the range of 260°C to 400°C
- Softness to up-hold structural integrity by relief of thermal stress
- Small volume expansion at reflow temperature to avoid break down of package
- Sufficient workability to be formed into thin wires or sheets
- Good electric and thermal conductivity
- Good mechanical properties, particularly fatigue resistance
- Air tightness not to break vacuum package

- Fluxless
- No alpha ray emission

Table 2.1 Usage of current high-temperature solders and their requirements.
(Suganuma, et al., 2009)

Field of use	Major Solders currently being used	Major Requirements
Die-attachment of power semiconductors and Application-Specific Integrated Circuit (ASIC)	High Pb alloys Au alloys	Reflow resistance High thermal/electric conductivity Thermal fatigue resistance
Flip-chip packages	High Pb alloys Au alloys	Reflow resistance Low A ray emission
Internal connection of passive components	High Pb alloys	Reflow resistance
Optical packages and modules including LEDs and laser devices	Au alloys	Fluxless Reflow resistance High thermal conductivity
Quartz device	High Pb alloys	Reflow resistance Air-tightness
Heat-resistant vehicle packages	High Pb alloys	Thermal fatigue resistance Heat exposure resistance
Module packages step soldering	High Pb alloys	Reflow resistance
Heat-sink joining & Leading pin joining	Au alloys	Thermal fatigue resistance High thermal conductivity Airtightness

2.5 High-Temperature Pb-Free Solder for Die Attach

In power modules, metallic solders are used for die attach because of their thermal and electrical conductivity. The solder material used to attach the die to the lead-frame can be categorized into two groups: hard solders and soft solders (Dennis & Howard, 1979). Hard solders are usually gold-based eutectics such as Au-3%Si, Au-12%Ge and Au-20%Sn. Those solders have high strength and do not quickly degrade from fatigue damage during power cycling. However, they are expensive and will transfer high stresses to the die, which may cause die fracture for any but the smallest die (<5mmx5mm). On the other hand, soft solders, including virtually all low-melting lead-,

tin- and indium- based solders, have low strength and high ductility. During temperature or power cycling, these solders transmit very little stress to the die. Therefore those solders can be used to join much larger die and are also relatively inexpensive. Of these solders, the ones with the highest melting points are high lead-solders ($T_{\text{melt}} > 290^{\circ}\text{C}$). As a result, high lead solders such as Pb5Sn, Pb10Sn are extensively used in the power semiconductor packages, despite the fact that they often experience extensive fatigue cracking.

There are increasing concerns nowadays about the use of lead-based solders in electronics which is health threat to human beings. The major concern is that lead from discarded consumer electronics products in landfills could leach into underground water and eventually into drinking water system (Figure 2.4) (Abtew & Selvaduray, 2000). In response to the concern over Pb used in electronic products and manufacturing applications, efforts have been on-going to find acceptable Pb-free solders. The U.S. National Electronics Manufacturing Initiative (NEMI) in USA recommends Sn-3.9Ag-0.6Cu for surface mount reflow soldering and Sn-0.7Cu for wave soldering, and the Japan Electronic Industry Development Association (JEIDA) selected

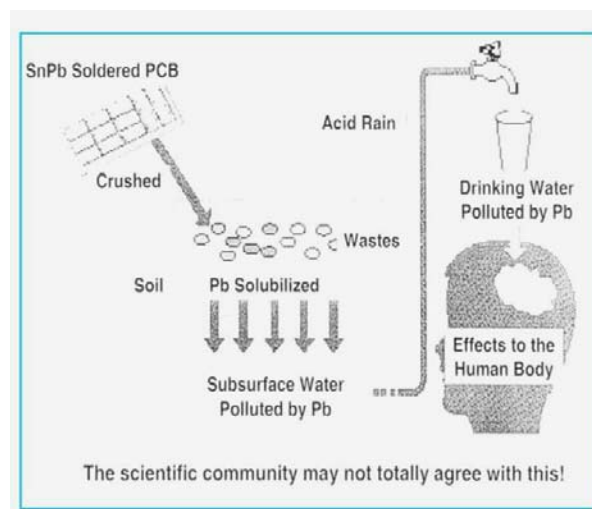


Figure 2.4 The schematic of how Pb from solder materials affects the human beings. (Jiang, 2008)

Sn-3.5Ag-0.75Cu, Sn-(2~5)Ag-(>5)Bi-(0.5~4)Cu, Sn-0.7Cu-0.3Ag and Sn-57Bi-1Ag (Nimmo, 1999). The IDEALS consortium in Europe preferred Sn-3.8Ag-0.7Cu for reflow soldering and Sn-3.8Ag-0.7Cu-0.25Sb for wave soldering. The SOLDERTEC lead-free roadmap in Europe recommends alloys in the range Sn-(3.4-4.1)Ag-(0.45-0.9)Cu for reflow and wave soldering.

High-lead solder die attach that used in power semiconductors packages are not subjected to ban, since the related applications are usually involves long life cycles and good candidates to replace high-lead solder in those applications is yet to be determined. Table 2.2 summarizes the possible high-temperature Pb-free solders including some Pb-based solders with their melting temperatures. Based on melting temperature requirement, Bi-based and Zn-Al-based alloys can be considered as a replacement of high-Pb alloys. These alloys show promises with some drawbacks which are discussed earlier. In this thesis, two Bi-based, two Zn-Al-based alloys and one SAC-Cu-epoxy solder are studied. In Bi-based alloys, Cu and Cu-In are added with Bi-Ag. Cu is added in the solder for increasing wettability on Cu lead-frame and In is added for improving ductility of the solder. In Zn-Al-based alloys, Ge and Mg-Ga are added. Ge is added for reducing the melting temperature and increasing the ductility of the alloy (U.S. patent No. US 6563225, 2003). Mg and Ga are added for reducing melting temperature solder. Furthermore, Mg prevents grain boundary corrosion but excessive amount of Mg makes the solder brittle (U.S. patent No. US 6563225, 2003). SAC-Cu-epoxy solder is also studied as a high-temperature Pb-free solder for die attach.

Table 2.2 Typical High-Temperature Solders.

Alloys	Composition (wt.%)	Solidus Temperature (°C)	Liquidus Temperature (°C)
High-Pb Alloy System Pb-Sn	Sn-65Pb	183	248
	Sn-70Pb	183	258
	Sn-80Pb	183	279
	Sn-90Pb	268	301
	Sn-95Pb	300	314
	Sn-98Pb	316	322
Pb-Ag	Pb-2.5Ag	304	304
	Pb-1.5Ag-1Sn	309	309
Sn-Sb Alloy System Sn-Sb	Sn-5Sb	235	240
	Sn-25Ag-10Sb (J-alloy)	228	395
Au Alloy System Au-Sn	Au-20Sn	280 (eutectic)	
	Au-Si	363 (eutectic)	
	Au-Ge	356 (eutectic)	
Bi Alloy System Bi-Ag	Bi-2.5Ag	263 (eutectic)	
	Bi-11Ag	263	360
Cu Alloy System Cu-Sn	Sn-(1-4)Cu	227	~400
	Sn-Cu particles composites	~230	
Zn Alloy System Zn-Al	Zn-(4-6)Al(-Ga, Ge, Mg, Cu)	300~340	
	Zn-Sn	199	360

(Courtesy of Senju Metals, Co., Ltd.)

2.6 Reliability of Die Attach Joint

In electronic package, solder provides both mechanical and electrical connection (die attach, wire bonding between die/lead-frame I/O terminals, etc) between and within the many levels of the package. The solder alloys used for power device die attachment are often subject to cyclic loading resulting from repeated thermal cycling, leading to fatigue failures of the die attach joint.

Thermal cycling refers to situations where the environment surrounding the electronic package undergoes cyclic thermal excursions. Generally, the cycle consists of a dwell at a high temperature, a ramp to a low temperature, a dwell at the low temperature, and a ramp to the high temperature, after which the cycle is repeated. Two common thermal cycling examples are the heating and cooling that occurs during a typical day during the morning and evening hours, and the heating and cooling of an automobile engine compartment upon a person's commute to and from his/her workplace. Electronic packages experience an isothermal temperature as they come to equilibrium with the environment during the high and low dwells. The CTE mismatch between the die or package and the lead-frame causes the die attach joints to deform and fatigue over many cycles.

Due to the extremes of planetary climate, the solder joint in space electronic packages must withstand much larger thermal fatigue loading and extended cold temperatures, and therefore the fatigue reliability of the solder joint becomes a critical issue in determining the lifetime of a functional device.

It is commonly accepted that under thermal fatigue conditions the following parameters are critical in determining the fatigue life of die attach or solder joint: 1) the temperature range (ΔT) during temperature cycling, 2) the two temperature extremes, 3) the temperature loading time (ramp rate, dwell time), and 4) the thickness of the die attach. The critical effects of both ΔT and the thickness of the die attach are logical since they are both related to the level of cyclic stress/strain due to a CTE mismatch between different packaging materials, the direct cause for die-attach fatigue failure. Cracks in die attach usually initiate from the edges and propagate toward the centre since cyclic stress/strain usually reaches its maximum at the edges first.

Extensive studies have been addressed PbSn solder interconnects and their fatigue reliability (Cressler, 2005; Glazer, 1995; Kirschman, et al., 2001), including fatigue testing of real joints (Hermida, et al., 2000; Kassner & Perez-Prado, 2004; Kim & Ledbetter, 1998; Zinov'ev & Vladislav, 1989), constitutive modelling of stresses and deformation in the joint (Shetty & Reinikainen, 2003), and bulk property measurements on solder alloys at normal temperature range ($>-40^{\circ}\text{C}$) (Leicht & Skipor, 2000; Pidaparti & Song, 1996; Shang, et al., 2007; Shetty, et al., 2001; Zhao, et al., 2003). The literature on thermal cycling of electronic components containing SnPb eutectic solder is abundant. But reliability tests of Zn-Al based alloys are very limited.

However, in the present study, the very harsh operational environment, including extended low temperatures, subjects the electronic modules to greater levels of thermal fatigue than normal commercial electronics or even electronics for military use, and assessment of its reliability have been tested in this thesis.

Intermetallics are not only formed during the die attachment but can also gradually grow during its operational period at high operating temperature. Therefore, the growth of intermetallics at high temperatures may result in more brittle fractures in the die attach joint. Studies of the effect of temperature on intermetallics of the die attach joint have also been conducted in this thesis.

CHAPTER 3 METHODOLOGY

3.1 Introduction

This chapter describes detail methods and techniques used for achieving the objectives of the study. Research in this work was conducted in three steps. In the first step, extensive literature survey was performed which is described in chapter 2. Based on previous work done by different researchers and their recommendations for high-temperature Pb-free solders, some alloys were selected for preliminary assessment. Some criteria were also set for the preliminary assessment which is required for a high-temperature die attach material. In the second step, preliminary assessment was performed which includes melting behavior of the solder, wettability on Cu lead-frame, die attach void, die shear strength, microstructure and interfacial reaction analysis at Si die/solder and lead-frame/solder interfaces. The solders which satisfy the preliminary assessment criteria were selected for the package reliability performance tests at accelerated condition. In the third step, package reliability performance test were conducted which includes autoclave (AC), temperature cycling (TC), high-temperature operating life (HTOL) and high-temperature storage life (HTSL) tests. Among these tests AC and TC tests were conducted with and without preconditioning (PC) of the samples. Failure mode was analyzed by scanning acoustic microscopy (SAM) test and cross-sectioning technique.

3.2 Preliminary Assessment of High-Temperature Pb-Free Solders

3.2.1 Melting behavior and microstructure analysis of solder

The melting behavior of the solder wire was determined from heating curve obtained by differential scanning calorimetric (DSC) measurement at a heating rate of 10° C/min. DSC is a thermoanalytical technique in which the difference in the amount of heat

required to increase the temperature of a sample and reference is measured as a function of temperature. Both the sample and reference are maintained at nearly the same temperature throughout the experiment. Figure 3.1 shows the inside of a DSC apparatus where small pans are placed into the compartments. In this study, aluminum (Al) pan was used and sample size was taken approximately 30 mg. DSC analysis was performed in air environment.

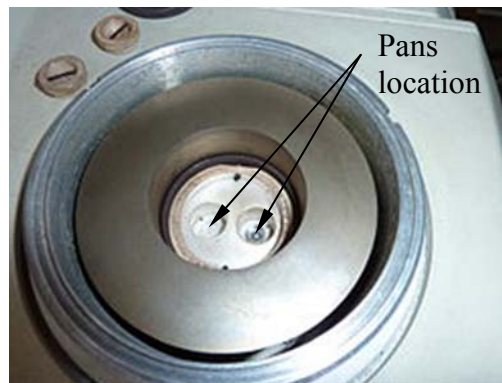


Figure 3.1 Inside of the DSC machine.

For microstructure analysis, solder wire was cast vertically in molding cup using a mixture of epoxy resin and epoxy hardener with a ratio of 5:1. Molding cup was kept in a vacuum chamber for removing air bubbles from the mixture which was trapped during mixing process. It was kept approximately 3 hours for hardening. After that it was polished with sand paper and polycrystalline diamond suspension (6 μm , 3 μm and 1 μm) for making cross-section. No etching reagent was used on polished surface of the sample. Cross-section of the solder wire was analyzed by optical microscope, scanning electron microscope (SEM) (Hitachi S-3400N) and energy dispersive x-ray (EDX) (EMAX-EX200).

3.2.2 Si die attachment

Automatic die attach machine (Brand: ESEC, Model: ESEC2005HR) was used for Si die attachment. Figure 3.2 shows the die attach machine which was used for dispensing solder wire. Die attach machine had eight zone heating tunnel. The first four zones was used for lead-frame pre-heating, solder was dispensed at zone five; at zone six die attachment was performed and the rest two zones were used for cooling the lead-frame. Between zone five and six, titanium/ceramic spanker was used for spreading the solder on lead-frame. For all experiments, commercial grade lead-frame (TAMAC 4) with 0.5 mm thickness and Ti/Ni/Ag metallized Si die were used. In one set of experiment, Ni metallized Cu lead-frame was used which is described in Article 3.2.2c and the rest of the experiments were performed on bare Cu lead-frame. Die back metallization thickness was used in the range of 700-2500 nm. Among these, Ti layer thickness varies from 100 to 150 nm, Ni layer thickness varies from 350 to 400 nm and Ag layer thickness varies from 200 to 2000 nm. In a single lead-frame, 20 single die can be attached with an array of 20x1. During die attachment, forming gas (95% N₂ with 5% H₂) was used in the heating tunnel. Each of the die was attached within a period of



Figure 3.2 Si die attach machine with solder wire as feed.
(Brand: ESEC, Model: ESEC2005HR)

approximately 0.8 to 1 second depending on the solder type. Total heating span (zone five to zone eight) of a single die was approximately 3.2 to 4 second. After the die attachment, lead-frames with Si dies come out from the heating tunnel and it was cooled down to room temperature by natural convection cooling. For each of the solder wire, die attach was performed at different temperatures and die attach properties were analyzed to find out most appropriate die attach temperature for each solder.

For SAC-Cu-epoxy solder, same die attach machine was used for Si die attachment with some modification in the solder dispense area. SAC-Cu-epoxy solder was dispensed on lead-frame at room temperature through showerhead nozzle. Different types of showerhead nozzles are available which can dispense one, two, four and five dots for single die attachment. Normally showerhead with higher number of dots is used for larger size die such that solder can spread uniformly in all directions. In the present experiments, two dots showerhead nozzle was used.

3.2.2(a) Die attach using Bi-Ag-Cu/ Bi-Ag-Cu-In solder

Solder wire of diameter 0.76 mm was used to attach Si die on bare Cu lead-frame using automatic die attach machine in an industrial environment. The size of the Si dies used in this experiment was approximately 2.7 mm x 2.4 mm x 0.4 mm. Die attach was performed in forming gas environment at temperatures 350°C and 450°C. Each of the die was attached within a period of approximately 0.8 second. Total heating span of a single die was approximately 3.2 second. It is to be mentioned that die attachment using Bi-10Ag-5Cu-In solder at temperature 350°C was performed with and without scrubbing action.

3.2.2(b) Die attach using Zn-Al-Ge solder

Zn-Al-Ge solder wire of diameter 0.5 mm was used to attach Si die on bare Cu lead-frame using automatic die attach machine in an industrial environment. The size of the Si dies used in this experiment was approximately 1.9 mm x 1.2 mm x 0.3 mm. Die attachment was performed in a forming gas environment at temperatures ranging from 370°C to 390°C. Each of the die was attached within a period of approximately 0.8 second. Total heating span of a single die was approximately 3.2 second.

3.2.2(c) Die attach using Zn-Al-Mg-Ga solder

Zn-Al-Mg-Ga solder wire of diameter 0.5 mm was used to attach Si die using automatic die attach machine in an industrial environment. Forming gas was used in the heating tunnel during die attachment. Each of the die was attached within a period of approximately 1 second. The total heating span of a single die was approximately 4 second.

Die attach using Zn-Al-Mg-Ga solder was performed for three sets of experiments. For first set of experiment, Si dies of approximately 2.03 mm x 1.73 mm x 0.3 mm were attached on bare Cu lead-frames at temperatures ranging from 370°C to 400°C. Optical images of the die attach samples with Zn-Al-Mg-Ga and standard Pb-5Sn solders are shown in Figure 3.3. Ag thicknesses used at the die back metallization were 200 nm and 2000 nm. Die attach area of the lead-frame used in this experiment was quite different from the others. At the center of the die attach area there was a square shaped dimple and four pedestals arranged in perpendicular direction to the four sides of the dimple. The function of dimple is to lock the solder at the center and the pedestals control the bond line thickness of the die attach joint. The schematic view of the die attach area of the lead-frame is shown in Figure 3.4.

For second set of experiment, Si dies of approximately 2 mm x 1.5 mm x 0.3 mm and 1.86 mm x 1.73 mm x 0.3 mm were attached on bare and Ni metallized Cu lead-frames respectively at temperature 380°C. For standard Pb-5Sn solder, Si dies of approximately 1.87 mm x 1.2 mm x 0.3 mm were attached on bare Cu lead-frame. Die attach area of the lead-frame used in this experiment was flat. Optical images of the die attach samples with Zn-Al-Mg-Ga and standard Pb-5Sn solders are shown in Figure 3.5.

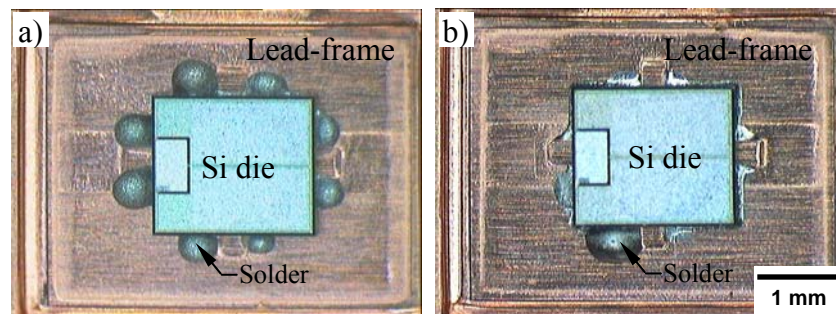


Figure 3.3 Optical images of the die attach samples using: a) Zn-Al-Mg-Ga solder at 380°C; b) standard Pb-5Sn solder.

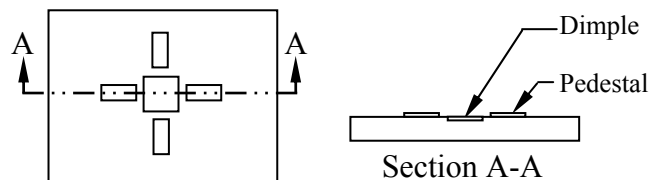


Figure 3.4 Schematic view of the die attach area of lead-frame.

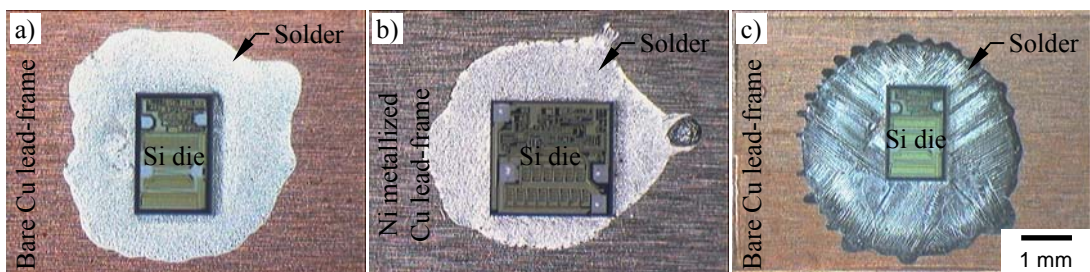


Figure 3.5 Optical images of the die attach samples using: a) & b) Zn-Al-Mg-Ga solder on bare & Ni metallized Cu lead-frame respectively, and c) standard Pb-5Sn solder on bare Cu lead-frame.

For third set of experiment, Si dies of approximately 2 mm x 1.5 mm x 0.3 mm were attached on bare Cu lead-frame at temperature 380°C. Die attach area of the lead-frame used in this experiment was flat.

3.2.2(d) Die attach using SAC-Cu-epoxy solder

SAC-Cu-epoxy solder was dispensed on bare Cu lead-frame with two dots showerhead nozzle at pressure 20 psig and Si die was placed on it using automatic die attach machine at room temperature. The size of the Si die used in this experiment was approximately 2.1 mm x 1.4 mm x 0.3 mm. For die bonding, the lead-frame with dies attached with epoxy was passed through reflow oven within 2 hours after solder dispense. Approximate profile used in reflow oven is shown in Figure 3.6. The peak temperature of the reflow profile was 245°C, ramp rate 1°C/min, time above 217°C was about 60 second and total reflow time was 5 minutes. At this stage, flux used in SAC-Cu-epoxy solder was activated and performed surface cleaning operation of the Cu particles and escaped from the solder. Conversion of some Cu_6Sn_5 and Cu_3Sn IMCs also takes place at this moment. After reflow treatment, lead-frame was kept in post cure oven at 175°C for 1 hour for further conversion of solder in to Cu-Sn IMCs.

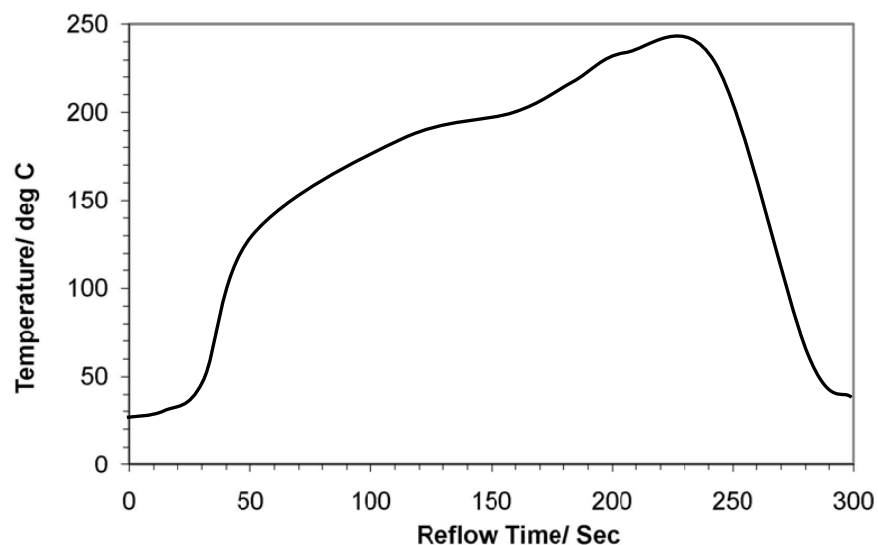


Figure 3.6 Reflow profile for SAC-Cu epoxy.

3.2.3 Investigation of bulk and interfacial microstructure

Die attach samples were singulated from the lead-frame and molded in molding cup with epoxy resin and hardener for making cross-section which is described earlier in article 3.2.1. No etching reagent was used on polished surface before SEM. Microstructure of the bulk solder and interfacial reactions at the Si die/solder and lead-frame/solder interfaces were analyzed by optical microscope, SEM, EDX and electron probe microanalyzer (EPMA) (CAMECA SX100). These analyses were performed to know the phases present in the solder joint and also to know the chemical composition of these phases. Interfacial reactions at the Si die/solder and lead-frame/solder interfaces and variation of thicknesses depending on die attach temperatures were also found from this analysis.

3.2.4 Wetting on Cu lead-frame

Solder wetting pertains to the formation of a relatively uniform, smooth, and unbroken film of solder that exhibits excellent adherence on the soldered surface. Non-wetting, on the other hand is the condition wherein the solder coating has contacted the surface but did not adhere completely to it, causing the surface or a part thereof to be exposed. When the hot solder comes in contact with a copper surface, a metal solvent action takes place. This solvent action is called wetting and forms IMC between the parts. In this study, wetting on Cu lead-frame was evaluated by measuring contact angle and wetting diameter of the soldered area. Contact angle and wetting diameter of the high-temperature Pb-free solder on Cu lead-frame were compared with the standard Pb-5Sn soldered samples. Formation of IMC between lead-frame and solder was also checked by cross-sectioning technique. For measuring the diameter of the soldered area, reference X and Y axis were set first. Then five points were picked at the periphery of the soldered area. Based on the reference axis and five points, wetting diameter was calculated using Smart scope software.

3.2.5 Void analysis

Regardless of the die attach process, the presence of voids in the die attach material affects the quality and reliability of the device itself. Large die attach voids results in low shear strength and low thermal/electrical conductivity, and produce large die stress that may lead to die cracking. In this study, voids under Si die attach joint was analyzed by back scanning method using SAM. Cumulative void area was calculated for each of the die attach samples using a mesh of 10 x 10 which was superimposing on die area of the SAM image. In some industrial practice, the maximum void rate allowed for high power application packages is 5% for single void and 10% for cumulative void. Die attach void of some alloys were also analyzed by cross-sectioning technique.

3.2.6 Die shear strength test

In this study, shear strength of the die attach samples was measured using a die shear machine (STORM INTELLI TEST FA1500) with a stroke length of 3000 μm and a test height of 100 μm from the lead-frame surface. Die shear strength of different high-temperature Pb-free soldered samples were compared with the shear strength of standard Pb-5Sn soldered samples. It is to be noted that the acceptable limit of the die shear strength depends on the size of the Si die. Standard followed by ON Semiconductor for the minimum die shear strength are given in Appendix-A.

3.3 Package Reliability Performance Test of Potential High-Temperature Pb-Free Solders

3.3.1 Sample preparation for reliability test

Based on the preliminary assessment results, die attachment was performed on Cu lead-frames with selected solders at optimum temperature. After that wire bonding was carried out in automatic wire bonding machine (SHINKAWA CUB45).



Figure 3.7 Wire bonding machine.
(Model: SHINKAWA CUB45)

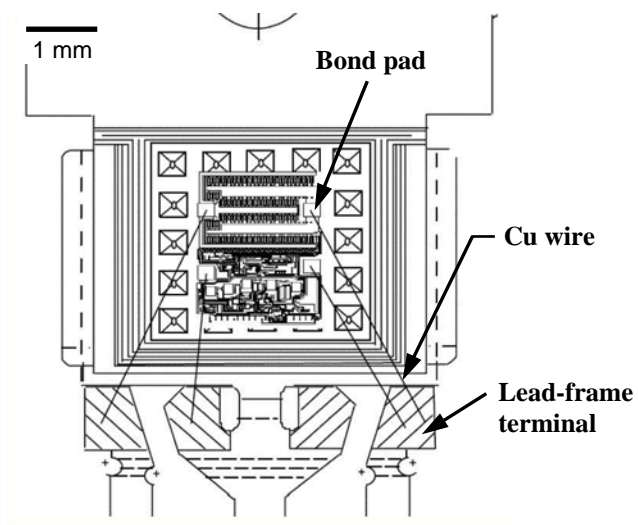


Figure 3.8 Wire bonding diagram.

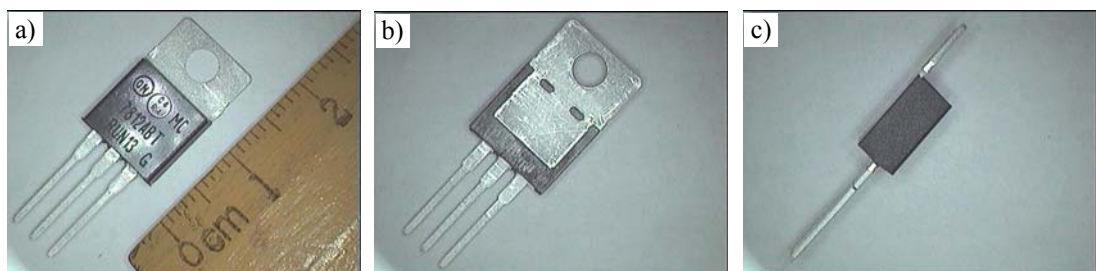


Figure 3.9 Optical images of the encapsulated package: a) front view; b) back side view; and c) side view.

Figure 3.7 shows the photograph of wire bonding machine. In the wire bonding operation input/output terminals of the Si die (bond pad) and lead-frame terminals were connected using 50 μm diameter Cu wire (99.99%). Wire bonding diagram is shown in Figure 3.8. At last, each of the wire bonded dies was encapsulated at temperature 180°C using E500HL epoxy mold compound. During encapsulation, bonded wires may be damaged. For that reason, electrical test was conducted for each of the molded samples and only good ones were selected for reliability tests. Figure 3.9 shows the optical images of one of the encapsulated sample.

3.3.2 Preconditioning

PC was performed according to JESD22-A113E standard. Before PC, electrical test was performed at 25°C and external visual observation was done by optical microscope at 40x magnification to ensure that no samples with external cracks or other damage were used in this test. All samples were placed in a clean, dry, shallow container so that the samples body do not touch or overlap each other. PC was performed in three stages. In first stage, dry back operation was performed in which all samples were baked in oven at 150 \pm 5°C for 24 hours for removing all moisture from the package. In second stage, all samples were kept in a chamber with 85°C/85% RH for 168 hours for moisture soaking. Moisture soaking was done within 2 hours from dry bake operation. In third stage, three times IR reflow was performed at 260°C. This operation was performed within 15 minute to 4 hours after moisture soak. At the end of PC, electrical test was performed again at 25°C.

3.3.3 Autoclave test

AC test was performed according to JESD22-A102D standard for evaluating the moisture resistance and robustness of the samples which forced delamination and corrosion in the package. It is a highly accelerated test which employs conditions of

pressure, humidity and temperature under condensing conditions to accelerate moisture penetration through the external protective material (encapsulant or seal) or along the interface between the external protective material and the metallic conductors passing through it. In this test, the samples were kept in a pressure cooker for 96 hours with 100% RH and temperature/pressure of $121.5 \pm 2^\circ\text{C}/15$ psig. This test was performed for two sets of samples: One set with PC and the other set without PC. Electrical test was performed for two sets of samples at zero and after 96 hours. Electrical test includes voltage, current and resistance. Cross-section was made for some samples for checking cracks, micro-structural change in the bulk solder and IMCs between Si die/solder and lead-frame/solder interfaces. SAM test was conducted on 10 samples before and after the AC test for checking delamination in the samples. Lot size for AC test was 80 samples and pass criteria was zero failure in electrical test.

3.3.4 Temperature cycling test

TC test was conducted according to JESD22-A104D standard for determining the ability of components and solder interconnects to withstand mechanical stresses induced by alternating high and low temperature extremes. In this test, the samples were kept in chamber where temperature changed from -65°C to $+150^\circ\text{C}$ alternatively. In this chamber, ramp rate was $10^\circ\text{C}/\text{min}$, holding time at the two extreme temperature peaks was 5 minutes and number of cycles was 2/hour. Total number of cycles completed in this test was 1000 cycles. This test was performed for two sets of samples: One with PC and the other one without PC. After completion of TC test, electrical test was performed for two sets of samples at zero, 500 and 1000 cycles. Cross-section was made for some samples for checking cracks, micro-structural change in the bulk solder and IMCs between Si die/solder and lead-frame/solder interfaces. SAM test was conducted on 10 samples before and after the TC test for checking delamination in the samples. Lot size for TC test was 80 samples and pass criteria was zero failure in electrical test.

3.3.5 High-temperature operating life test

HTOL test was conducted according to JESD22-A108D standard for determining the effects of bias conditions and temperature on samples over time. In this test, the samples were kept in chamber for 1008 hours at temperature 125°C. At this time, maximum rated voltage was applied in each sample. This test was conducted for one set of samples without PC. Electrical test was carried out for all samples at 0, 504 and 1008 hours of operation. Cross-section was made for some samples for checking cracks, micro-structural change in the bulk solder and IMCs between Si die/solder and lead-frame/solder interfaces. SAM test was conducted on 10 samples before and after the HTOL test for checking delamination in the samples. Lot size for HTOL test was 80 samples and pass criteria was zero failure in electrical test.

3.3.6 High-temperature storage life test

HTSL test was conducted according to JESD22-A103D standard for determining the effects of time and temperature, under storage conditions, for thermally activated failure mechanisms and time-to-failure distributions of the samples. In this test, the samples were kept in different chambers at temperature 125, 150 and 175°C for 1008 hours without applying electrical condition. Some samples were collected from each chamber after 48, 96, 168, 336, 504 and 804 hours. Cross-section was made for some samples for checking cracks and change of IMCs thicknesses at lead-frame/solder interfaces.

3.4 Failure Mode Analysis

Failure of the samples was analyzed by SAM test and cross-sectioning technique. SAM test method was used to determine delamination in the package. Sonix scan, Model: UHR 2000 was used in this study. Thru scan method was used for this analysis. For checking cracks in the solder joint, cross-sectioning technique was used.

CHAPTER 4 RESULTS AND DISCUSSION

4.1 Introduction

This chapter presents the results and discussion of this research work. In this dissertation, two Bi-based alloys, two Zn-Al-based alloys and one SAC-Cu-epoxy solder were selected based on literature survey for investigation as high-temperature Pb-free solder for Si die attachment. Investigation includes, melting behavior and microstructure of solder wire, microstructure of die attach joint, interfacial reactions at Si die/solder and lead-frame/solder interfaces, die attach properties such as wetting on Cu lead-frame, void and die shear strength for preliminary assessment. Based on preliminary assessment results, reliability tests of some selected solders were performed at accelerated condition and the results obtained from these tests are also described in the chapter.

4.2 Die Attachment Using Bi-Based Alloys

In this study, two Bi-based alloys were selected as a high-temperature Pb-free die attach material. These were Bi-Ag-Cu and Bi-Ag-Cu-In. These alloys were used in wire form.

4.2.1 Bi-Ag-Cu solder

4.2.1(a) Microstructure and melting behavior of Bi-Ag-Cu solder wire

Figure 4.1 shows the cross-sectional SEM micrograph of the Bi-Ag-Cu solder wire. It consists of three phases. According to the EDX analysis, the brighter contrast phases (point A) are 100 wt.% of Bi, medium gray particles (point B) are Ag-rich phase containing an average of 97.6 wt.% of Ag and dark particles (point C) are 100 wt.% of Cu.

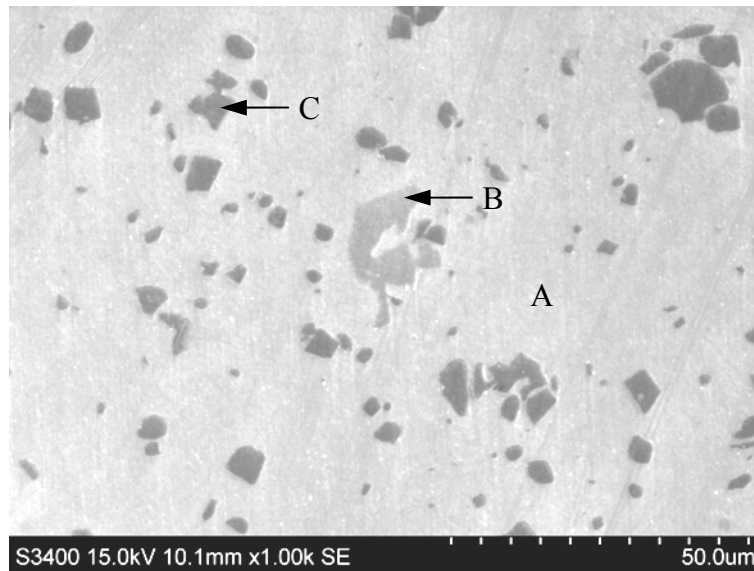


Figure 4.1 SEM micrograph of Bi-Ag-Cu solder wire.

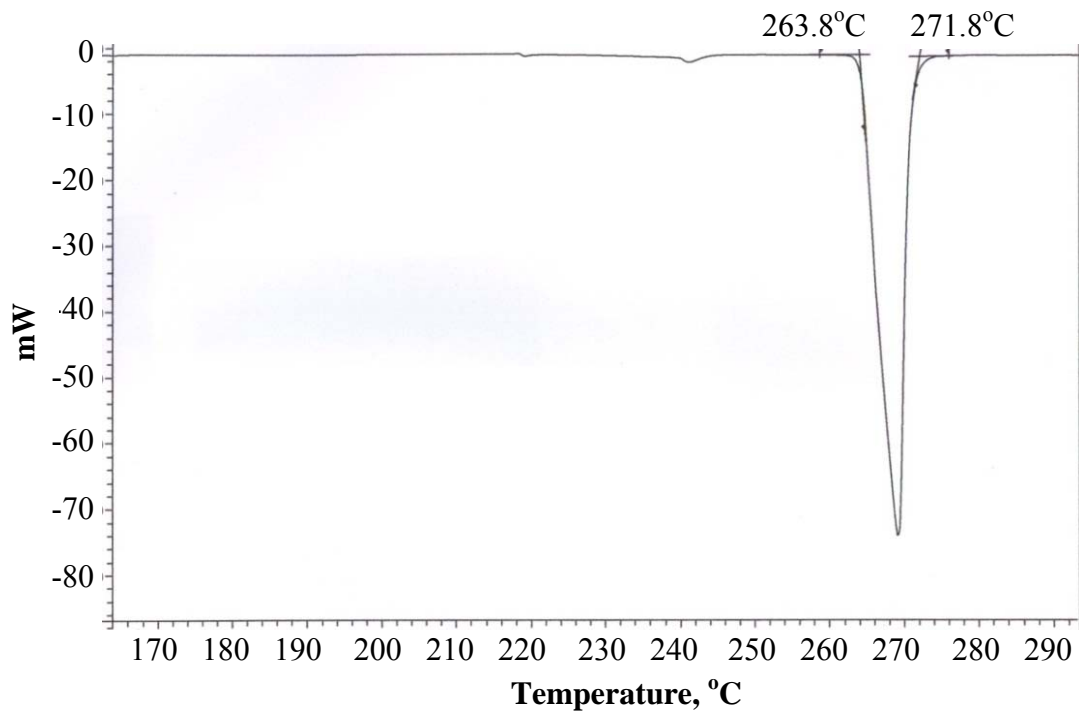


Figure 4.2 DSC curve of Bi-Ag-Cu solder wire.

The melting behavior of the solder wire was determined from heating curve obtained by DSC measurement at a heating rate of $10^{\circ}\text{C}/\text{min}$ which is shown in Figure 4.2. From this figure, one large endothermic pick is found where the alloy starts melting at 263.8°C and melting completed at 271.8°C .

4.2.1(b) Microstructure of die attach joint

Figure 4.3 shows SEM micrograph of Si die-solder-copper system for which die attach was performed with Bi-Ag-Cu solder at 350°C. The microstructure of the bulk solder consists of mainly three phases: one with a brighter contrast and the other two are medium gray and dark contrast phases under SEM. EDX analysis was carried out on

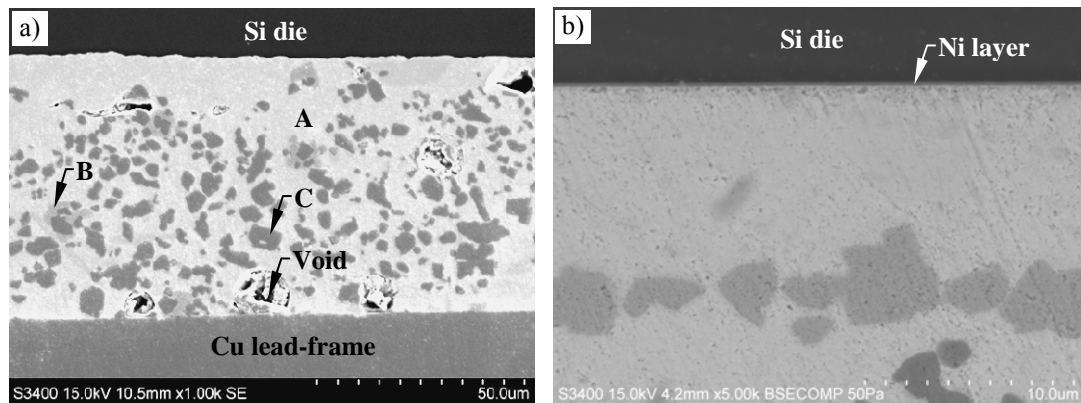


Figure 4.3 SEM micrograph of die attach sample with Bi-Ag-Cu solder at 350°C: a) cross-section of the joint; b) Si die/solder interface at higher magnification.

these points. The brighter contrast phases (point A) are 100 wt.% of Bi phase. The medium gray particles (point B) are Ag rich phase containing about 94.4 wt.% of Ag with 5.6 wt.% of Bi and the dark particles (point C) are 100 wt.% of Cu phase. It is observed from the EDX analysis that the chemical compositions of the phases present in the solder joint are almost same as the phases in solder wire. Therefore, it can be concluded that no diffusion was occurred in between solder and lead-frame during soldering process. At the Si die/solder interface (Figure 4.3b) with Ti/Ni/Ag metallization at the die back; IMC layer could not be detected by SEM at present magnification, however it has been reported that Ni react with Bi and forms NiBi and NiBi₃ IMCs (Lalena, et al., 2002; Song, et al., 2006). Very thin Ni layer could be one of the reasons for not detecting IMC layers by SEM at this magnification.

4.2.1(c) Wetting and void analysis of Bi-Ag-Cu soldered samples

Wetting of Bi-Ag-Cu solder on Cu lead-frame was analyzed by measuring contact angle which is shown in Figure 4.4. It is observed from the figure that contact angle is very large for both the die attach temperatures 350°C and 450°C. Result obtain from this test indicates limited wettability of the solder on Cu lead-frame. Such contact angle will initiate crack at the interface upon thermal cyclic loading. It is also observed that die area is not fully covered by the solder which also indicate limited spreading of solder on lead-frame. It is to be mentioned that extreme die attach temperature 450°C was selected only for checking the effect of temperature on wettability of the solder on Cu lead-frame though it is beyond the allowable temperature limit of Si die.

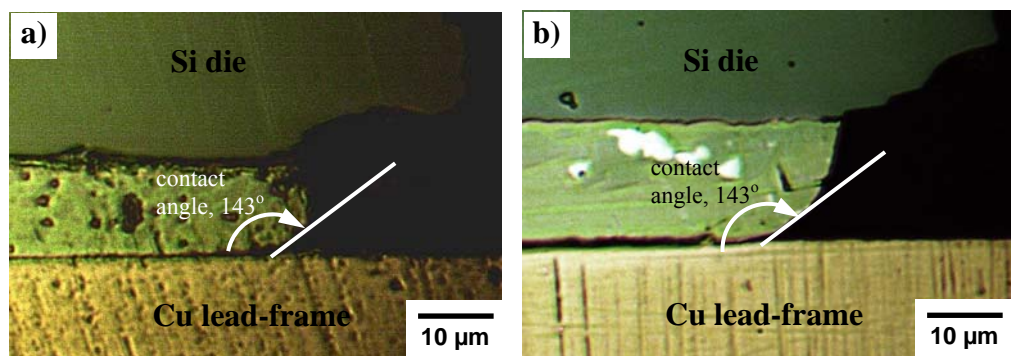


Figure 4.4 Contact angle of Bi-Ag-Cu solder on Cu lead-frame: a) at 350°C; b) at 450°C.

A lot of voids were observed in the cross-section of die attach samples (Figure 4.5). For checking consistency of the void condition, cross-sectional analysis was conducted on multiple samples. Series of voids were found in the bulk solder for each of the samples. Figure 4.5a, b, c are some of the optical images of a sample where die attach was performed at 350°C and 4.5d, e, f at 450°C. It is observed that die attach sample at 450°C exhibits smaller void as compared with that at 350°C.

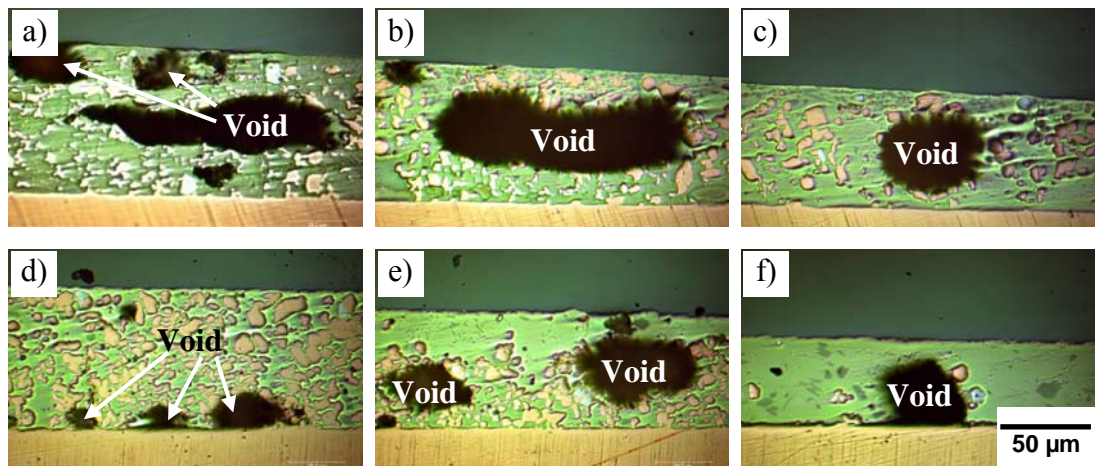


Figure 4.5 Voids in the die attach samples with Bi-Ag-Cu solder on Cu lead-frame: a), b) & c) at 350°C; and d), e) & f) at 450°C.

4.2.1(d) Summary

From the preliminary assessment results, it was found that Bi-Ag-Cu solder is not suitable for die attachment on bare Cu lead-frame due to poor wetting, less spreading and excessive voids. Fewer voids were found in the die attach samples at 450°C but there is no improvement of wetting and spreading on Cu lead-frame which is commonly used in electronic industries.

4.2.2 Bi-Ag-Cu-In solder

4.2.2(a) Microstructure and melting behavior of Bi-Ag-Cu-In solder wire

Figure 4.6 shows the cross-sectional SEM micrograph of the Bi-Ag-Cu-In solder wire. It consists of three phases. According to the EDX analysis, the brighter contrast phases (point A) are 100 wt.% of Bi, medium gray particles (point B) are Ag-rich phase containing an average of 87.3 wt.% of Ag and dark particles (point C) are 100 wt.% of Cu.

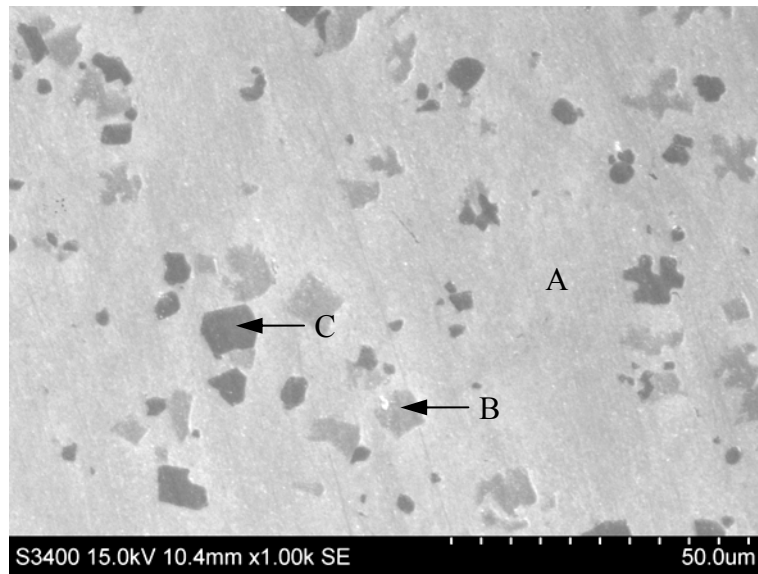


Figure 4.6 SEM image of Bi-Ag-Cu-In solder wire.

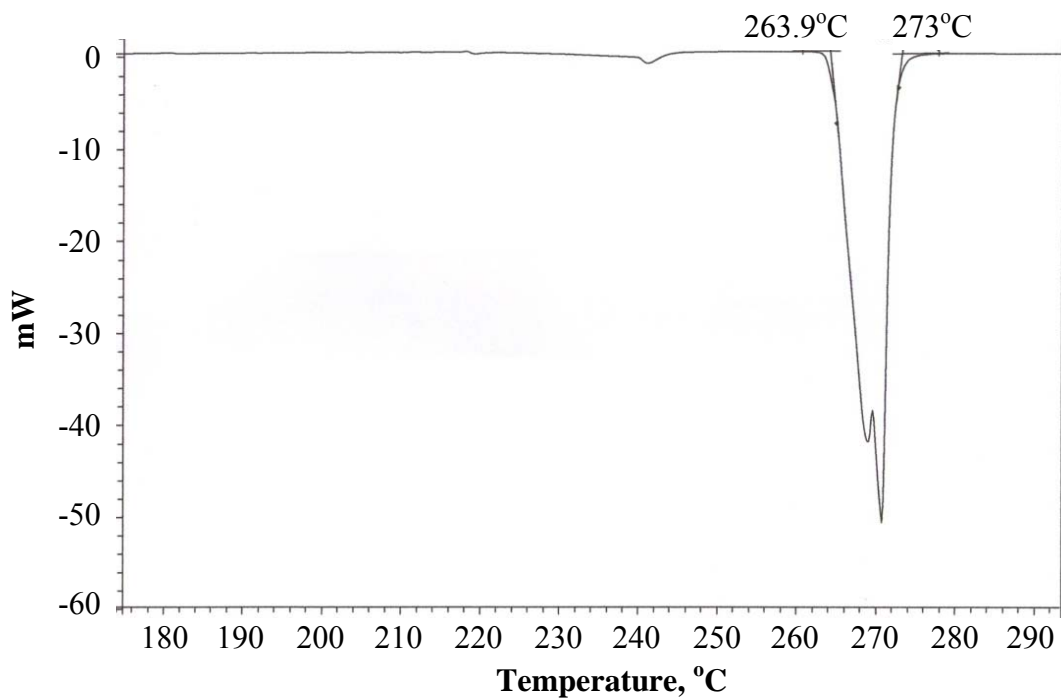


Figure 4.7 DSC curve of Bi-Ag-Cu-In solder wire.

The melting behavior of the solder wire was determined from heating curve obtained by DSC measurement at a heating rate of 10°C/min which is shown in Figure 4.7. From this figure, one large endothermic pick is found where the alloy starts melting at 263.9°C and melting completed at 273°C.

4.2.2(b) Microstructure of die attach joint

Figure 4.8 shows optical and SEM micrographs of a Si die-solder-copper system where die attach was performed with Bi-Ag-Cu-In solder at 350°C. Optical micrograph of the bulk solder (Figure 4.8a) shows four phases. Under optical microscope these phases

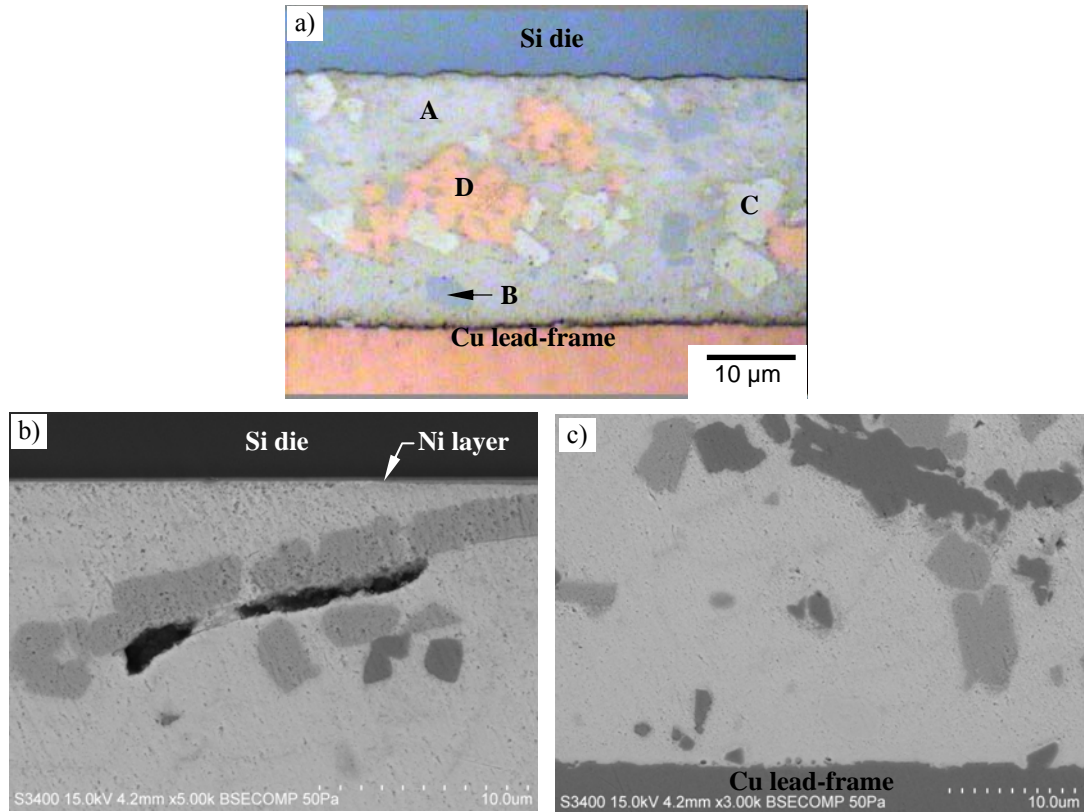


Figure 4.8 Optical and SEM micrographs of die attach sample with Bi-Ag-Cu-In solder at 350°C: a) optical micrograph of the cross-section; b) SEM micrograph of Si die/solder interface at higher magnification; c) SEM micrograph of lead-frame/solder interface at higher magnification.

appear light gray, sky blue, bright and orange. EDX analysis was carried out on the individual phases. The light gray phase (point A) is a Bi rich phase containing about 60.8 wt.% of Bi. The sky blue phase (point B) are also Bi rich phase containing about 59.7 wt.% of Bi. The bright phase (point C) are Ag rich phase containing about 57.8 wt.% of Ag and orange phase (point D) are Cu rich phase containing about 85.6 wt.% of Cu. Measured compositions of these phases are given in Table 4.1. From table it is found that sky blue phase contains Ni which comes from the die back metallization. At

the Si die/solder interface (Figure 4.8b) with Ti/Ni/Ag metallization at the die back; IMC layer could not be detected by SEM at present magnification, however it has been reported that Ni react with Bi and forms NiBi and NiBi₃ IMCs (Lalena, et al., 2002; Song, et al., 2006). At the lead-frame/solder interface (Figure 4.8c), no reaction layer was observed by SEM.

Table 4.1 EDX analysis results of the bulk microstructure of die attach sample using Bi-Ag-Cu-In solder.

Element	Point A	Point B	Point C	Point D
	Wt.%	Wt.%	Wt.%	Wt.%
Bi M	60.8	59.7	37.8	12.5
Ag L	1.7	1.7	57.8	1.9
Cu L	37.5	33.7	-	85.6
In L	-	-	4.4	-
Ni K	-	4.9	-	-

4.2.2(c) Wetting and void analysis of Bi-Ag-Cu-In soldered samples

Wetting of Bi-Ag-Cu-In solder on Cu lead-frame was analyzed by measuring contact angle which is shown in Figure 4.9. It is observed from the figure that contact angle is very large for both the die attach temperatures 350°C and 450°C. It indicates limited wettability of the alloy on Cu lead-frame (Figures 4.9a & b). Such contact angle will initiate crack at the interface upon thermal cyclic loading. Contact angle was found 80° at temperature 350°C when scrubbing force was applied on dispensed solder by Si die during die placement (Figure 4.9c). But the contact angle is still too large.

Void of the die attach samples was evaluated by cross-sectional technique. Cross-section was made only for the die attach samples at 350°C with and without scrubbing conditions. For checking consistency of the void condition, cross-sectional analysis was

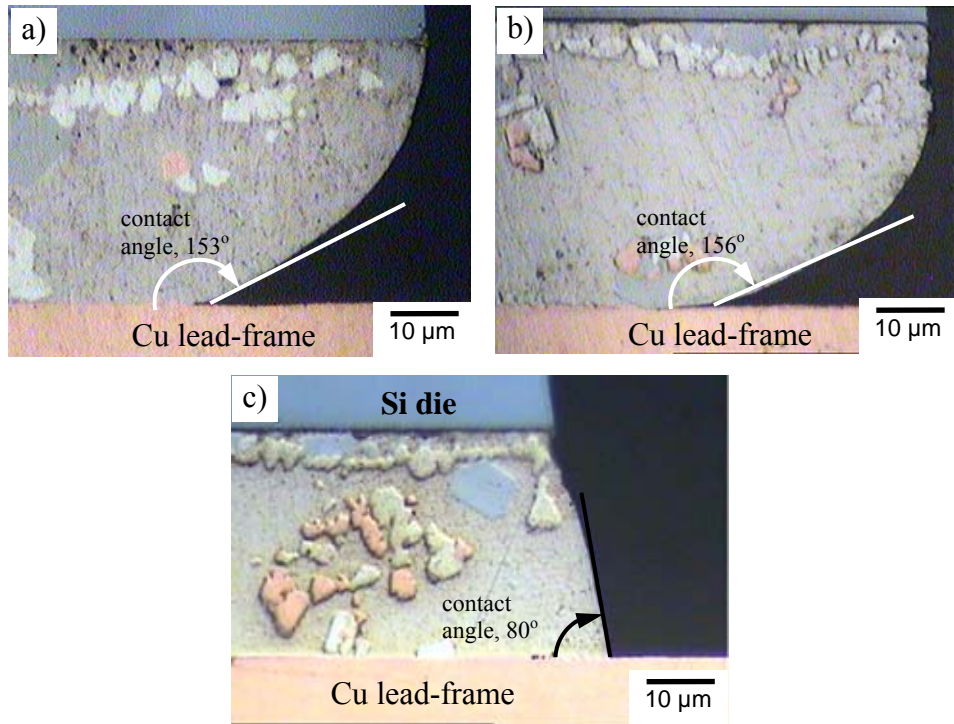


Figure 4.9 Contact angle of Bi-Ag-Cu-In solder on Cu lead-frame: a) at 350°C; b) at 450°C; and c) at 350°C with scrubbing.

conducted on multiple samples. Figure 4.10 a, b & c are some of the optical images of a sample where die attach was performed at 350°C without scrubbing and 4.10 d & e with scrubbing. From these figures, fewer voids are found for scrubbed samples as compared with that for without scrubbed samples. Thus, scrubbing action has significant impact on die attach void. On the other hand, solder splashing was observed in some die attach samples due to scrubbing action which is shown in Figure 4.11. There is a possibility of lead-frame as well as Si die contamination from splashed solder. Since wetting of Bi-Ag-Cu-In solder on Cu lead-frame is poor, there is a possibility of unwetted area on lead-frame. During die placement, trapping of air occurred at the unwetted lead-frame area which is one of the reasons for solder joint void (Singer, et al., 2003). This trapped air escaped from the solder joint while scrubbing force is applied by Si die. For the same reason, solder splashing was observed in the scrubbed samples.

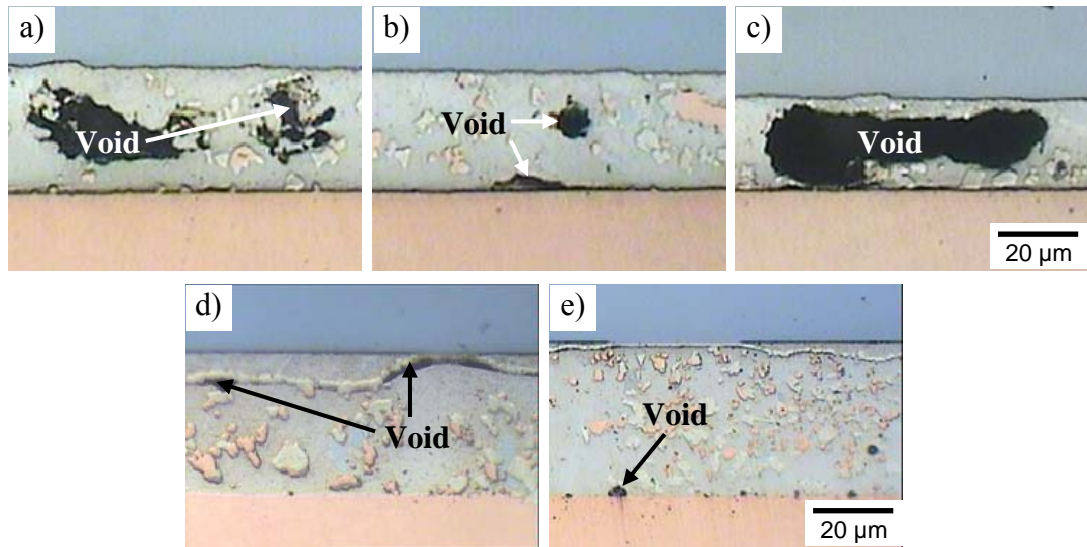


Figure 4.10 Voids in the die attach samples with Bi-Ag-Cu-In solder on Cu lead-frame at 350°C: a), b) & c) without scrubbing; and d) & e) with scrubbing.

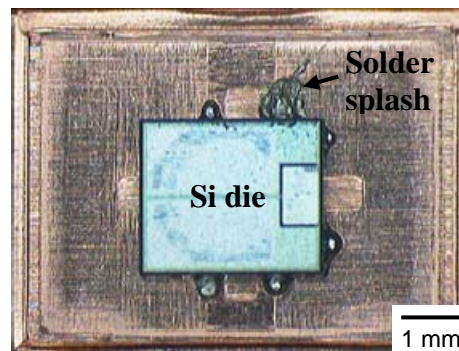


Figure 4.11 Optical image of the die attach sample with Bi-Ag-Cu-In solder on Cu lead-frame at 350°C with scrubbing.

4.2.2(d) Observation during wire bonding operation

Before wire bonding operation, die attachment was performed on Cu lead-frame in automatic die attach machine at 350°C. Wire bonding operation was conducted in automatic bonding machine with Cu wire. After wire bonding operation, it was observed that dies were shifted from its original place. Wire bonding with Cu wire is normally performed at higher temperature and pressure compared with Au and Al wire bond. In this experiment, wire bonding was performed at temperature 290°C with bond force of 2.16 N. Since wetting of Bi-Ag-Cu-In solder on Cu lead-frame was limited and lots of voids were found in the die attach joint, therefore it is expected that the bonding

strength of this solder with lead-frame was poor. For that reason, joint failure occurred due to apply of bond force as well as increase of temperature during wire bonding process. As a consequence, wire bonding operation was not successful with Bi-Ag-Cu-In solder.

4.2.2(e) Summary

The above results shows that Bi-Ag-Cu-In solder is not suitable for die attach on bare Cu lead-frame due to poor wetting and voids conditions. Scrubbing action slightly improves the wetting on Cu lead-frame and also reduces void in the solder joint. On the other hand, solder splashing was observed which can contaminate the lead-frame as well as Si die. So scrubbing is not the solution for increasing wetting on lead-frame and reduction of void in the solder joint. Moreover, melting temperature of this alloy is low (about 270°C) as compare to standard Pb-5Sn solder. For that reason, wire bonding operation with Cu wire was not successful. Based on above analysis it is concluded that the present Bi-Ag-Cu-In solder alloy is not well-suited as a high-temperature Pb-free solder for Si die attachment under the present experimental conditions.

4.3 Die Attachment Using Zn-Al-Based Alloys

In this study, two Zn-Al-based alloys were selected as a high-temperature lead-free die attach materials. These were Zn-Al-Ge and Zn-Al-Mg-Ga. These alloys were used in wire form.

4.3.1 Zn-Al-Ge solder

4.3.1(a) Microstructure and melting behavior of Zn-Al-Ge solder wire

Figure 4.12 shows the cross-sectional microstructure of the Zn-Al-Ge solder wire. It consist of primary hexagonal close-packed (hcp) Zn, Zn-rich face centered cubic (fcc)

and Ge rich phases (Takaku, et al., 2008). According to the EDX analysis, the bright grains represents the hcp (Zn) (94.2 wt.% Zn) and the dark particles with a complex microstructure represent the Zn-rich fcc phase (71.9 wt.% Zn), which was decomposed into Al-rich fcc + hcp (Zn) by the monotectoid reaction during cooling (Okamoto, 1995). Medium gray particles are Ge rich phase containing 61.1 mass% Ge.

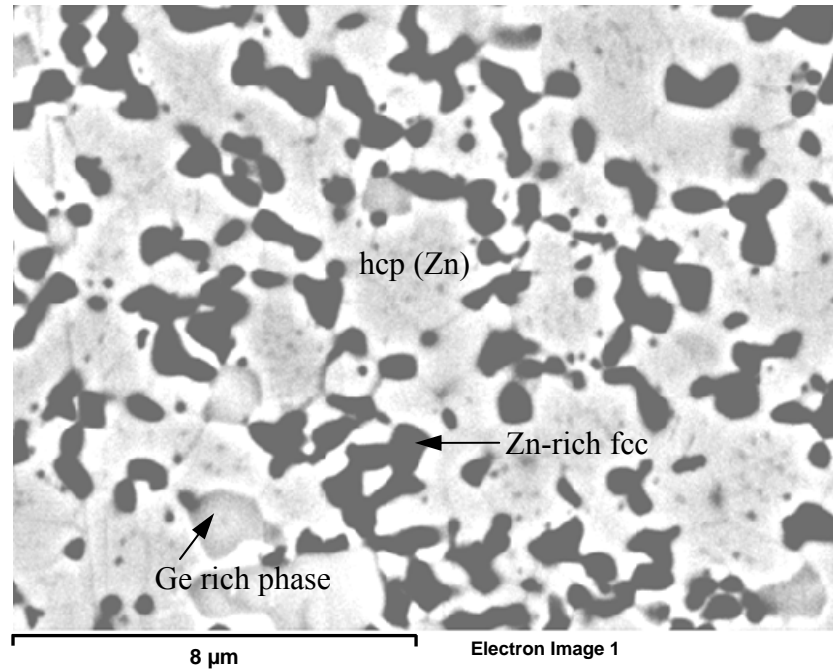


Figure 4.12 SEM image of Zn-Al-Ge solder wire.

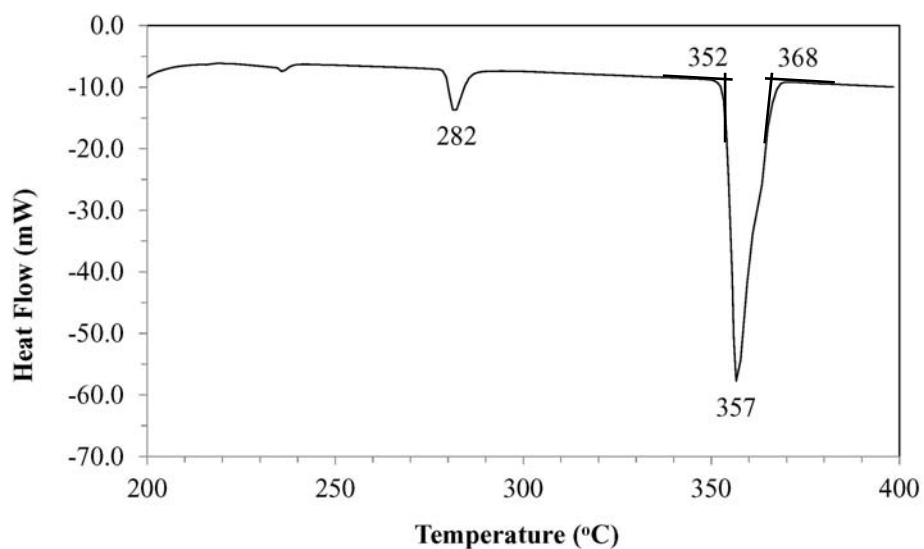


Figure 4.13 DSC curve of Zn-Al-Ge solder wire.

DSC analysis was performed for measuring the melting temperature of the solder wire. Figure 4.13 shows the DSC heating curve of Zn-Al-Ge solder wire. There are two endothermic peaks in the DSC heating curve; one is at 282°C and the other one is at 357°C. At the first endothermic peak, monotectoid reaction occurred where Al-rich face centered cubic (fcc) and hexagonal close-packed (hcp) (Zn) converted to

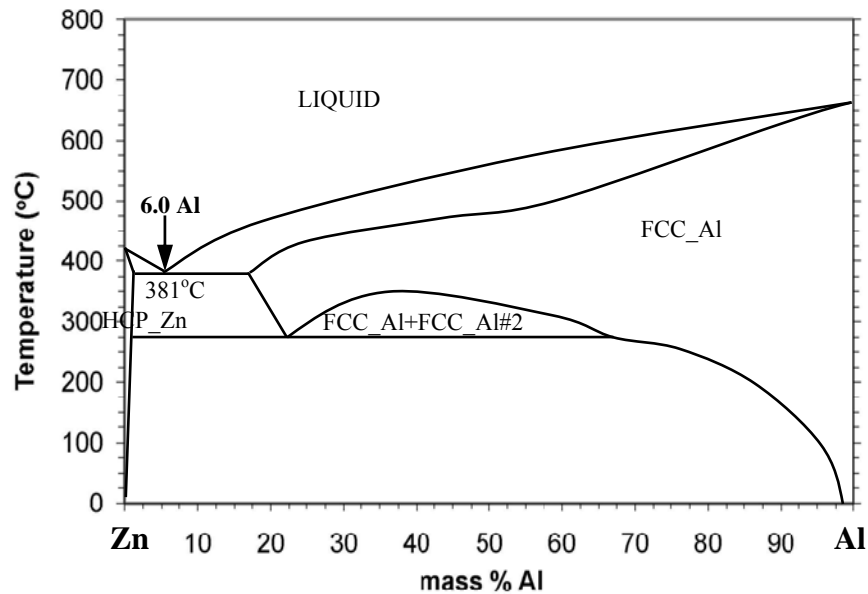


Figure 4.14 Zn-Al binary phase diagram. (Okamoto, 1995).

Al-rich fcc (Okamoto, 1995). In the second large endothermic peak, eutectic melting reaction occurred where Al-rich fcc and hcp (Zn) becomes liquid in this stage. Though the eutectic melting temperature of Zn-Al binary system is 381°C (Figure 4.14), it is found lower due to the addition of Ge in this alloy. Solidus and liquidus temperature of this solder was found 352 °C and 368°C respectively.

4.3.1(b) Microstructural characterization of Zn-Al-Ge solder on Cu lead-frame

Figure 4.15 shows SEM images of typical bulk and interfacial microstructure of a Si die-solder-copper system where die attach was performed at 390°C. Zn-Al-Ge solder wetted well and IMC layers are clearly observed at the Cu lead-frame/solder interface. The microstructure of the bulk solder consists of mainly two phases: one with a brighter

contrast and the other one being a mixture of light and dark phases. EDX analysis was carried out on these points. The phase with brighter contrast (point A) is a zinc rich phase containing about 85.3 wt.% Zn. The mixture (point B) contains a higher percentage of zinc phase about 65.4 wt.% Zn. In addition, some small particles with brighter appearance (point C) are observed at different places in the bulk solder (Figure 4.15b). Details of these particles are discussed later. EDX analysis results of the bulk solder are presented in Table 4.2. From this Figure 4.15b, it is clearly observed that the mixture phase is a combination of fine layers of bright and dark phases. It indicates that after die bond operation, solidification process ends through eutectic reaction.

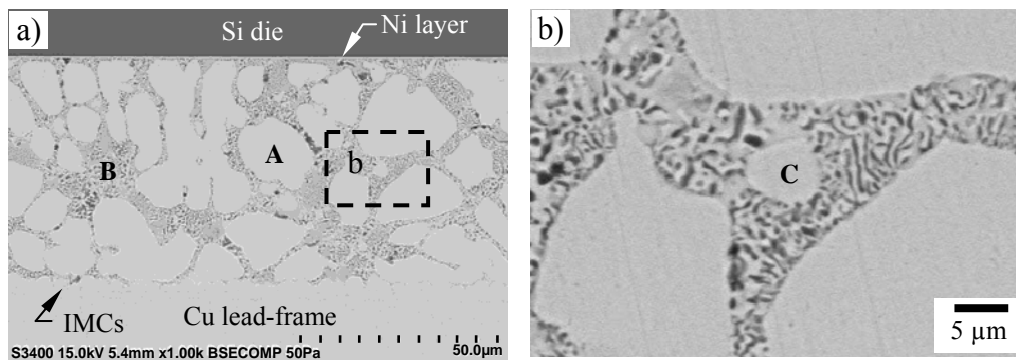


Figure 4.15 SEM images of die attach sample at 390°C with Zn-Al-Ge solder on Cu lead-frame: a) cross-section of the solder joint; b) SEM image at higher magnification.

Table 4.2 EDX analysis results of the bulk microstructure of die attach sample using Zn-Al-Ge solder.

Element	Point A	Point B	Point C
	Wt.%	Wt.%	Wt.%
Zn L	85.3	65.4	80.1
Al K	2.8	22	-
Ge L	0.9	3.7	-
Cu L	11	8.9	19.9

Figure 4.16 shows the interfacial reactions between Si die/solder and lead-frame/solder interfaces of the die attach sample at 390°C on bare Cu lead-frame. From Figure 4.16a, Ti and Ni layer is found intact and another thin layer is observed just below the Ni layer. EDX analysis was carried out on this layer. According to EDX analysis, it contains 57.5 at.% of Al and 42.5 at.% of Ni which is close to the composition of Al_3Ni_2 IMC. It comply with other researcher work that Ni react with Al and forms Al_3Ni_2 IMC (Takaku et al., 2009). Figure 4.16b shows the interfacial reactions between

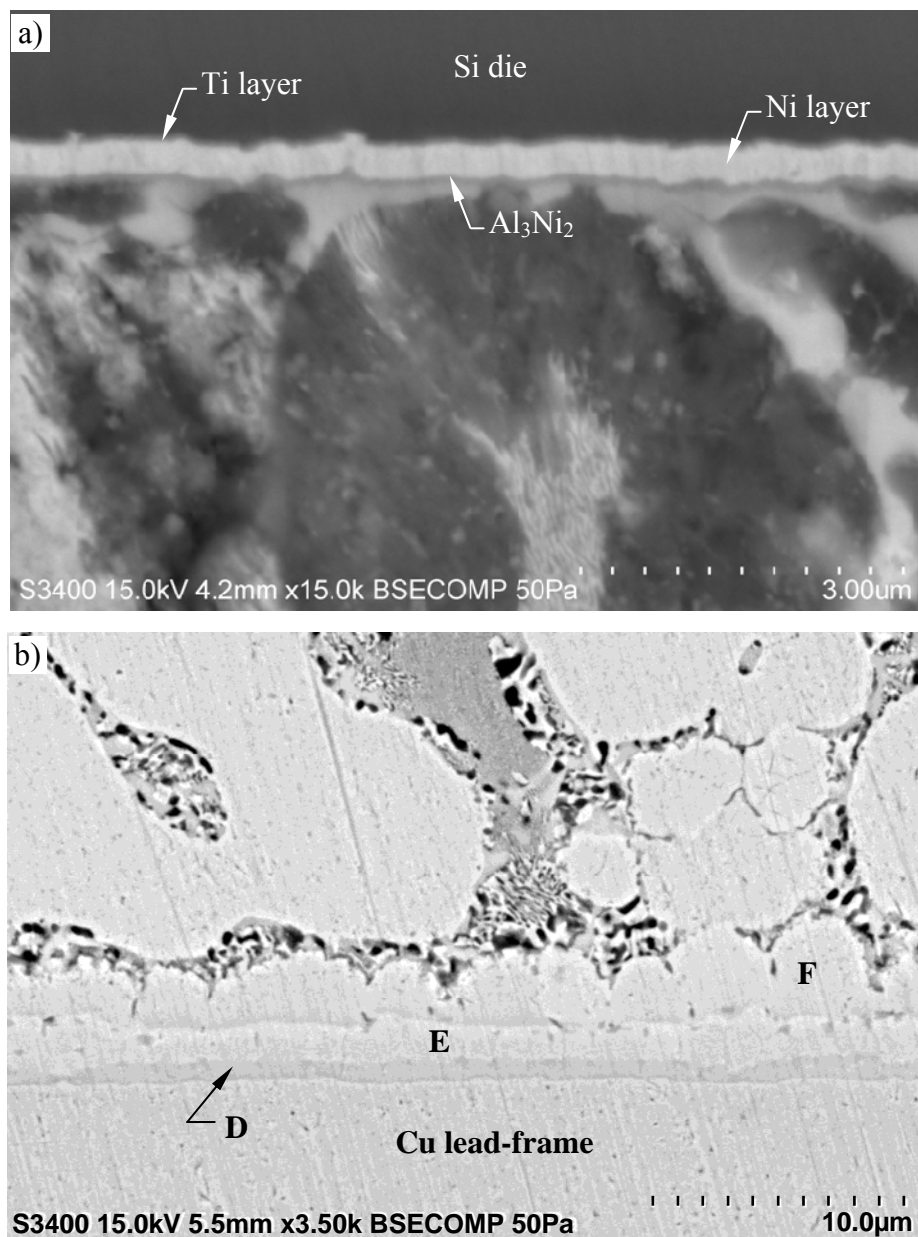


Figure 4.16 Interfacial reactions of the die attach sample on Cu lead-frame at 390°C with Zn-Al-Ge solder at: a) Si die/solder interface; b) lead-frame/solder interface.

lead-frame/solder interfaces. From this figure it is evident that there are three distinct IMC layers. EDX analysis was performed to determine the chemical composition of these IMC layers. The measured compositions of these IMC layers are given in Table 4.3. From this table, it is found that the composition of the layer D, E and F is close to CuZn, Cu₅Zn₈ and CuZn₄ IMC respectively. Formation of such IMCs at the interface between Cu lead-frame and Zn-Al solder has been reported in different literatures (Takaku, et al., 2008). Therefore, it is confirmed that the thin layer (D) is β'-CuZn forms close to copper lead-frame, scallop shaped layer (F) is ε-CuZn₄ forms at the solder side and while γ-Cu₅Zn₈ layer (E) forms at the middle. The thickness of IMC layers varies depending on die attach temperature. Higher die attach temperature corresponds to greater IMCs thickness. The average thickness of thin β'-CuZn layer varies from about 0.5 to 0.84 μm, γ-Cu₅Zn₈ layer from about 1.1 to 1.7 μm and ε-CuZn₄ layer from about 2.2 to 3.4 μm depending on temperature at which die attachment was performed.

Table 4.3 EDX analysis results of IMC layers at lead-frame/solder interface using Zn-Al-Ge solder on bare Cu lead-frame.

Element	β'-CuZn (D)	γ-Cu ₅ Zn ₈ (E)	ε-CuZn ₄ (F)
	At.%	At.%	At.%
Zn L	48.1	61.8	76.6
Cu L	51.9	38.2	23.4

The small size brighter particles (point C) that was observed at different places (C in Figure 4.15b) in the bulk solder are rich in zinc and their composition (20.3 at.% Cu and 79.7 at.% Zn) closely resembles that of scallop type CuZn₄ IMC which forms at the solder side of the lead-frame/solder interface. The shape and size of these particles are similar to that of CuZn₄ scallop. It is therefore suggested that these particles are CuZn₄ IMC which have been spalled from the interface during soldering.

Figure 4.17 presents the EPMA elemental mapping of the die attach sample at 370°C. It is seen from the mapping that Zn and Cu exist at the same locations. On the other hand, Ge coexists with Al. The binary phase diagrams shows that the eutectic melting temperatures for the systems Al-Ge and Ge-Zn (Figure 4.18 & 4.19) are 416°C and 402°C respectively. Ge content at the eutectic point of Al-Ge binary system is about 28 wt.% which is higher than the Ge content of Ge-Zn binary system (5 wt.%). Since eutectic melting temperature as well as concentration of Ge in Al-Ge binary system is higher than that in the Ge-Zn binary system, it is expected that during solidification, the Al-Ge binary eutectic with higher Ge contents forms before Ge-Zn eutectic. This explains why Al and Ge coexists.

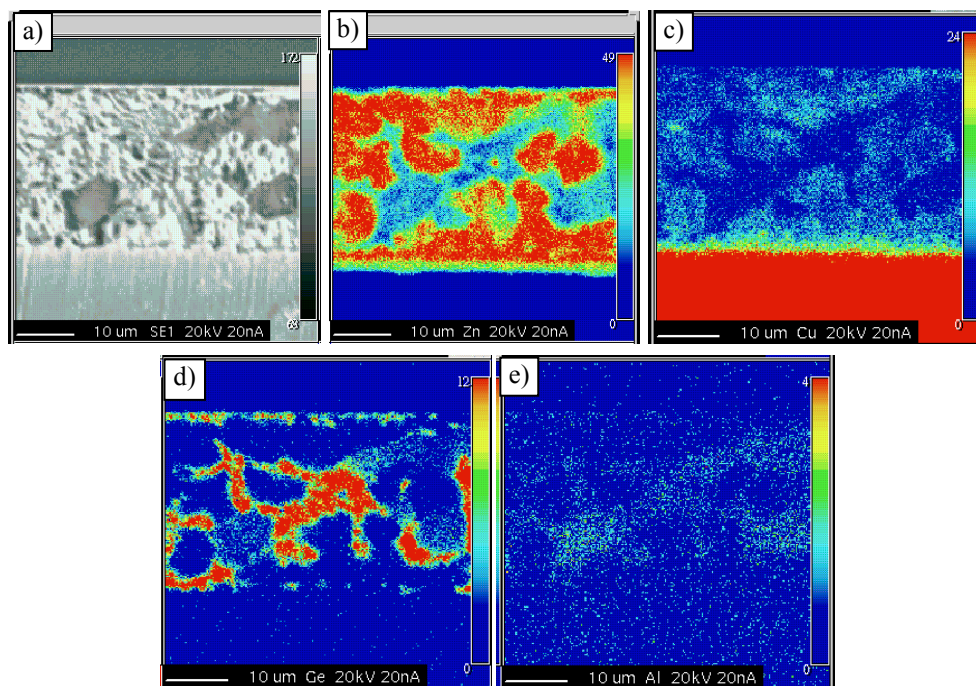


Figure 4.17 EPMA elemental mapping of the solder joint at 370°C with Zn-Al-Ge solder: (a) SEM image of the mapping region; and element maps of (b) Zn; (c) Cu; (d) Ge; and (e) Al.

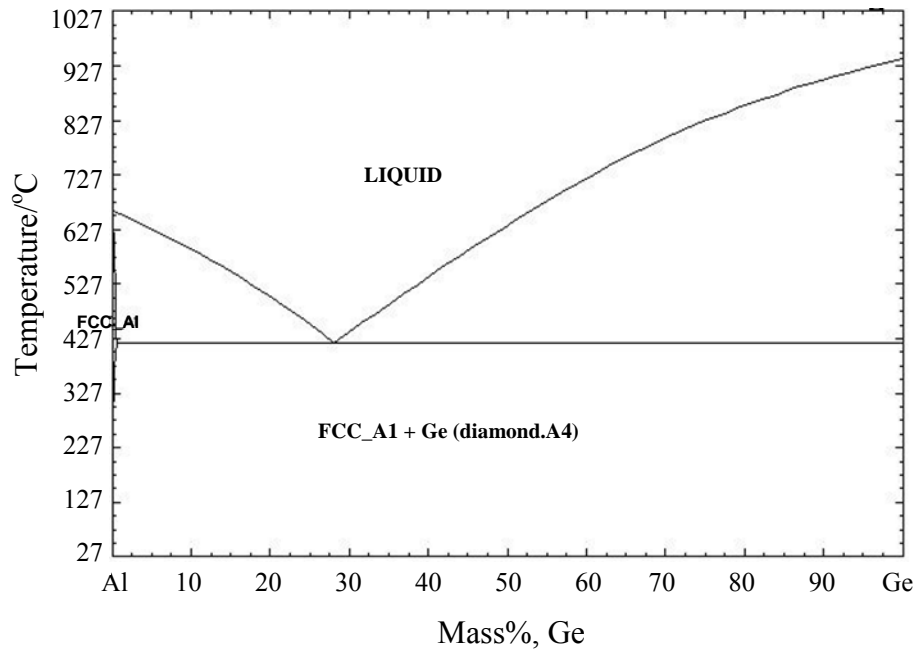


Figure 4.18 AL-Ge binary phase diagram.
(SGTE Alloy Phase Diagrams, 2004)

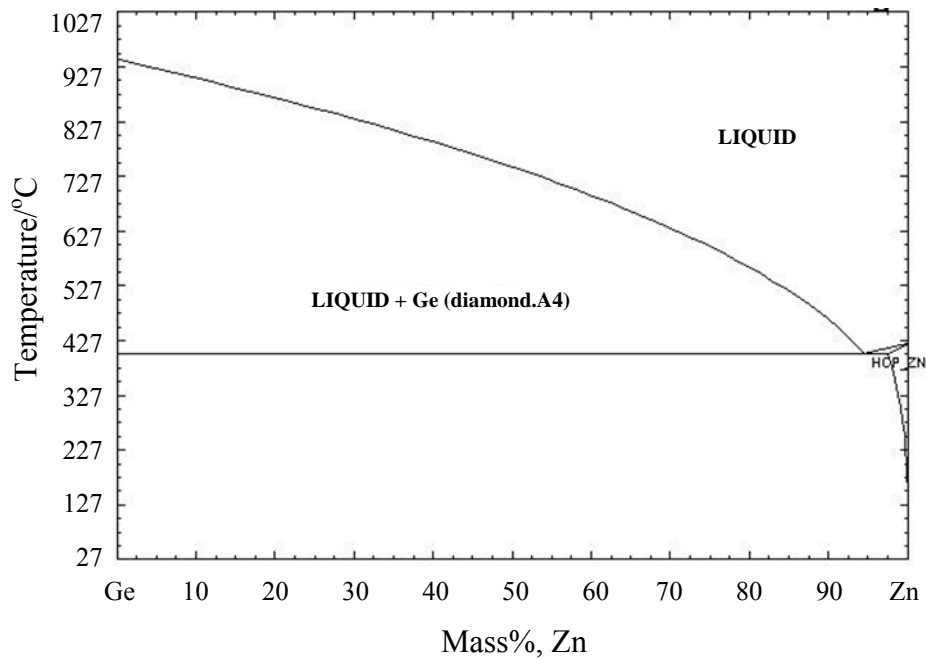


Figure 4.19 Ge-Zn binary phase diagram.
(SGTE Alloy Phase Diagrams, 2004)

4.3.1(c) Wetting and void analysis of Zn-Al-Ge soldered samples

Voids under Si die attach joint was analyzed by back scanning method using SAM. From each set of die attach samples, 20 samples were scanned for void analysis. Based on void conditions, the best and average back scanning images for each set of die attach

samples are shown in Figure 4.20. In these images, the darker rectangular area is Si die and the outer approximately circular area is wetting area of the solder. The white spots within the dark rectangular die area represents void. In some industrial practice, the maximum void rate allowed for high power applications is 5% for single void and 10% for cumulative void. Cumulative void area was measured manually for each of the die attach samples using a mesh of 10 x 10 which was superimposed on die area of the SAM image. Figure 4.21 shows the cumulative void analysis result. From this figure, it is evident that less voids were found for the die attach joint at temperature 380°C compared with that at 370 and 390°C. It is expected that low wetting at 370°C and oxidation at 390°C are the possible reasons for more voids in the die attach joints. It is to be mentioned that out of 20 samples, 15% samples were found more than 10% void for die attach joint at temperature 380°C. On the other hand, 40% and 30% samples were found more than 10% void for die attach joint at temperatures 370 and 390°C respectively. Such happened for the inconsistency of solder wetting on lead-frame for the corresponding die attach temperature. Standard deviation of the void analysis was also lower for the die attach temperature of 380°C (3.8) as compared with 370-390°C (4.7-5.1). Die attach samples with standard Pb-5Sn solder have almost no voids.

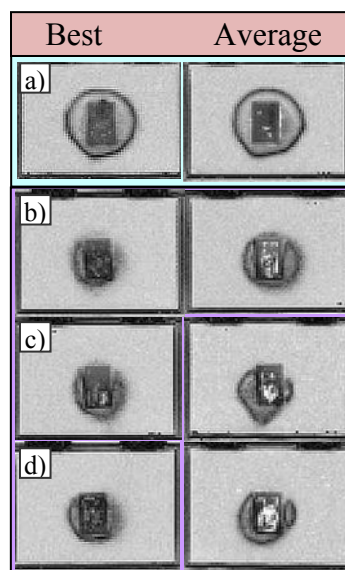


Figure 4.20 Back scan SAM images of die attach samples: a) Standard Pb-5Sn solder wire was used, and Zn-Al-Ge solder wire was used at b) 370°C, c) 380°C, & d) 390°C.

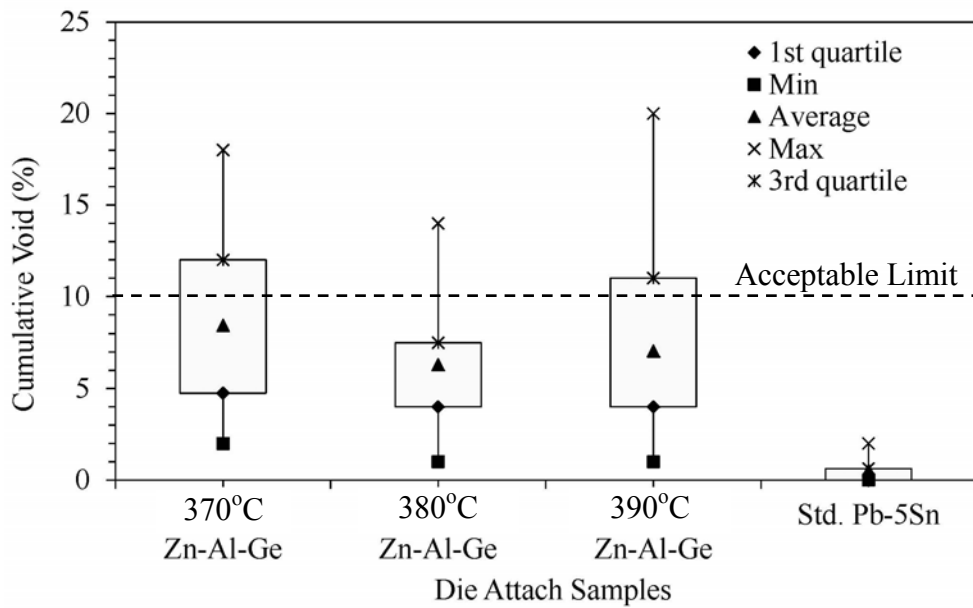


Figure 4.21 Cumulative void % of die attach samples calculated from back scanning images.

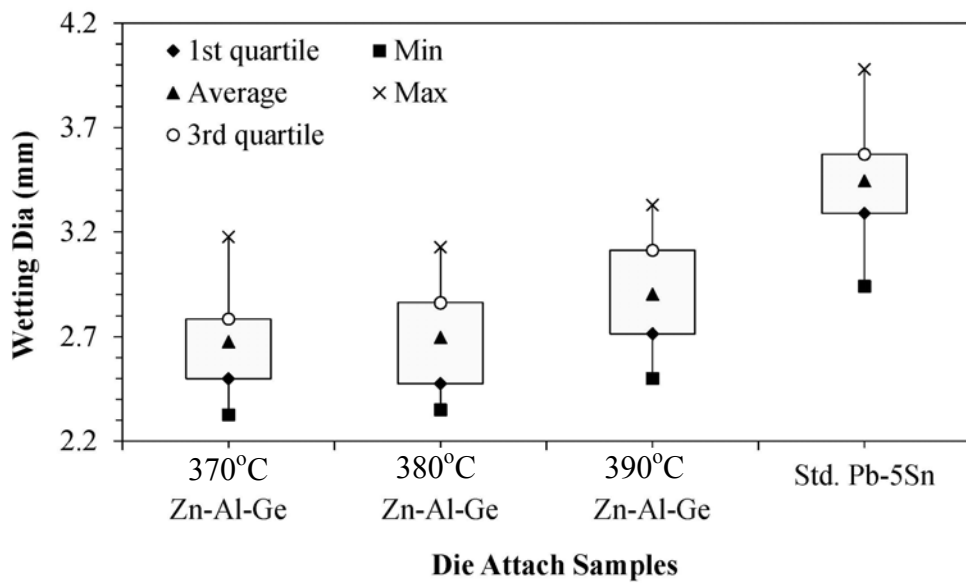


Figure 4.22 Comparison of wetting diameter of Zn-Al-Ge soldered samples with standard Pb-5Sn soldered samples.

Wetting of Zn-Al-Ge solder on Cu lead-frame was analyzed by measuring the wetting diameter of Zn-Al-Ge soldered samples and compared with the standard Pb-5Sn soldered sample which is shown in Figure 4.22. In general, the larger the wetting area the better the wetting. It is to be mentioned that same amount of solder was dispensed

for each of the die attach conditions. 20 samples were taken for measuring wetting diameter. From this figure, it is found that the average wetting diameter of Zn-Al-Ge soldered samples increases with the increase of die attach temperature. It is also found that the average wetting diameter of standard Pb-5Sn soldered samples is higher as compared with that of Zn-Al-Ge soldered samples.

4.3.1(d) Die shear strength of Zn-Al-Ge soldered samples

Die shear strength of Zn-Al-Ge soldered samples at different die attach temperatures was measured and compared with that of standard Pb-5Sn soldered samples (Figure 4.23). It is found that the average die shear strength is higher at the die attach temperature of 390°C (22.3 MPa) as compared with those obtained for 370-380°C (15.5-17.4 MPa). Average die shear strength of standard Pb-5Sn soldered samples

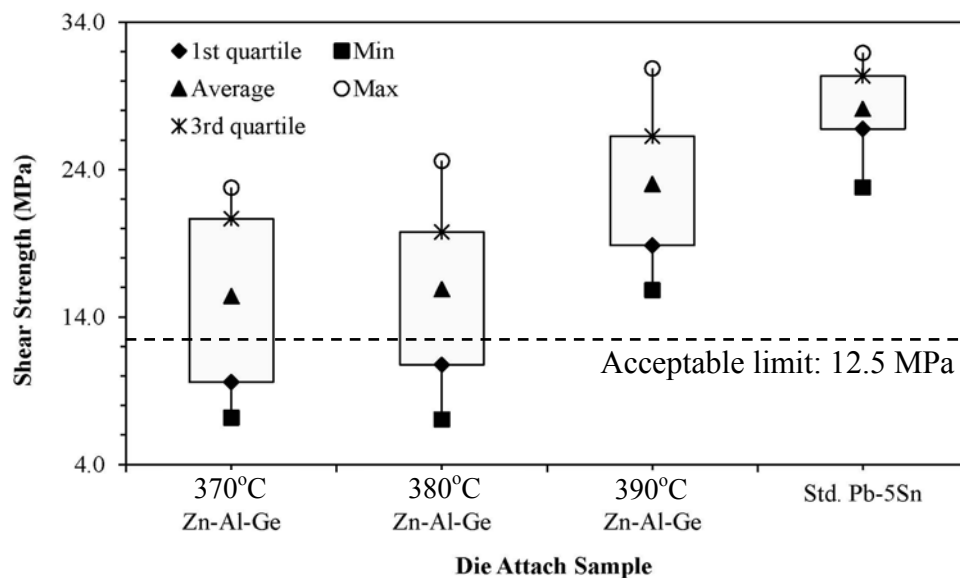


Figure 4.23 Comparison of die shear strength of Zn-Al-Ge soldered samples at different die attach temperatures with standard Pb-5Sn soldered samples.

was found 28.2 MPa. Die shear strength depends on the strength of solder material, wetting on lead-frame and bonding strength of Si die/solder interface. Since Zn-Al-Ge solder is strong enough and wetting diameter increases with the increase of die attach

temperature, therefore it is expected that the die shear strength is increased with die attach temperature. It is also found that the shear strength data points at the die attach temperature of 390°C are above the industry acceptable limit. It is to be noted that the acceptable limit of the die shear strength depends on the size of the Si die. According to the ON Semiconductor standard, the acceptable limit for this die is considered as 12.5 MPa.

The failure mode of Zn-Al-Ge soldered samples was found different from that of the standard Pb-5Sn soldered samples which are shown in Figure 4.24. For Zn-Al-Ge soldered samples, shear occurred by cracking of Si die regardless of the die attach temperature. Figure 4.24a shows the sheared surface of the Zn-Al-Ge soldered sample

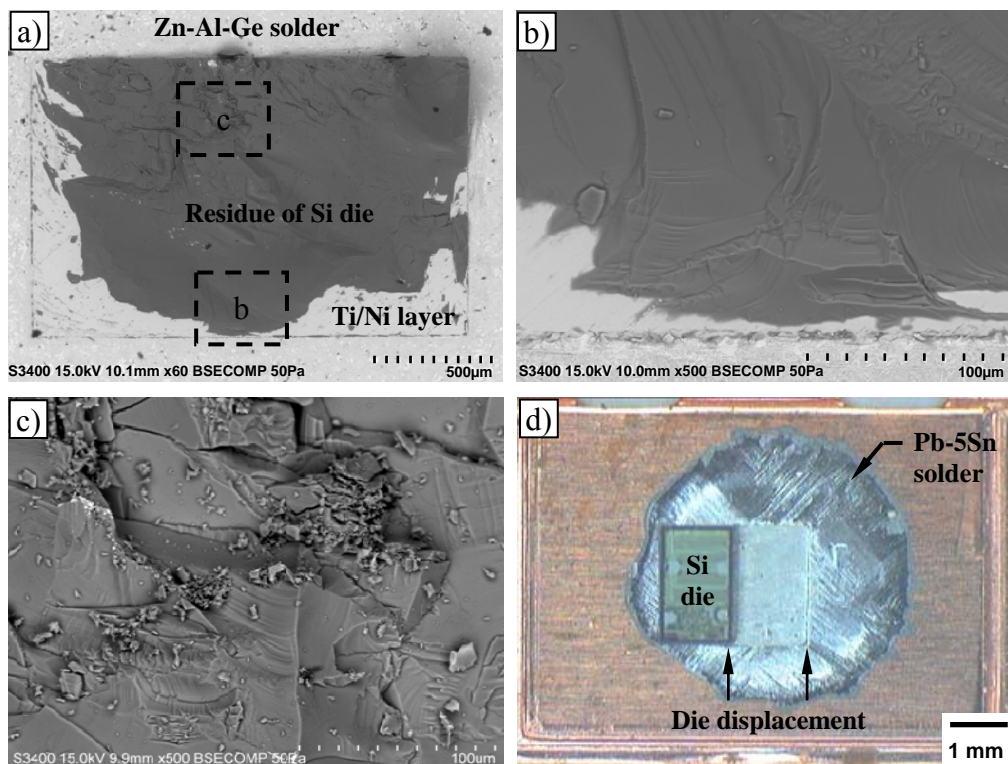


Figure 4.24 SEM/Optical images of the die sheared surface: a) Zn-Al-Ge soldered sample at 380°C; b) & c) SEM image at higher magnification; d) standard Pb-5Sn soldered sample.

at 380°C. From this figure, two shades are observed within the rectangular die area: one with brighter appearance and the other one being darker. For confirmation of these shades, EDX element mapping was performed which is described later. Figure 24b & c are magnified image of the fractured die surface. For standard Pb-5Sn soldered samples, die shear occurred at bulk solder (Figure 4.24d). Since Zn-Al-Ge solder is strong compare to standard Pb-5Sn solder and it forms IMCs at Si die/solder and lead-frame/solder interfaces, therefore failure of Zn-Al-Ge soldered samples on bare Cu lead-frame was occurred by cracking of Si die. On the other hand, standard Pb-5Sn solder is ductile and has strong interfacial bonding with Si die and lead-frame. Therefore, shear failure of standard Pb-5Sn soldered samples occurred at the bulk solder.

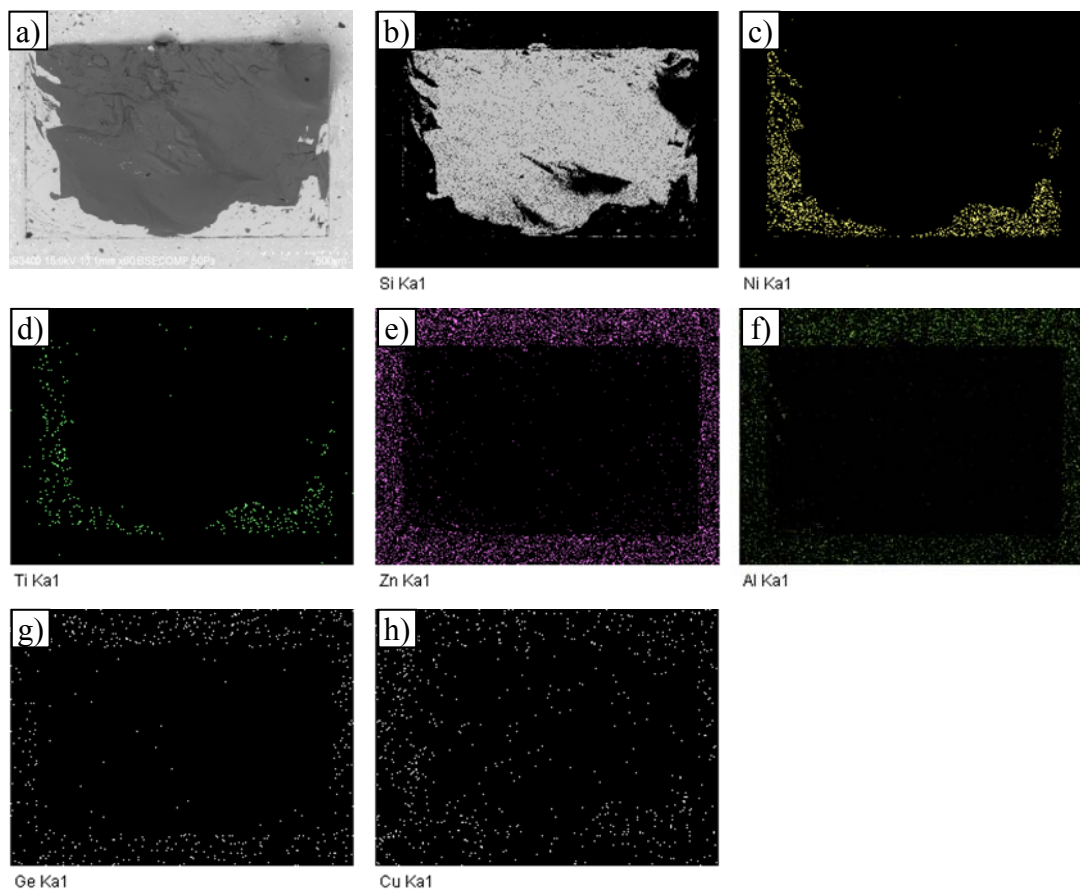


Figure 4.25 EDX elemental mapping of the sheared surface of the soldered sample with Zn-Al-Ge solder: (a) SEM image of the mapping region; and element maps of (b) Si; (c) Ni; (d) Ti; (e) Zn; (f) Al; (g) Ge; and (h) Cu.

Figure 4.25 shows the EDX element mapping of the sheared surface of the die attach sample with Zn-Al-Ge on bare Cu lead-frame. From this mapping, it is found that within the rectangular die area, the dark shaded surface contains Si and bright shaded surface contains Ni and Ti. No other elements are detected within the rectangular die area. Zn, Al and Ge found outside the rectangular die area. From this element mapping analysis, it can be concluded that die shear initiated just above the Ti/Ni layer at the die back and ends by cracking of entire Si die. Shear failure mechanism of Zn-Al-Ge soldered samples is drawn which is shown in Figure 4.26.

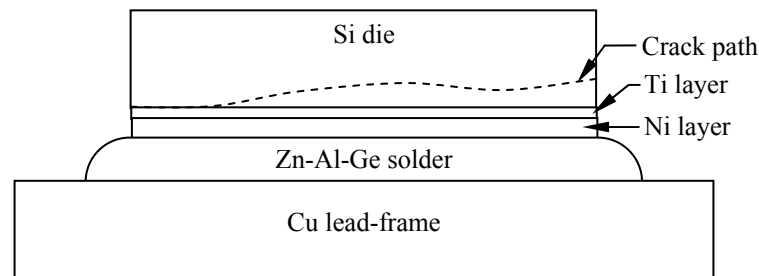


Figure 4.26 Failure mechanism of Zn-Al-Ge soldered samples during die shear.

4.3.1(e) Summary

From the preliminary assessment results of Zn-Al-Ge solder, wetting was found better at 390°C but, it was not as good as in a standard Pb-5Sn solder. Cumulative void was found to be more than 10% for all die attach samples using Zn-Al-Ge solder. But comparatively fewer voids were found in the samples at 380°C. Die shear strength was found within acceptable limit only for die attach samples at 390°C. Based on above analysis it is concluded that the present Zn-Al-Ge solder alloy is not well-suited as a high-temperature Pb-free solder for Si die attachment under the present experimental conditions.

4.3.2 Zn-Al-Mg-Ga solder

4.3.2(a) Introduction

Performance evaluation of Zn-Al-Mg-Ga solder as an alternative to high-Pb solder as a die attach material was conducted in three different sets of experiments. First set of experiment was designed to evaluate the die attach performance Zn-Al-Mg-Ga solder on bare Cu lead-frame at different die attach temperatures. Effect of Ag thickness at the die back metallization on interfacial reaction was also investigated in this experiment. In second set of experiment, comparative study of Si die attachment with Zn-Al-Mg-Ga solder on bare and Ni metallized Cu lead-frame were conducted. For both experiments, interfacial reactions at Si die/solder and lead-frame/solder interfaces, bulk microstructures, and die attach properties such as wetting, voids and die shear strength were investigated. Die attach properties were also compared with the standard Pb-5Sn soldered samples. In third set of experiment, reliability tests of Zn-Al-Mg-Ga soldered samples were performed at accelerated condition. Reliability tests include AC, TC, HTOL and HTSL.

4.3.2(b) Microstructure and melting behavior of Zn-Al-Mg-Ga solder wire

Figure 4.27 shows the SEM microstructure of the Zn-Al-Mg-Ga solder wire. It consist of primary hexagonal close-packed (hcp) Zn, Zn-rich face centered cubic (fcc) and Mg_2Zn_{11} IMC (Takaku, et al., 2008). According to the EDX analysis, the bright grains represents the hcp (Zn) (97.5 wt.% Zn) and the dark particles with a complex microstructure represent the Zn-rich fcc phase (85.2 wt.% Zn), which was decomposed into Al-rich fcc + hcp (Zn) by the monotectoid reaction during cooling (Okamoto, 1995). Light gray particles are Mg_2Zn_{11} . Based on EDX analysis, the composition of Mg_2Zn_{11} is 13.7 at.% of Mg and 86.3 at.% of Zn.

DSC analysis was performed for measuring the melting temperature of the solder wire. Figure 4.28 represents the DSC heating curve of Zn-Al-Mg-Ga solder wire. Three distinct endothermic peaks were observed at temperature 260.4, 339.2 and 365.4°C. Among these peaks, monotectoid reaction was occurred at the first peak where Al-rich face centered cubic (fcc) and hexagonal close-packed (hcp) (Zn) converted to Al-rich fcc (Okamoto, 1995). At the second peak, eutectic melting reaction was occurred at which Al-rich fcc & hcp (Zn) converted to liquid in this stage. At the third peak, Mg_2Zn_{11} IMC converted to liquid phase (SGTE Alloy Phase Diagrams, 2004). In Zn-Al binary system, monotectoid and eutectic melting reactions occur at temperature 282 and 381°C respectively (Figure 4.14). Due to addition of Mg and Ga in this alloy, these reactions take place at lower temperature than the Zn-Al binary system.

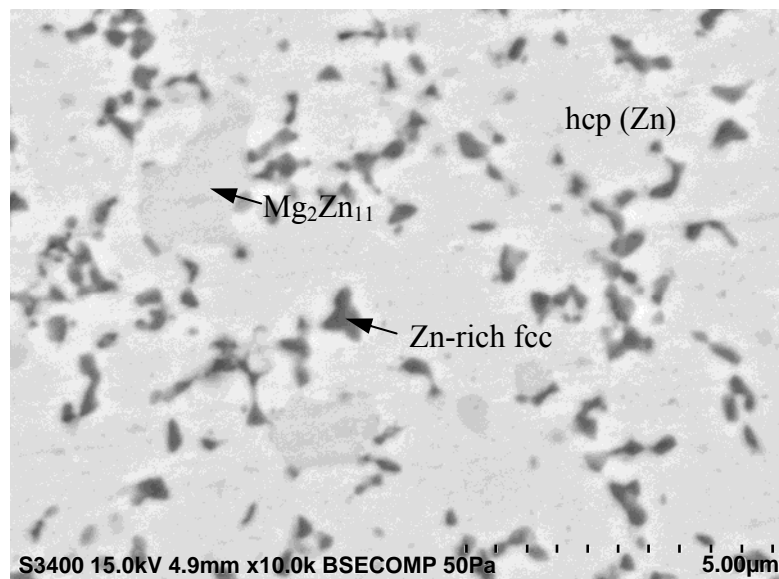


Figure 4.27 SEM image of Zn-Al-Mg-Ga solder wire.

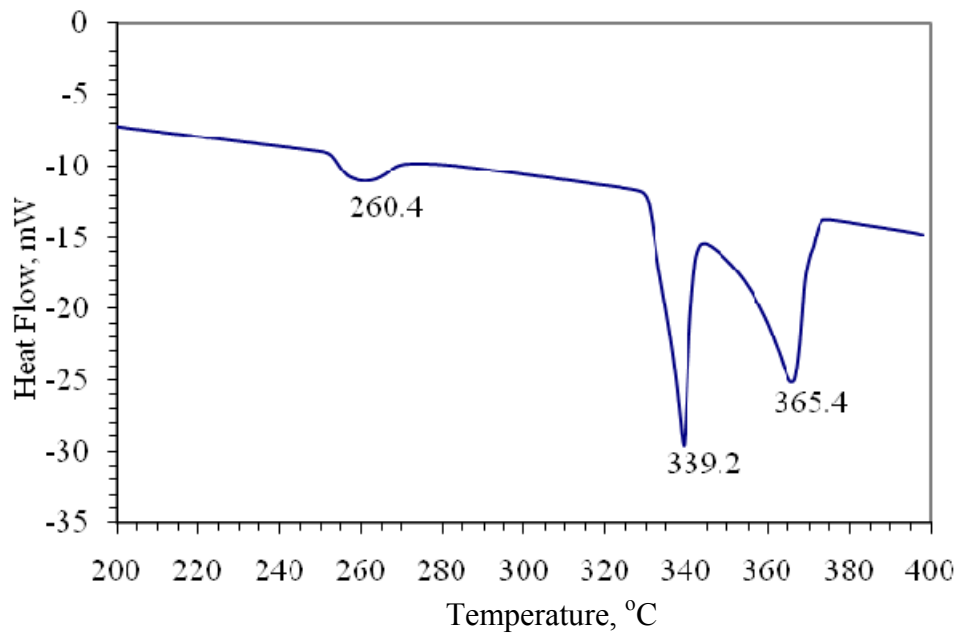


Figure 4.28 DSC curve of Zn-Al-Mg-Ga solder wire.

4.3.2(c) Microstructural characterization of Zn-Al-Mg-Ga solder on Cu lead-frame

Figure 4.29a shows the typical interface microstructure of the Si die attachment with Zn-Al-Mg-Ga solder on bare Cu lead-frame at temperature 390°C. Zn-Al-Mg-Ga solders wetted well with Si die and Cu lead-frame, and reaction layers were clearly observed at the Si die and Cu lead-frame interfaces. From Figure 4.29b it is evident that there are three distinct IMC layers formed at the Cu lead-frame/solder interface. A scallop shaped ϵ -CuZn₄ layer (A) forms at the solder side, a thin layer (C) of β' -CuZn forms close to copper lead-frame and while γ -Cu₅Zn₈ layer (B) forms at the middle (Takaku, et al., 2008). The average thickness of each IMC layer was measured for different die attached temperature. Higher die attached temperature corresponds to greater IMCs thickness. Thickness of scallop shaped ϵ -CuZn₄ layer varies from about 1.6 to 3.3 μm , γ -Cu₅Zn₈ layer from about 0.8 to 1.3 μm and β' -CuZn layer from about 0.4 to 0.5 μm depending on die attached temperature. The microstructure of the bulk solder (Figure 4.29c) consists of mainly two phases: one with a

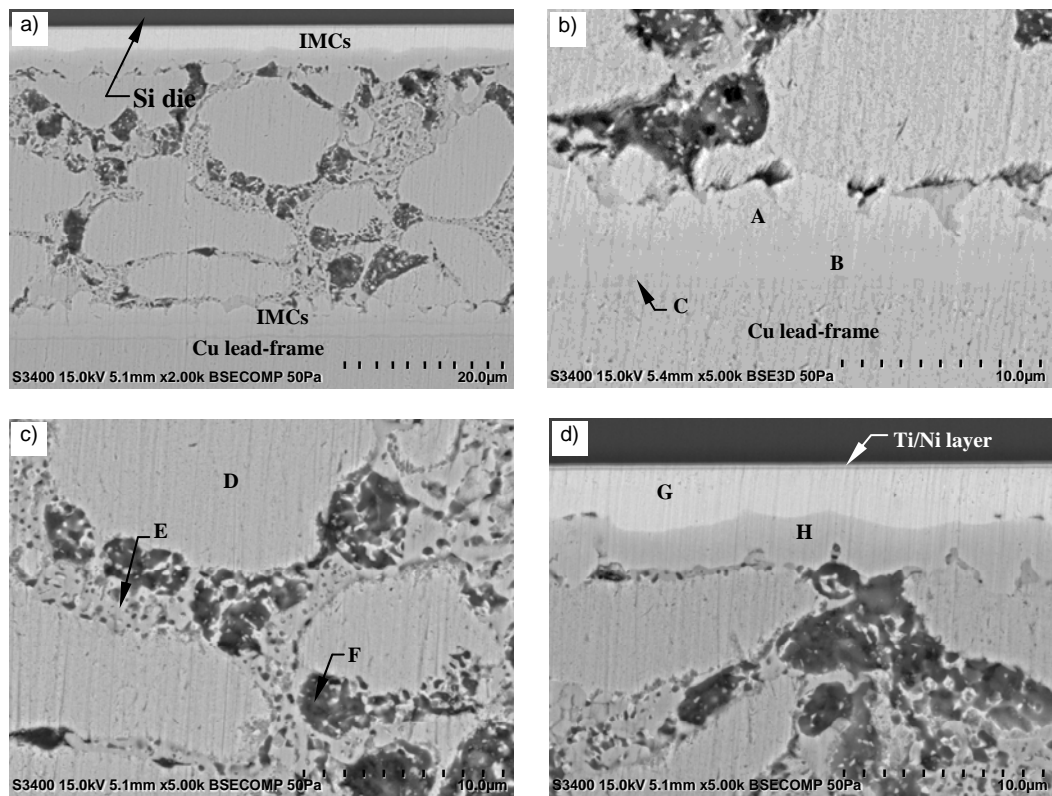


Figure 4.29 SEM micrograph of the die attach sample at 390°C using 2000 nm Ag thickness at the die back: a) cross-section of the joint; b) IMC layers at solder/lead-frame interface; c) bulk solder micrograph at higher magnification d) IMC layers at Si die/solder interface.

brighter contrast and the other one being a mixture of light and dark phases. EDX analysis was carried out on these points. The phases with brighter contrast particles (point D) are Zn rich phase containing about 80.9 wt.% of Zn. The light particles (point E) in the mixture phase are also Zn rich, which contain an average of 73.7 wt.% of Zn. The dark particles (point F) in the mixture phase are Al rich phase containing an average of 45 wt.% Al. Measured compositions of these phases are given in Table 4.4. The mixture phase is a combination of fine layers of light and dark particles. It indicates that after die bond operation, solidification process ends through eutectic reaction. Figure 4.29d shows the interfacial microstructure at Si die/solder interface. Ti/Ni/Ag metallized Si die with 2000 nm Ag thickness forms two IMC layers at the interface. EDX analysis was performed to determine the chemical composition of these IMC

layers. The measured compositions of these IMC layers are given in Table 4.5. From this table, it is found that the composition of the layer G is close to AgZn but the composition of H is not as close as AgZn₃. From binary phase diagram of Ag-Zn (Figure 4.30), it is expected that these two IMC layers are AgZn and AgZn₃.

Table 4.4 EDX analysis results of bulk microstructure of die attach sample using Zn-Al-Mg-Ga solder on bare Cu lead-frame with 2000 nm Ag thickness at the die back.

Element	Point D	Point E	Point F
	Wt.%	Wt.%	Wt.%
Zn K	80.9	73.7	38.8
Al K	2.7	4.8	45
Mg K	-	4.9	-
Ga K	-	-	3.7
Cu K	13.6	15.1	12.5
Ag L	2.8	1.4	-

Table 4.5 EDX analysis results of IMC layers at Si die/solder interface using Zn-Al-Mg-Ga solder with 2000 nm Ag thickness at the die back.

Element	Point G	Point H
	At.%	At.%
Zn L	53.6	86.4
Ag L	46.4	13.6

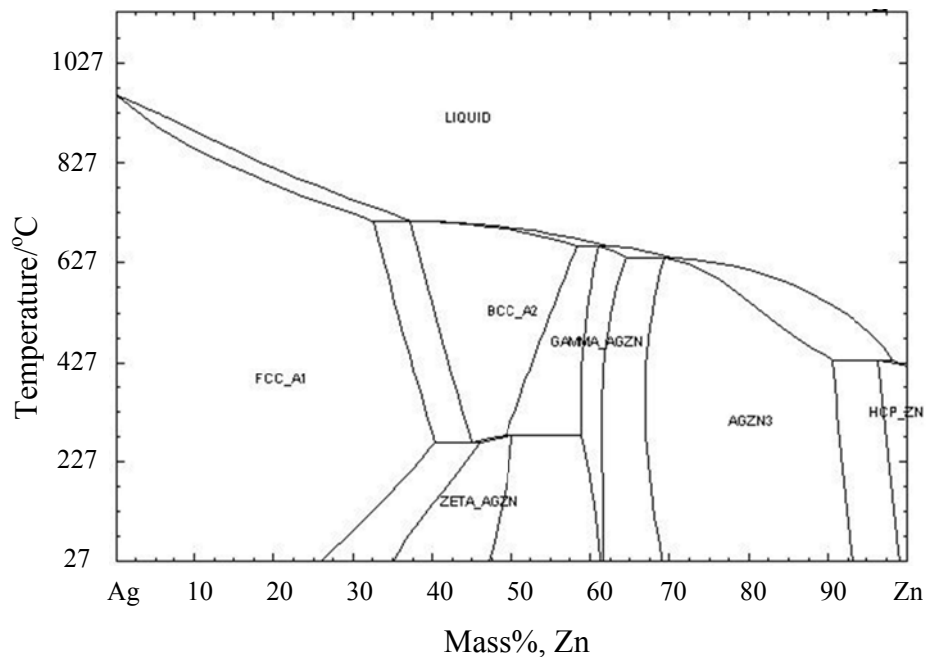


Figure 4.30 Ag-Zn binary phase diagram. (SGTE Alloy Phase Diagrams, 2004)

Using 200 nm Ag thicknesses at the die back, a thin IMC layer was observed at the Si die/solder interface while die attach was performed at 390°C on bare Cu lead-frame which is shown in Figure 4.31. EDX analysis was carried out on this layer. According to EDX analysis, it contains 58.3 at.% of Al and 41.7 at.% of Ni which is close to the composition of Al_3Ni_2 IMC. It complies with other researcher work that Ni reacts with Al and forms Al_3Ni_2 IMC (Takaku, et al., 2009). Microstructure of the bulk solder was found as similar as the samples using 2000 nm Ag thickness at the die back (Figure 32). Moreover, some particles (point L) with brighter appearance are observed at different locations in the bulk solder. These particles are rich in zinc and their shape, size and composition closely resemble that of scallop type CuZn_4 IMC. It is therefore suggested that these particles are CuZn_4 IMC which have been spalled from the interface during soldering. EDX analysis results of bulk solder are given in Table 4.6. From Tables 4.4 & 4.6, it is observed that Mg and Ga coexist in the eutectic reaction zone of the bulk solder

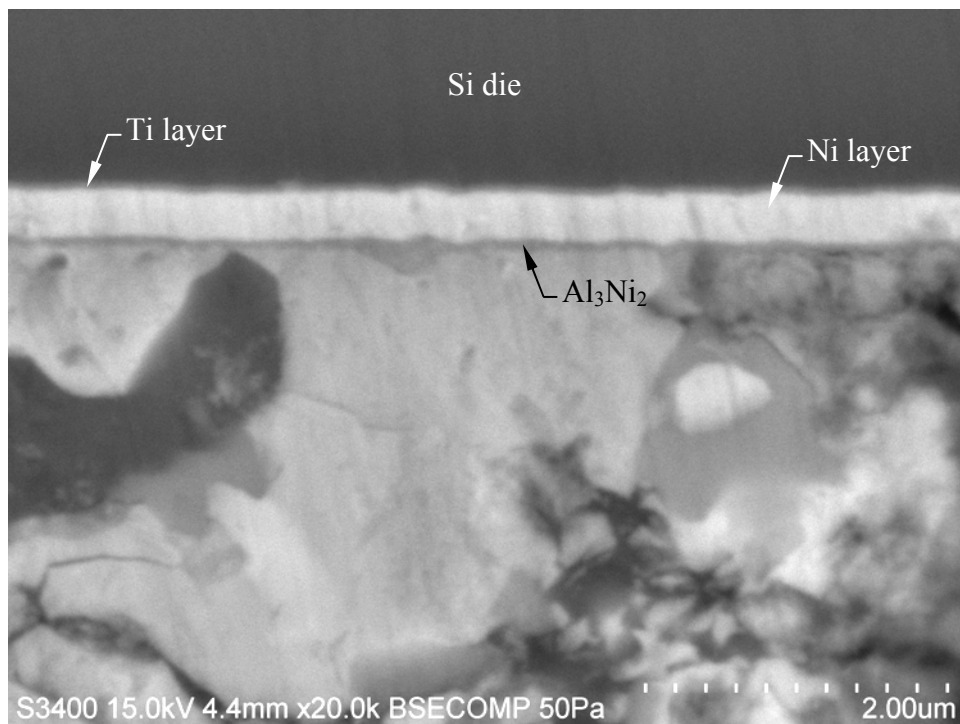


Figure 4.31 SEM image at the Si die/solder interface of the die attach sample on Cu lead-frame at 390°C with Zn-Al-Mg-Ga solder using 200 nm Ag thickness at the die back.

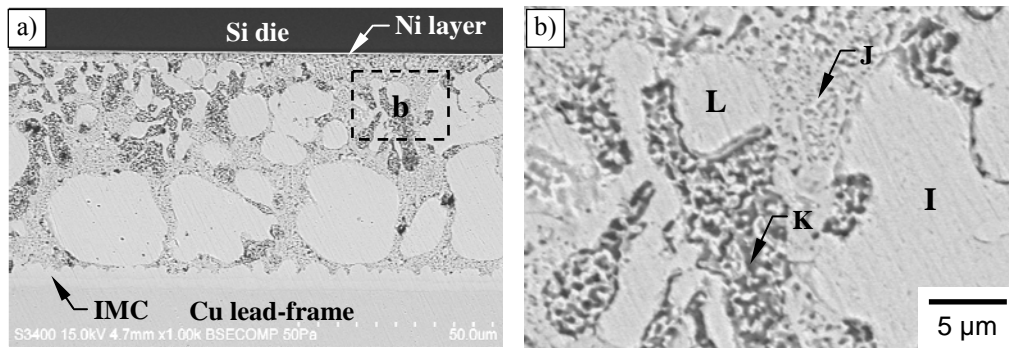


Figure 4.32 Typical SEM micrograph of the die attach sample at 380°C using 200 nm Ag thickness at the die back: a) cross-section of the joint; b) SEM image at higher magnification.

with Zn rich and Al rich phases respectively. Since Zn and Mg forms $Zn_{11}Mg_2$ IMC in the solder wire, it is expected that same IMC was formed again after soldering process. It is to be noted that solid solubility of Mg in hcp Zn is negligible at room temperature (SGTE Alloy Phase Diagrams, 2004). For that reason, it is expected that Mg coexists with Zn in the eutectic reaction zone. On the other hand, solid solubility of Ga in fcc Al is higher than the hcp Zn at room temperature (Figures 4.33 & 34). Therefore, it is expected that Ga coexists with Al.

Table 4.6 EDX analysis results of bulk microstructure of die attach sample using Zn-Al-Mg-Ga on bare Cu lead-frame with 200 nm Ag thickness at the die back.

Element	Point I	Point J	Point K
	Wt.%	Wt.%	Wt.%
Zn K	82.5	72.5	48
Al K	2.4	4.6	32.4
Mg K	-	5.1	-
Ga K	-	-	4
Cu K	15.1	17.8	15.6

Figures 4.35 & 4.36 represents the thickness changes of the IMC layers at lead-frame/solder and Si die/solder interfaces as a function of die attach temperature. For both the interfaces, higher die attach temperature corresponds to greater IMC thicknesses. Total IMC layer thicknesses for both the interfaces were measured and

presented in Figure 4.37 against corresponding die attach temperatures. It is observed that total IMC layer thickness at the lead-frame/solder interface increases more rapidly as compare to the IMC layer thickness at the Si die/solder interface with the increase of die attach temperature.

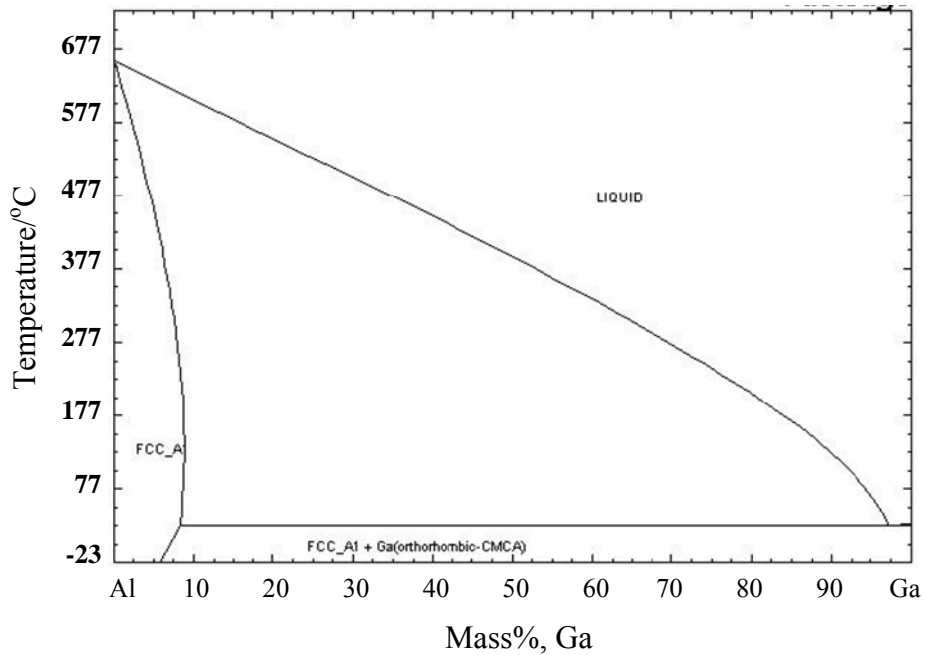


Figure 4.33 Al-Ga binary phase diagram.
(SGTE Alloy Phase Diagrams, 2004)

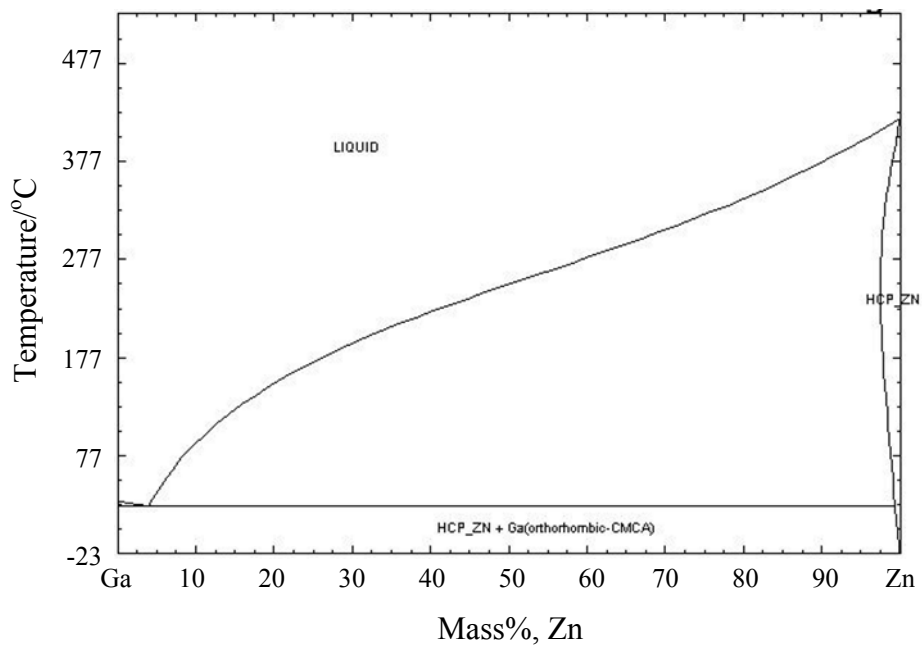


Figure 4.34 Ga-Zn binary phase diagram.
(SGTE Alloy Phase Diagrams, 2004)

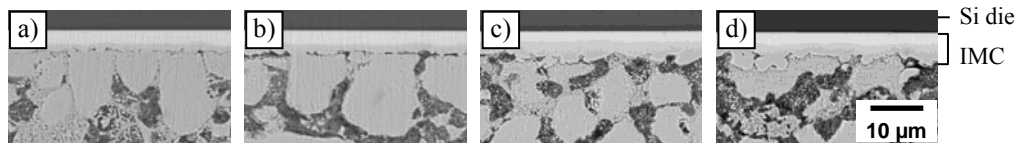


Figure 4.35 Effect of die attach temperature on thickness of IMCs layers at Si die/solder interface with Zn-Al-Mg-Ga solder: (a) 370°C, (b) 380°C, (c) 390°C and (d) 400°C.

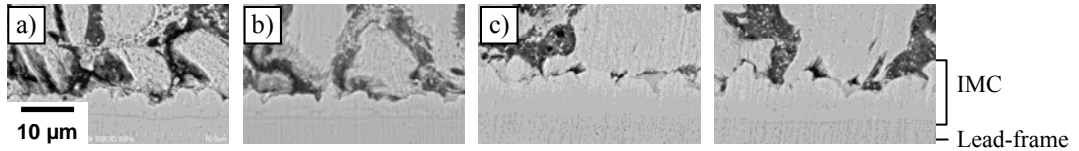


Figure 4.36 Effect of die attach temperature on thickness of IMCs layers at lead-frame/solder interface with Zn-Al-Mg-Ga solder: (a) 370°C, (b) 380°C, (c) 390°C and (d) 400°C.

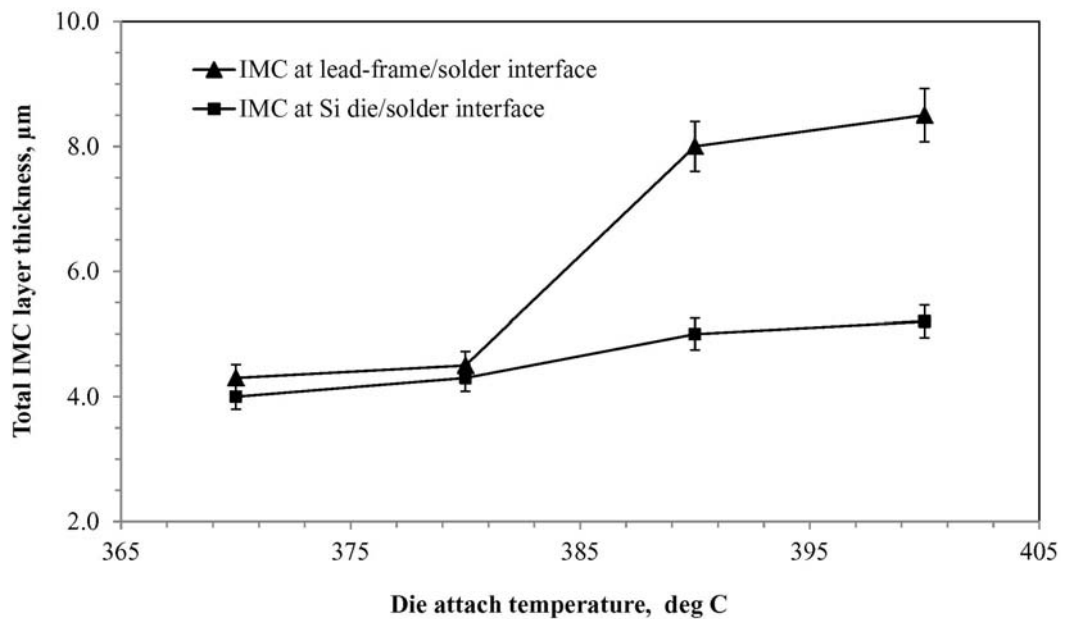


Figure 4.37 Total IMC layer thicknesses with respect to die attach temperature.

EDX elemental mapping of the die attach joint is shown in Figure 4.38 which was prepared at 390°C with Zn-Al-Mg-Ga solder on bare Cu lead-frame. It is seen from the mapping that the concentration of Zn is more in the brighter contrast areas and Al concentration is more in the darker contrast areas. Since small amount of Mg and Ga are added in the solder, these two elements were not detected well by EDX element

mapping. From Cu mapping it is found that Cu exists everywhere in the bulk solder since Cu diffused to the solder during soldering process. On the other hand, Zn diffused to the Cu lead-frame as well as Ag layer at the die back and forms IMCs at lead-frame/solder and Si die/solder interfaces.

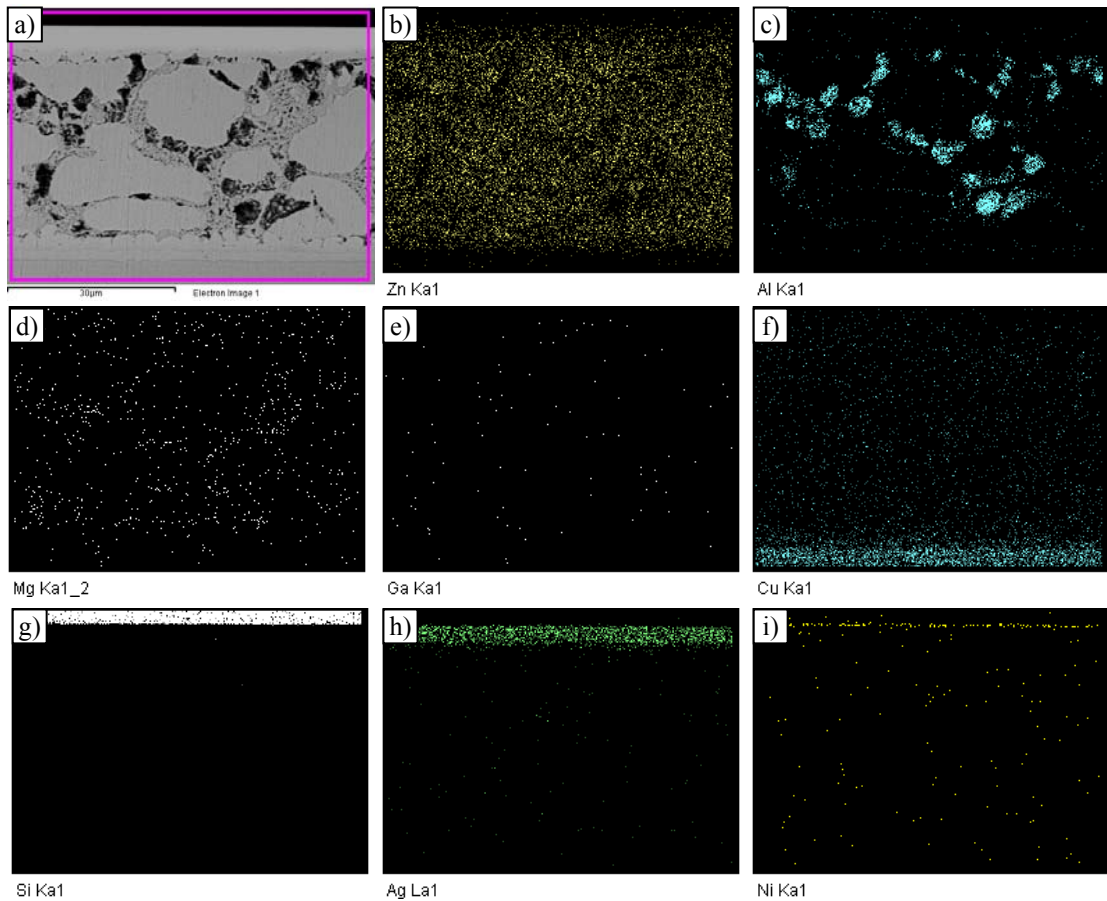


Figure 4.38 Element mapping of the die attach joint at 390°C on bare Cu lead-frame: (a) SEM image of the mapping region and element maps of (b) Zn; (c) Al; (d) Mg; (e) Ga; (f) Cu; (g) Si; (h) Ag and (i) Ni.

4.3.2(d) Wetting and void analysis of Zn-Al-Mg-Ga soldered samples on Cu lead-frame

Back scanning method was used for analyzing the void conditions in the solder joint. From each set of die attach samples, 20 samples were scanned for void analysis. Based on void conditions, the best and average back scanning images for each set of die attach samples are shown in Figure 4.39. In the SAM images, the rectangular dark area marked

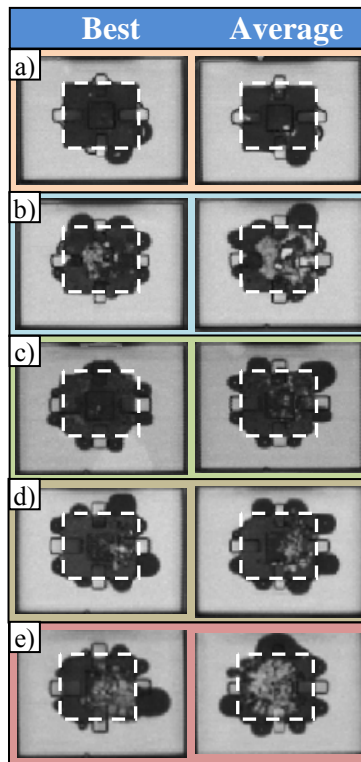


Figure 4.39 SAM images of the die attach samples using back scanning method: a) standard Pb-Sn soldered sample; and Zn-Al-Mg-Ga soldered samples at b) 370°C; c) 380°C; d) 390°C; e) 400°C.

with white dashed line is the Si die and the white spots within the dark rectangular area of the die are represented as voids. Cumulative void area was measured manually for each of the die attach samples using a mesh of 10 x 10 which was superimposed on die area of the SAM image. Figure 4.40 shows the cumulative void analysis results. From this analysis it is found that die attach samples at 380 and 390°C have less void which is within industry acceptable limit. Almost all the die attach samples at 370 and 400°C have more than 10% voids. It is expected that low wetting at 370°C and oxidation at 400°C are the reasons for more void. The standard Pb-5Sn soldered samples have almost no void. On the other hand, Zn-Al-Mg-Ga solder wetted well on Cu lead-frame, covered entire die area and flowed in all directions under the Si die. It is also observed from the Zn-Al-Mg-Ga soldered samples that the amount of oozed solder around the Si die is more compared with that of standard Pb-5Sn soldered samples. For this issue, the

amount of solder dispense need to be optimized. It is to be mentioned that the die attach area of the lead-frame used in this experiment was quite different from the others which is mentioned earlier in Article 3.2.2c. Wetting pattern of Zn-Al-Mg-Ga and Pb-5Sn solder (Figure 3.3) are found similar but different from the previous experiments. For that reason, contact angle was not measured for checking wettability on lead-frame.

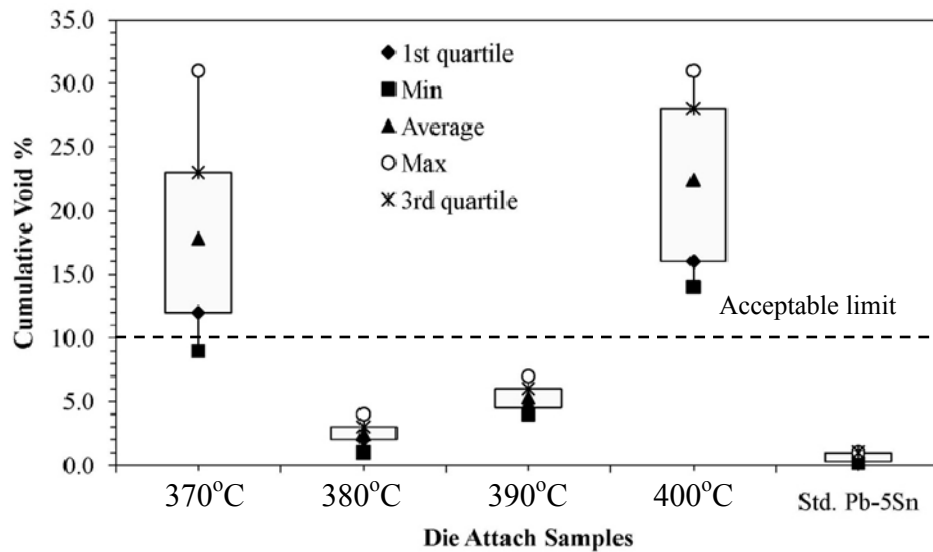


Figure 4.40 Comparison of cumulative voids of Zn-Al-Mg-Ga soldered samples at different die attach temperatures with standard Pb-5Sn soldered samples.

4.3.2(e) Die shear strength of Zn-Al-Mg-Ga soldered samples on Cu lead-frame

Figure 4.41 shows the comparison of the die shear strength of Zn-Al-Mg-Ga soldered samples on bare Cu lead-frames at different die attach temperatures with standard Pb-5Sn soldered sample. It is found that die shear strength of Zn-Al-Mg-Ga soldered samples increases with the die attach temperature. Average die shear strength of Zn-Al-Mg-Ga soldered samples varies from 21.8 MPa to 29.4 MPa with the corresponding die attach temperature of 370°C and 400°C. Die shear strength depends on the strength of solder material, wetting on lead-frame and bonding strength of Si die/solder interface. Since Zn-Al-Mg-Ga solder is strong enough and wetting increases with the increase of die attach temperature, therefore it is expected that the die shear strength is increased

with die attach temperature. Average die shear strength of standard Pb-5Sn soldered samples was found 29.3 MPa. It is also found that shear strength of all the samples are above the industry acceptable limit. It is to be noted that the acceptable limit of the die shear strength depends on the size of the Si die. According to the ON Semiconductor standard, the acceptable limit for this die is considered as 12.5 MPa.

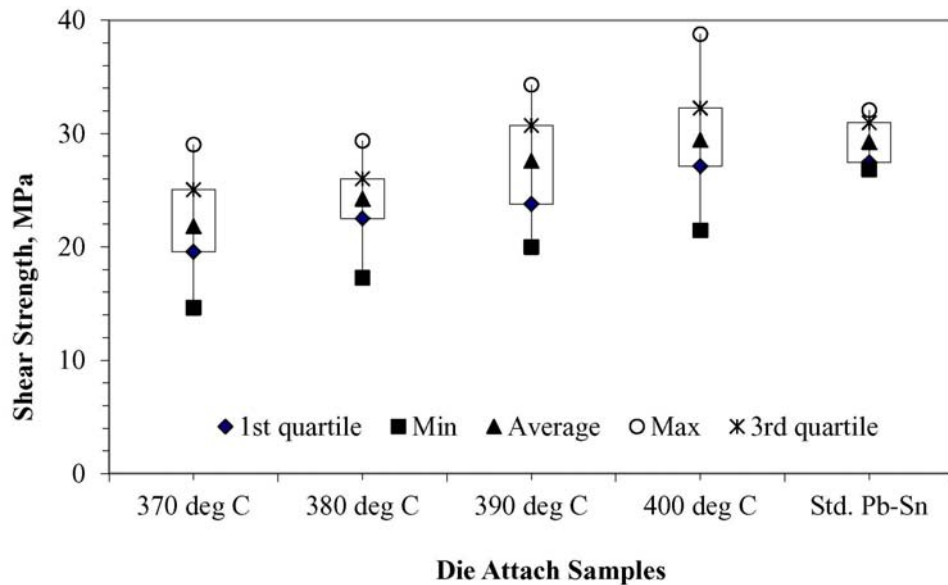


Figure 4.41 Comparison of die shear strength of Zn-Al-Mg-Ga soldered samples at different die attach temperatures with standard Pb-5Sn soldered samples.

The failure mode of Zn-Al-Mg-Ga soldered samples during die shear was found different from that of the standard Pb-5Sn soldered samples which are shown in Figure 4.42. For Zn-Al-Mg-Ga soldered samples, shear occurred by cracking of Si die regardless of the die attach temperature. Figure 4.42a shows the sheared surface of the Zn-Al-Mg-Ga soldered sample. From this figure, two shades are observed within the rectangular die area: one with brighter appearance and the other one being darker. For confirmation of these shades, EDX element mapping was performed on the sheared surface which is described later. From Figure 4.42b, it is found that fracture also occurred in IMC layers at Si die/solder interface. For standard Pb-5Sn soldered samples, die shear occurred at bulk solder (Figure 4.42c). Since Zn-Al-Mg-Ga solder is strong

compare to standard Pb-5Sn solder and it forms IMCs at Si die/solder and lead-frame/solder interfaces, therefore failure of Zn-Al-Mg-Ga soldered samples on bare Cu lead-frame was occurred by cracking of Si die. On the other hand, standard Pb-5Sn solder is ductile and has strong interfacial bonding with Si die and lead-frame. Therefore, shear failure of standard Pb-5Sn soldered samples occurred at the bulk solder.

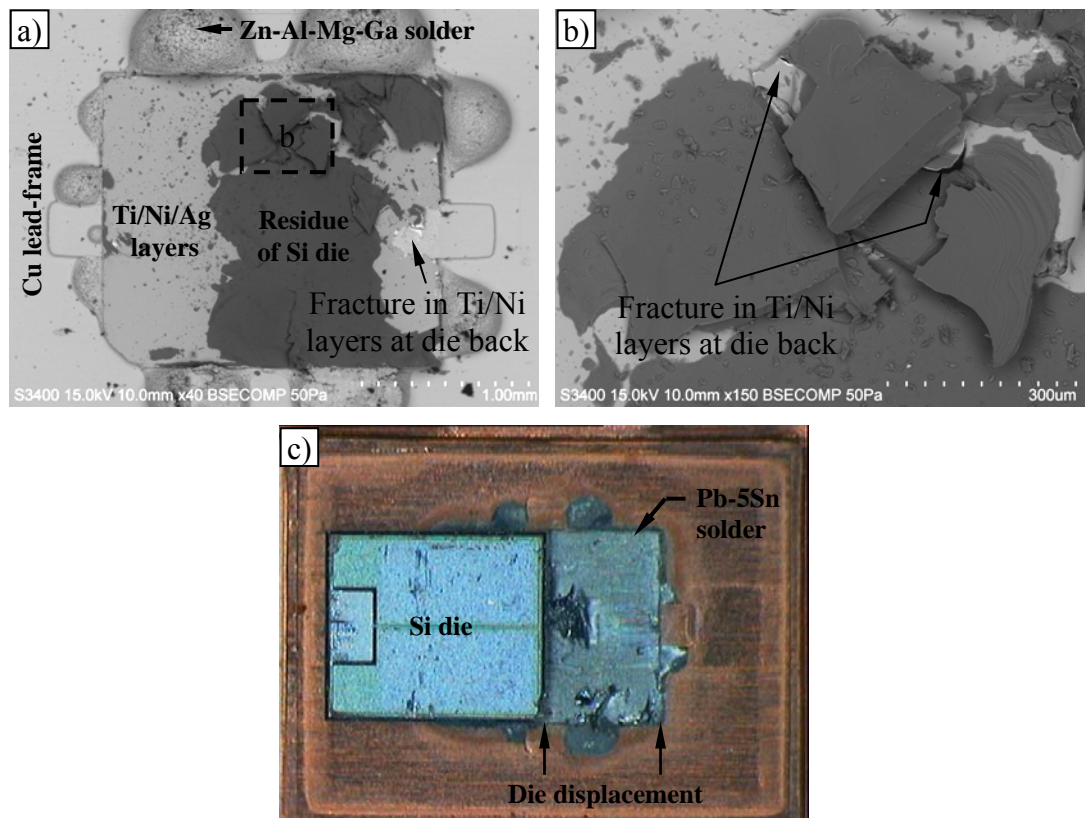


Figure 4.42 SEM/Optical images of the die sheared surface: a) Zn-Al-Mg-Ga soldered sample; b) SEM image at higher magnification; c) standard Pb-5Sn soldered sample.

Figure 4.43 shows the EDX element mapping of the sheared surface of the die attach sample with Zn-Al-Mg-Ga on bare Cu lead-frame. From this mapping, it is found that within the rectangular die area, the dark shaded surface contains Si and bright shaded surface contains Ti, Ni and Ag. No other elements are detected within the rectangular die area except Zn which is found at the middle of right hand side of the rectangular die

area. At this location, Ti and Ni are not found. It indicates that fracture also occurred at Ti/Ni layers at the die back. Zn, Al and Cu are found outside the rectangular die area. From this element mapping analysis, it can be concluded that die shear of Zn-Al-Mg-Ga soldered samples was started just above the Ti/Ni layer at the die back, and damaged Ti/Ni layer in some places and ended by cracking of Si die. Schematic view of the shear failure mechanism is shown in Figure 4.44.

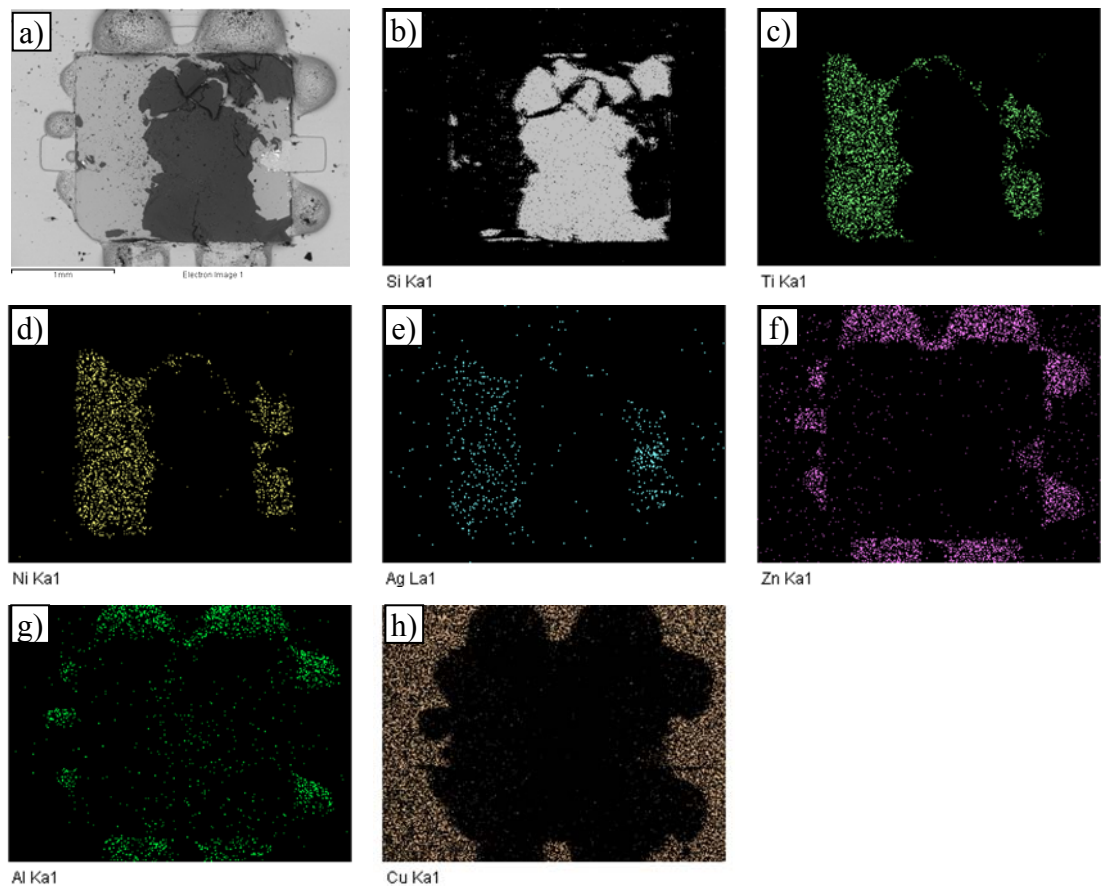


Figure 4.43 EDX elemental mapping of the sheared surface of the soldered sample with Zn-Al-Mg-Ga solder: (a) SEM image of the mapping region; and element maps of (b) Si; (c) Ti; (d) Ni; (e) Ag; (f) Zn; (g) Al; and (h) Cu.

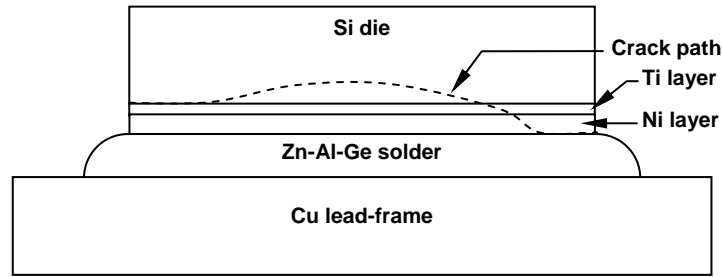


Figure 4.44 Failure mechanism of Zn-Al-Mg-Ga soldered samples during die shear

4.3.2(f) Microstructural characterization of Zn-Al-Mg-Ga solder on Ni metallized Cu lead-frame

Figure 4.45 shows the typical interfacial microstructure of the Si die attachment on Ni metallized Cu lead-frame with Zn-Al-Mg-Ga solder at 380°C. A sound die attachment was achieved, and no Cu-Zn IMCs were observed at the lead-frame/solder interface. The bulk solder consists of mainly three phases (Figure 4.45a). These are smooth textured brighter phase, smooth textured slightly darker phase and coarse textured phase. EDX analysis was carried out on these phases and found all are rich in Zn. The phase with smooth textured brighter particles (point A) containing about 85.3 wt.% Zn, smooth textured slightly darker particles (point B) containing about 72.9 wt.% Zn and coarse textured particles (point C) containing about 69.1 wt.% Zn.

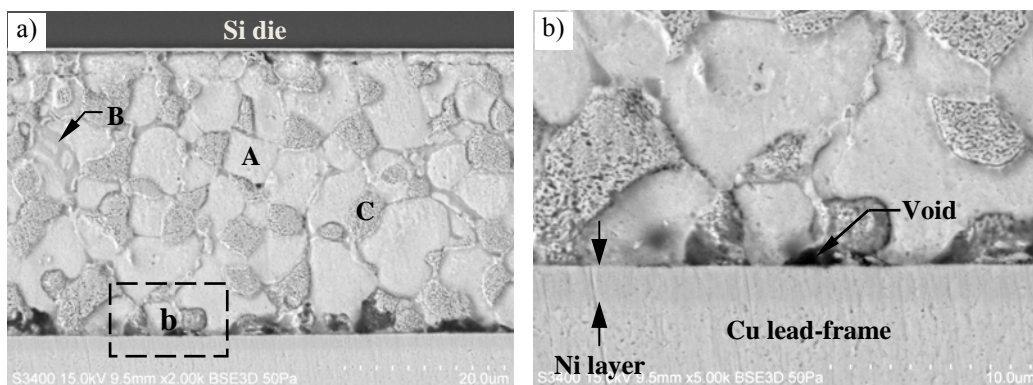


Figure 4.45 Typical microstructure of the die attached joint on Ni metallized Cu lead-frame. (a) cross-section of the joint; (b) SEM image at higher magnification.

The measured compositions of these phases are given in Table 4.7. It is to be noted that small size voids were observed at the lead-frame/solder interface which is shown in Figure 4.45b. It is suggested that these voids formed due to uneven wetting of Zn-Al-Mg-Ga solder on Ni metallized Cu lead-frame. Moreover, EDX analysis was also carried out on the Ni metallized layer of the lead-frame at two different locations. One point was taken at the solder side and the other point was taken at the middle. EDX analysis results are given in Table 4.8. From this Table, it is found that Ni layer reduced Zn diffusion to Cu lead-frame a lot. On the other hand, concentration of Cu is found almost uniform throughout the Ni layer.

Table 4.7 EDX analysis results of bulk microstructure of die attach sample using Zn-Al-Mg-Ga solder on Ni metallized Cu lead-frame.

Element	Point A	Point B	Point C
	Wt.%	Wt.%	Wt.%
Zn K	85.3	72.9	69.1
Al K	2.7	2.8	18.2
Mg K	-	13.6	-
Cu K	12	10.7	12.7

Table 4.8 EDX analysis results of Ni layer on Cu lead-frame.

Element	At the solder side	At the middle
	Wt.%	Wt.%
Ni K	60.4	73.2
Al K	2	1.6
Cu K	19.7	19.1
Zn K	17.9	6.1

Figure 4.46 represents the EDX element mapping of the die attached joint constructed with Zn-Al-Mg-Ga solder on Ni metallized Cu lead-frame. Al concentration was found higher in the coarse textured areas. It is seen from the mapping that Ni layers are found

intact on both the interfaces. Though Ni layer was found intact, Cu diffused through Ni layer and found everywhere in the bulk solder.

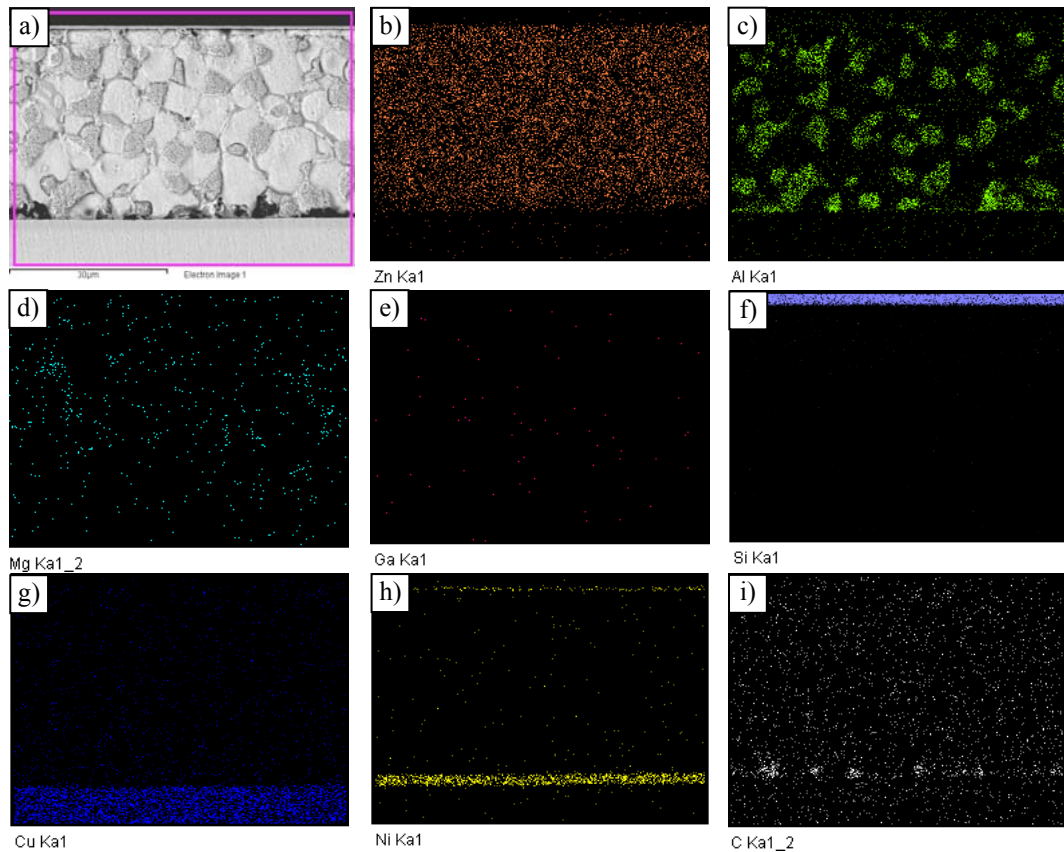


Figure 4.46 Element mapping of the die attached joint on Ni metallized Cu lead-frame. (a) SEM image of the mapping region and element maps of (b) Zn; (c) Al; (d) Mg; (e) Ga; (f) Si; (g) Cu; (h) Ni and (i) C.

4.3.2(g) Wetting and void analysis of Zn-Al-Mg-Ga soldered samples on Ni metallized Cu lead-frame

Die attach samples on bare and Ni metallized lead-frame using Zn-Al-Mg-Ga solder was analyzed using SAM for checking void condition in the solder joints and compared these images with the standard Pb-5Sn soldered samples. Figure 4.47 shows the back scanning images from SAM. The darker rectangular area is Si die and the outer approximately circular area is wetting area of the solder. The white spots within the dark rectangular area of the die are represented as voids. Cumulative void was measured

and compared with the standard Pb-5Sn soldered samples which are shown in Figure 4.48. From the back scan analysis it is found that die attached samples on Ni plated lead-frame have less void as compare to bare Cu leaf-frame. Die attach samples using standard Pb-5Sn solder have almost no void.

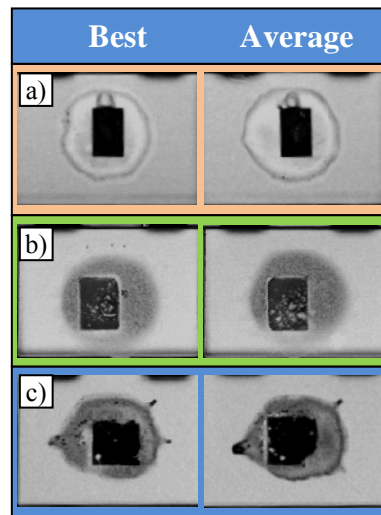


Figure 4.47 Back scanning images of the die attach samples: a) using standard Pb-5Sn solder; and using Zn-Al-Mg-Ga solder at 380°C on b) bare Cu lead-frame; and c) Ni metallized Cu lead-frame.

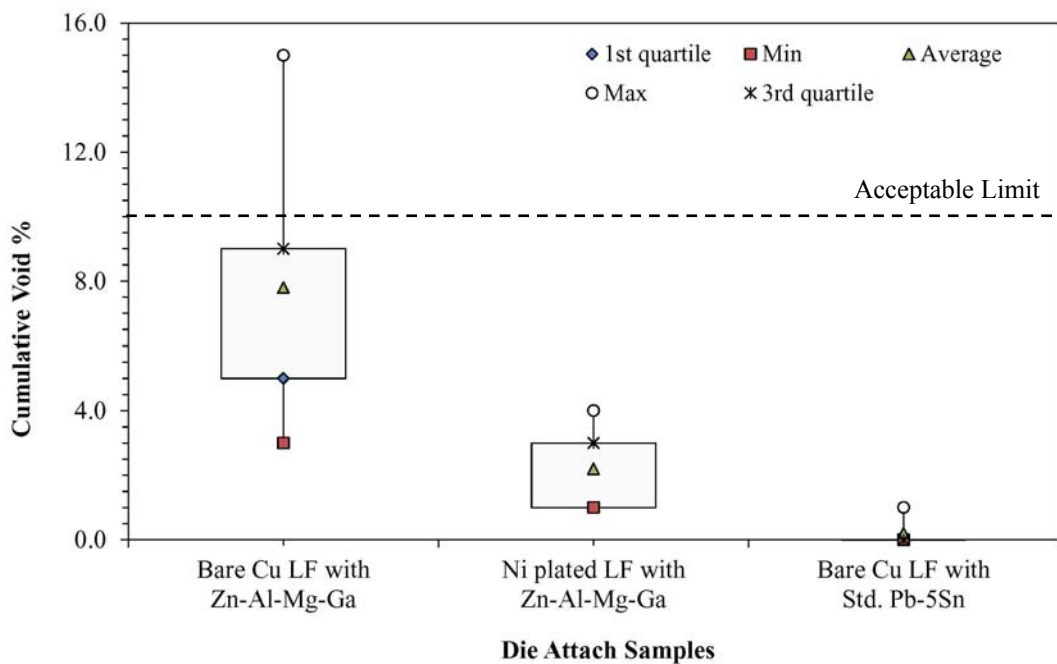


Figure 4.48 Comparison of cumulative voids of Zn-Al-Mg-Ga soldered samples on different lead-frames with standard Pb-5Sn soldered samples.

Wetting of Zn-Al-Mg-Ga solder was found better on bare Cu lead-frame as compare to Ni metallized Cu lead-frame. Contact angles of Zn-Al-Mg-Ga solder on bare and Ni metallized Cu lead-frame and standard Pb-5Sn solder are shown in Figure 4.49. From the optical images, it is found that the contact angle of Zn-Al-Mg-Ga solder on bare Cu lead-frame is similar (± 1 degree) to standard Pb-5Sn solder.

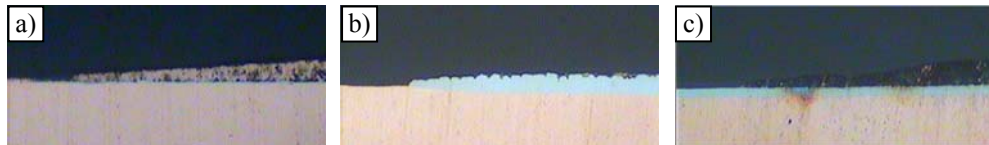


Figure 4.49 Optical images representing wetting angle: a) standard Pb-5Sn solder; and Zn-Al-Mg-Ga solder on b) bare Cu lead-frame; c) Ni metallized Cu lead-frame.

4.3.2(h) Die shear strength of Zn-Al-Mg-Ga soldered samples on Ni metallized Cu lead-frame

Die shear strength of Zn-Al-Mg-Ga soldered samples on bare and Ni metallized Cu lead-frames were measured and compared with the shear strength of standard Pb-5Sn soldered samples (Figure 4.50). It is found that average die shear strength is lower

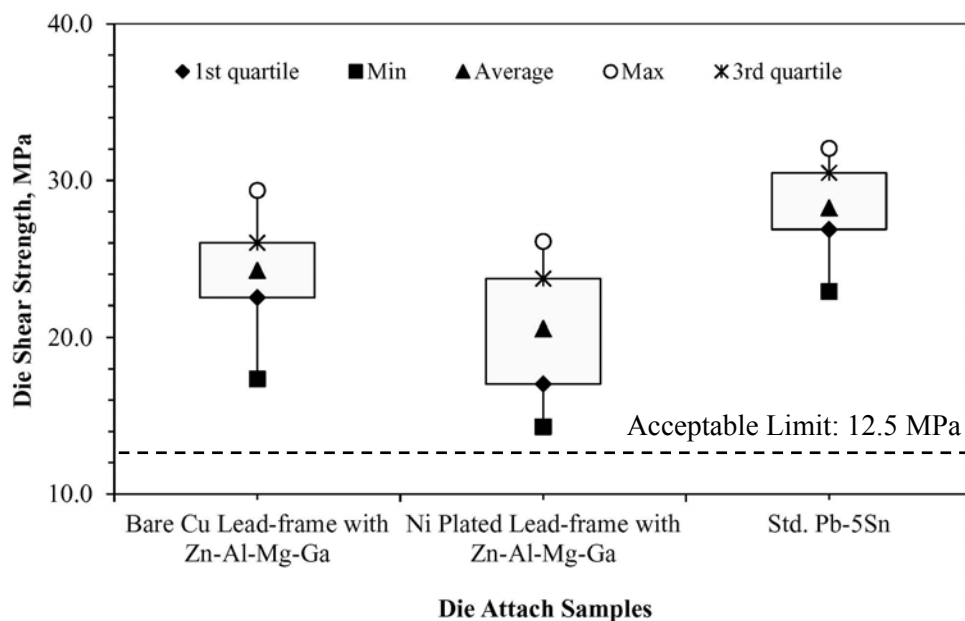


Figure 4.50 Comparison of die shear strength of Zn-Al-Mg-Ga soldered samples on different lead-frame conditions with standard Pb-5Sn soldered samples.

on Ni metallized Cu lead-frame (20.5 MPa) as compared to bare Cu lead-frame (24.2 MPa). Due to less wetting on Ni metallized Cu lead-frame, bonding strength of the die attach joint becomes low. For that reason, average die shear strength was found less on Ni metallized Cu lead-frame compare to bare Cu lead-frame. Average die shear strength of standard Pb-5Sn soldered samples is found to be 28.2 MPa which is higher than the shear strength of Zn-Al-Mg-Ga soldered samples. According to the ON Semiconductor standard, the acceptable limit for these dies is considered as 12.5 MPa.

Shear failure modes of each type of samples were also analyzed and found different from the standard Pb-5Sn soldered samples which are presented in Table 4.9. Similar type of failure was found for Zn-Al-Mg-Ga soldered samples on bare Cu lead-frame which mentioned earlier. Shear failure of die attach samples on Ni metallized Cu lead-frame occurred at lead-frame/solder interface. For confirmation of failure mode, EDX element mapping was performed on sheared surface which is shown in Figure 4.51. From this mapping, Ni is found inside the square size die area and there is no Zn found within this area. It indicates that shear failure was occurred at lead-frame/solder interface. Concentration of Cu is also found more within the die area (Figure 4.51e) which indicates diffusion of Cu through Ni layer. For that reason Cu was found everywhere in the bulk solder. Shear failure of standard Pb-5Sn soldered samples was occurred at bulk solder. Since Zn-Al-Mg-Ga solder is strong compare to standard Pb-5Sn solder and it forms IMCs at Si die/solder and lead-frame/solder interfaces,

Table 4.9 Shear failure mode of die attach samples using standard Pb-5Sn and Zn-Al-Mg-Ga solder.

Solder used	Die attach on	Failure mode
Std. Pb-5Sn	Bare Cu lead-frame	Bulk solder
Zn-Al-Mg-Ga	Bare Cu lead-frame	Cracking of Si die
Zn-Al-Mg-Ga	Ni plated Cu lead-frame	Lead-frame/solder interface

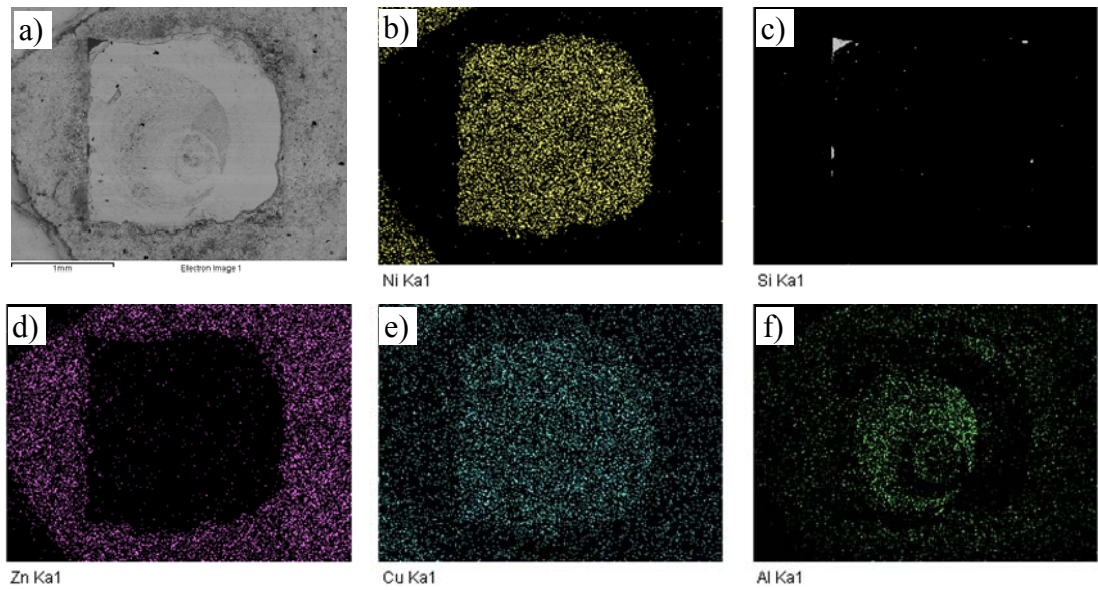


Figure 4.51 EDX elemental mapping of the sheared surface of the soldered sample with Zn-Al-Mg-Ga solder on Ni metallized Cu lead-frame: (a) SEM image of the mapping region; and element maps of (b) Ni; (c) Si; (d) Zn; (e) Cu; (f) Al.

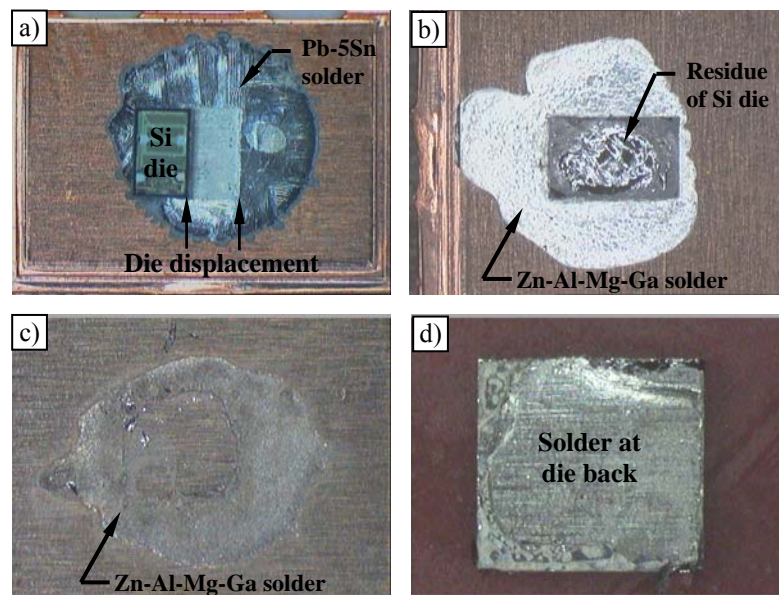


Figure 4.52 Optical images of die shared samples with: a) standard Pb-5Sn solder; and Zn-Al-Mg-Ga solder b) on bare Cu lead-frame; c) on Ni metallized Cu lead-frame; d) backside of the die with solder lifted from Ni metallized Cu lead-frame.

therefore failure of Zn-Al-Mg-Ga soldered samples on bare Cu lead-frame occurred by cracking of Si die. On the other hand, wetting of Zn-Al-Mg-Ga solder was found less on Ni metallized Cu lead-frame as compare to bare Cu lead-frame. Therefore, bonding

strength of Zn-Al-Mg-Ga solder with Ni metallized Cu lead-frame was not strong enough as compare to bare Cu lead-frame. Accordingly, failure occurred at the lead-frame/solder interface. Since standard Pb-5Sn solder is ductile and has strong interfacial bonding with Si die and lead-frame, therefore failure occurred at the bulk solder. Optical images of the sheared samples are shown in Figure 4.52.

4.3.2(i) Reliability tests

Pass criteria for AC, TC and HTOL tests were zero failure in electrical test out of 80 samples. For all these reliability tests, electrical test was performed and found OK without failure. Since the electrical test results were found similar for all these tests, only electrical test result for TC test is presented graphically in this dissertation.

Autoclave test

This test was performed for two sets of samples: One with PC and the other one without PC. Electrical test was performed for two sets of samples and all samples were found OK without failure. Cross-section was made for some samples for checking cracks and micro-structural change in the bulk solder and at the interfaces which is shown in

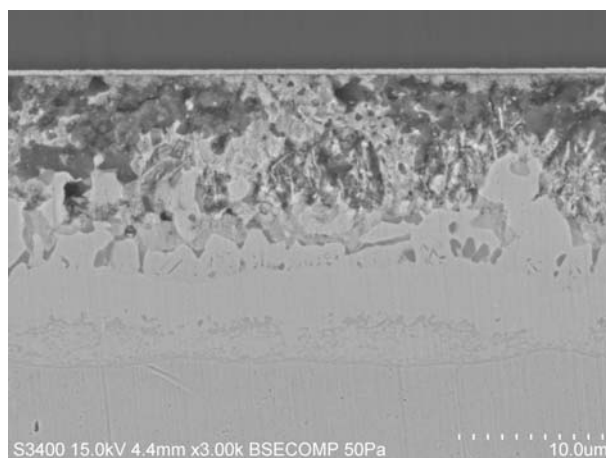


Figure 4.53 SEM micrograph of molded die attach sample soldered with Zn-Al-Mg-Ga solder after AC test with PC.

Figure 4.53. From this figure, it is found that IMC thickness at lead-frame/solder interface increased a lot which is approximately 8.2 μm . In bulk microstructure, amount of brighter contrast phases found lower compare to that of dark phases. It indicates that during AC test, Zn diffused more to the Cu lead-frame and forms thicker IMCs at the interface. No crack was found in the bulk solder as well as at the interfaces.

Temperature cycling test

TC 1000 cycles test was performed for two sets of samples: One with PC and the other one without PC. Electrical test was conducted for all samples before and after TC test. In this test, output voltage was measured for each sample, and the amount of deviations was calculated. Graphical presentation of the electrical test result is shown in Figure 4.54. From this test, maximum deviation was found 12.1%. According to ON Semiconductor standard, maximum output voltage deviation is considered as 20%. Cross-section was made for some samples for checking cracks and micro-structural change in the bulk solder and interfaces which is shown in Figure 4.55. From this figure, it is found that IMC thickness at lead-frame/solder interface increased further which is approximately 19.8 μm . For that reason amount of brighter contrast phase

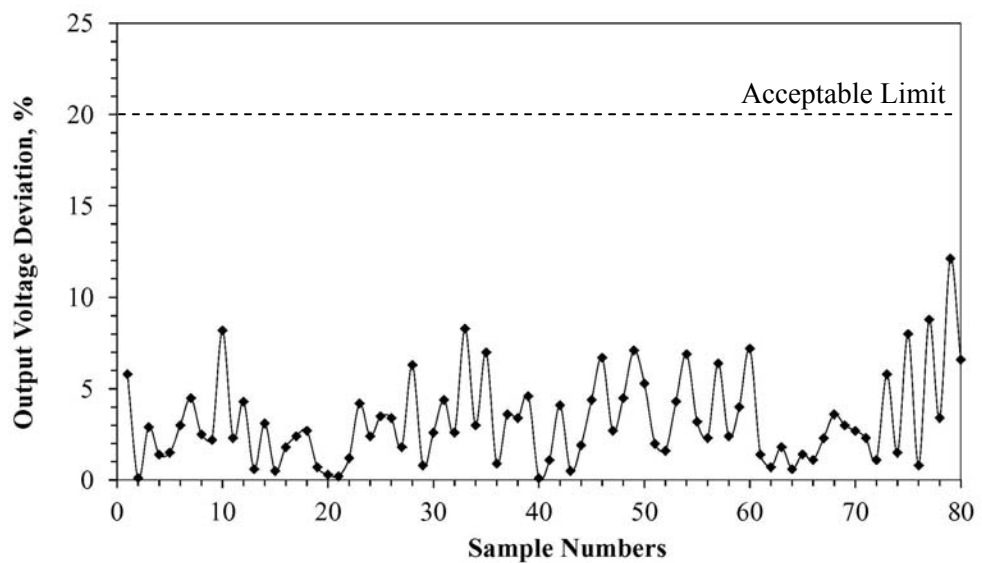


Figure 4.54 Deviation of output voltage after completion of TC test with PC.

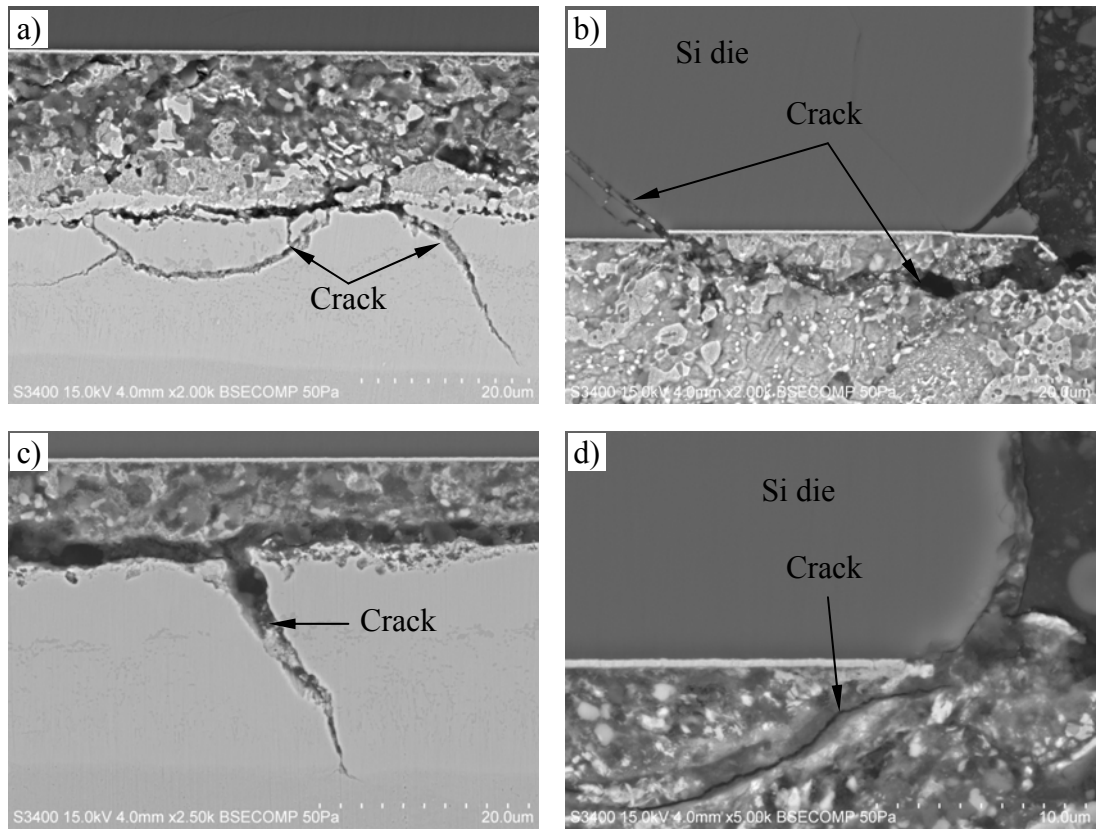


Figure 4.55 SEM micrograph of TC test samples soldered with Zn-Al-Mg-Ga solder: a) & b) after 1000 TC without PC; c) & d) after 1000 TC with PC test.

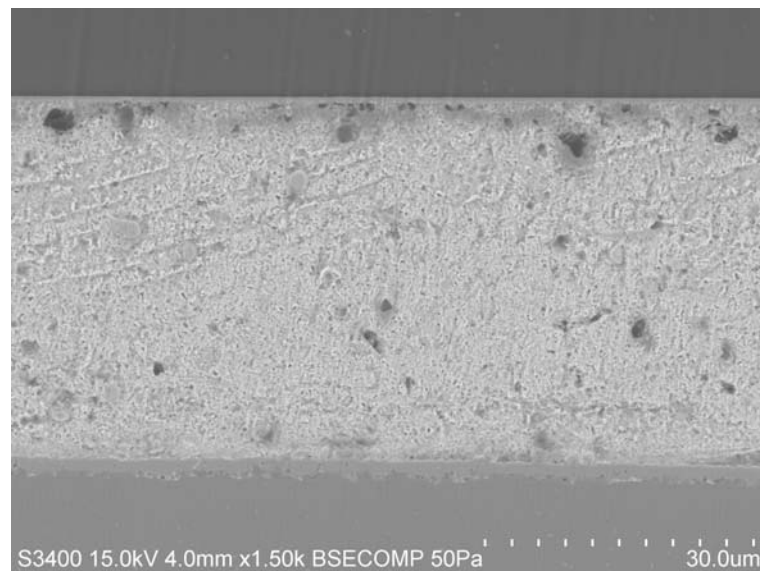


Figure 4.56 SEM micrograph of standard Pb-5Sn soldered sample after TC 1000 cycles with PC.

reduced further in bulk solder. Crack was found in the IMCs at lead-frame/solder interface and bulk solder for both PC and without PC samples. Crack also found in Si die for some samples. TC 1000 cycles test was also performed on standard Pb-5Sn soldered samples with and without PC. From cross-section, no crack was found for standard Pb-5Sn soldered samples (Figure 4.56).

High-temperature operating life test

This test was conducted for one set of sample without PC. Electrical test was carried out for all samples at 0, 504 and 1008 hours of operation and found OK with zero failure. Cross-section was made for some samples after 1008 hours of operation for checking cracks and micro-structural change in the bulk solder and interfaces which is shown in Figure 4.57. From this figure, it is found that IMC thickness at lead-frame/solder is approximately 20.1 μm . Amount of brighter contrast phase almost nil in bulk solder. Crack was found in the IMC layer at lead-frame/solder interface. It is also observed that an empty space is developed just above the IMC layer due to Zn diffusion in the Cu lead-frame.

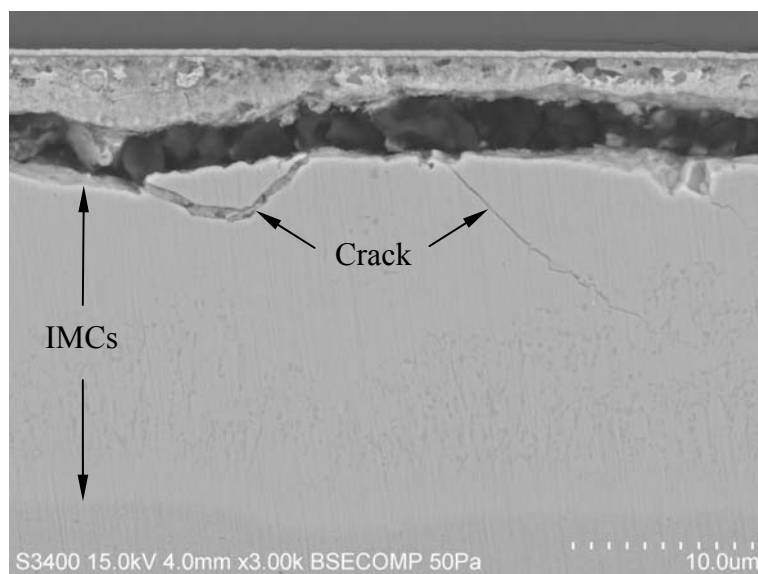


Figure 4.57 SEM micrograph of HTOL test samples soldered with Zn-Al-Mg-Ga solder after 1008 hours of operation.

High-temperature storage life test

HTSL test was performed at three different temperatures and aged up to 1008 hours. Cross-section was made for some samples in each ageing conditions for checking cracks and changes of IMCs thicknesses at lead-frame/solder interface. Optical images of some samples are shown in Figure 4.58. From this figure, it is found that IMCs thickness at lead-frame/solder increases with ageing time. Crack was found in the IMCs layer after 1008 hours of ageing. The changes of IMCs thickness for all ageing conditions are summarized in Table 4.10. From this table, it is found that bond line thickness (BLT) has significant impact on growth of IMCs over ageing temperature and time.

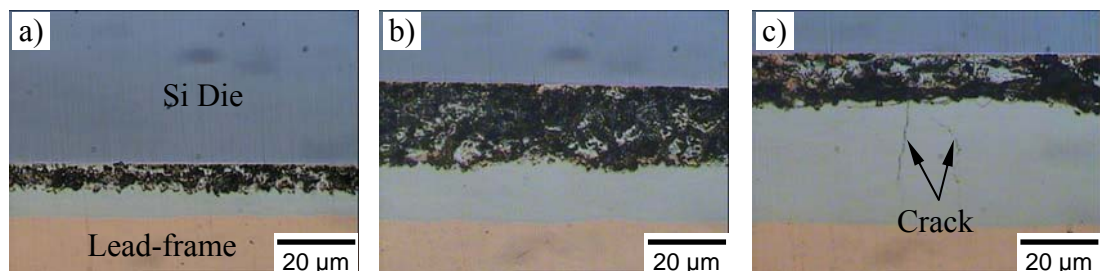


Figure 4.58 Optical images of die attach samples aged at 175°C for: a) 48 hours; b) 168 hours; and c) 1008 hours.

Table 4.10 Effect of ageing time and storage temperature on IMC thicknesses at lead-frame/solder interface.

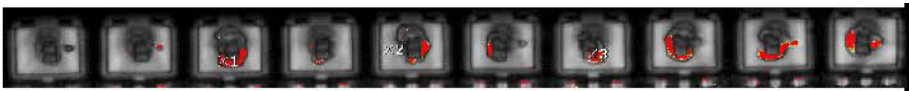
Ageing Time (Hours)	Storage Temperature								
	125°C			150°C			175°C		
	BLT (µm)	IMC thickness		BLT (µm)	IMC thickness		BLT (µm)	IMC thickness	
(µm)		St. Dev.	(µm)		St. Dev.	(µm)		St. Dev.	
48	13.0	3.2	0.25	13.0	5.5	0.19	16.5	8.8	0.52
96	13.9	4.0	0.22	13.2	6.6	0.37	20.7	12.7	0.52
168	12.1	4.2	0.18	25.5	14.2	0.52	17.8	11.9	1.11
336	10.9	4.8	0.23	22.0	13.6	3.69	19.9	14.2	1.55
504	15.5	7.8	0.72	15.0	9.9	1.59	14.3	10.5	0.39
840	17.3	10.2	0.81	13.5	9.4	1.79	13.9	10.4	0.78
1008	19.3	11.9	0.55	39.7	28.3	0.57	17.9	13.4	0.67

Highest IMCs thickness was found 28.3 μm for the sample which has highest BLT and aged at 150°C for 1008 hours. Since BLT of the samples are not same and it influences the IMC growth, therefore activation energy and diffusion coefficient of the Zn-Cu IMCs are not calculates in this study.

Scanning acoustic microscopy test

SAM test was conducted on 10 samples before and after PC for checking delamination in the die surface, flag, wire bond post area and die attachment. For this test, pass criteria is zero failure out of 10 samples. SAM test result is summarized in Table 4.11. From this table, it is found that there is no delamination in the die attach joint. But delamination is found in the die surface, flag and wire bond post areas. Therefore, it does not fulfill the pass criteria according the SAM test.

Table 4.11 SAM test result of Zn-Al-Mg-Ga soldered samples before and after PC.

	SAM image	Result
Before PC		Minor delamination in flag area-Pass
		Delamination in wire bond post area-Fail
		No delamination in at die attach- Pass
After PC		Delamination in die surface flag area-Fail
		Delamination in wire bond post area-Fail
		No delamination in at die attach- Pass

4.3.2(j) Summary

In this analysis, Zn-Al-Mg-Ga solder was evaluated as a high-temperature die attach material on bare and Ni metallized Cu lead-frame at temperature ranging from 370 to 400°C. Wetting was found better on bare Cu lead-frame compare to Ni metallized Cu lead-frame. Cumulative void was found less than 10% for die attach samples at 380 and 390°C. Die shear strength was found within acceptable limit for all die attach temperatures and lead-frame conditions. Based on wetting, void and die shear strength it is found that die attach temperature 380°C is more appropriate of Zn-Al-Mg-Ga solder for Si die attachment on bare and Ni metallized Cu lead-frame which is 20°C less than the maximum operating temperature of Si die. In reliability tests, AC, TC and HTOL test results were found acceptable with zero failure. Creak was found in IMC layer at lead-frame/solder interface and bulk solder after TC 1000 cycles test which may affect in the reliability for long term use. Delamination was found in the die surface, flag and wire bond post areas before and after PC test. But no delamination was found in the die attachment.

4.4 SAC-Cu-Epoxy Solder

It is mixture of Sn-3Ag-0.5Cu (SAC) powder, Cu micro particles and polymer with flux in the form of past. The size of Cu and SAC particles is about 5-7 μm and 15 μm respectively. The main principal of this solder is to convert SAC alloy and Cu particles in to Cu_3Sn and Cu_6Sn_5 IMCs during reflow and post cure operation in oven. Since the melting temperature of Cu_3Sn and Cu_6Sn_5 IMCs are about 400°C, therefore it can be used as a high-temperature die attach material.

4.4.1 Microstructure characterization of SAC-Cu-epoxy solder

Figure 4.59 shows the typical SEM microstructure of Si die attachment with SAC-Cu-epoxy on bare Cu lead-frame after reflow and post cure operation. SAC-Cu-epoxy

wetted well with Si die and Cu lead-frame, and conversion of Cu-Sn IMCs was clearly observed in the bulk as well as Cu lead-frame interface. The microstructure of the bulk solder consists of four phases: one with dark contrast phase and the other three are deep gray, light gray, brighter contrast phases under SEM (Figure 4.59a). EDX analysis was carried out at these points. The dark contrast phases (point A) are trapped polymer with some Cu particles. These Cu particles are found intact as there was no takes place with Sn. The deep gray particles (point B) are 100 wt.% of Cu which remain unconverted after post cure operation. Light gray phases are Cu_6Sn_5 IMC which converted during reflow and post cure operation. The brighter contrast phases (point D) are Sn rich phase containing about 72.8 wt.% of Sn (SAC alloy) which remain unconverted after post cure

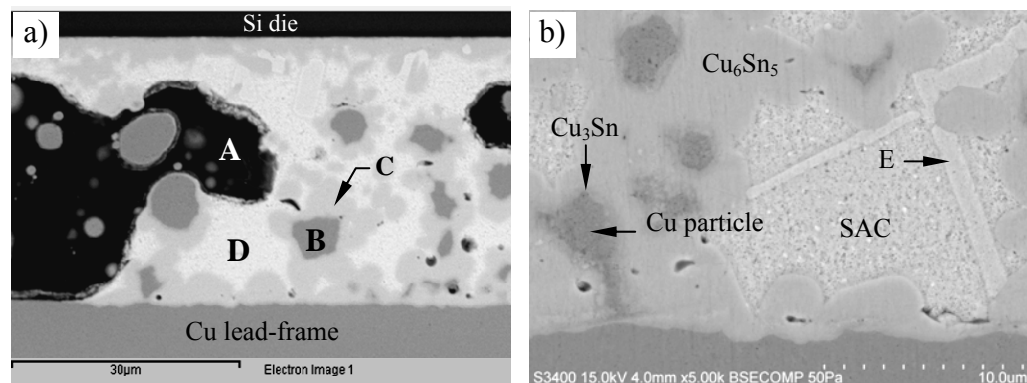


Figure 4.59 SEM micrograph of die attach sample with SAC-Cu epoxy: a) cross-section of the die attach sample; and b) SEM image at higher magnification.

operation. Figure 4.59b shows the magnified image of lead-frame/solder interface region. From this figure it is evident that there is only one layer of IMC formed at the lead-frame/solder interface which is Cu_6Sn_5 . On the other hand, a thin layer of Cu_3Sn IMC is found around the Cu particles. Moreover, a brighter contrast particle (point E) is observed in the unconverted SAC alloy region. According to EDX analysis, it is Ag rich phase containing about 51.6 wt.% of Ag with 24.4 & 24 wt.% of Sn and Cu respectively. Conversion of Cu-Sn IMCs was estimated from some cross-sectional

images of die attach samples after reflow and post cure operation (Figure 4.60). From this analysis, it is found that about 25% area of the solder joint was occupied by trapped polymer (Figure 4.60a). Out of 75% area which contains solders, about 55% area is covered by Cu-Sn IMCs, 40% area is covered by unconverted SAC alloy and 5% area is covered by unconverted Cu particles (Figure 4.60b). It is also observed that some Cu particles are trapped within the polymer areas. On the other hand, there is a lack of Cu particles in the unconverted SAC alloy areas. For that reasons, conversion of Cu-Sn IMCs is found less. IMC conversion can be improved by adding more Cu particles with finer size.

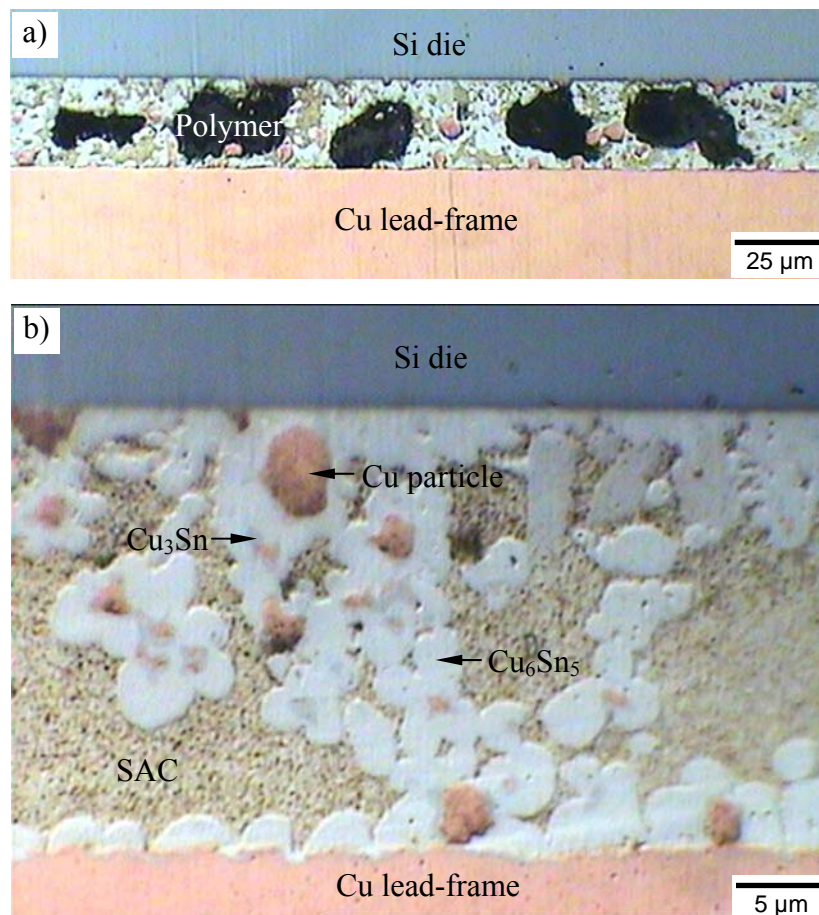


Figure 4.60 Optical image of the die attach sample with SAC-Cu epoxy: a) at lower magnification; and b) at higher magnification.

4.4.2 Die shear strength test

Die shear strength of SAC-Cu-epoxy soldered samples were measured for comparison with the shear strength of standard Pb-5Sn soldered samples. Minimum, maximum and average shear strength values of SAC-Cu-epoxy soldered samples were found 14.7, 23.8 and 18.1 MPa respectively. Average die shear strength of standard Pb-5Sn soldered samples was found 29.3 MPa. According to the ON Semiconductor standard, the acceptable limit for this die is considered as 12.5 MPa.

4.4.3 Reliability tests

4.4.3(a) Autoclave test

This test was performed for two sets of samples: One with PC and the other one without PC. Electrical test was performed for two sets of samples and all samples were found OK without failure. Cross-section was made for some samples for checking cracks and micro-structural change in the bulk solder which is shown in Figure 4.61. From this figure, fewer amounts of unconverted Cu particles are found in the bulk solder and Cu_6Sn_5 & Cu_3Sn IMCs are clearly observed around the Cu particles as well as Cu lead-frame/solder interface. There is no crack found in the bulk solder.

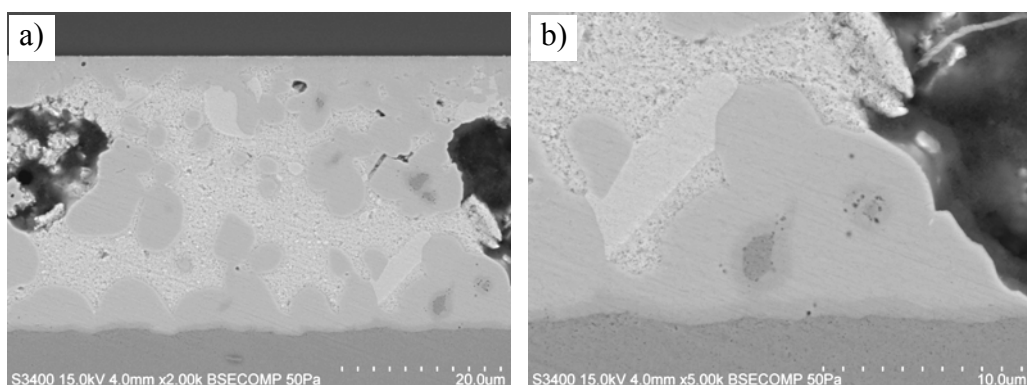


Figure 4.61 SEM micrograph of molded die attach sample soldered with SAC-Cu-epoxy after autoclave test without preconditioning: a) cross-section of the sample; and b) SEM image at higher magnification.

4.4.3(b) Temperature cycling test

This test was performed for two sets of samples: One with PC and the other one without PC. Electrical test was performed for two sets of samples and all samples were found OK without failure. Cross-section was made for some samples for checking cracks and micro-structural change in the bulk as well as at the interfaces. From Figure 4.62, crack is found in the bulk solder for both PC and without PC samples. It is also observed that most of the time crack propagates through the unconverted SAC alloy which is the weakest area in the bulk solder. Crack was also found in the trapped polymer.

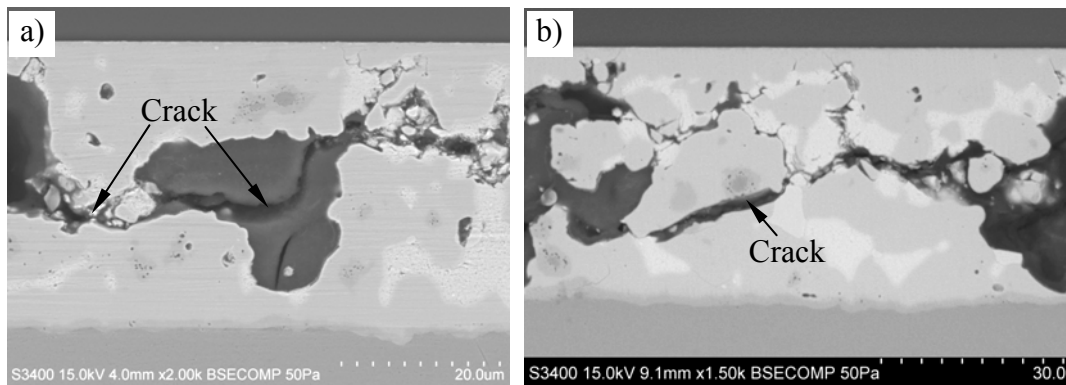


Figure 4.62 SEM micrographs of molded die attach samples soldered with SAC-Cu-epoxy after 1000 temperature cycle test: a) without preconditioning; and b) with preconditioning.

4.4.3(c) Scanning acoustic microscopy test

SAM test was conducted for 10 samples after completion of AC and TC for checking delamination in the samples and compared it with the fresh samples. Figure 4.63 shows the comparative SAM test results of AC and TC samples with fresh one. From this figure, no delamination is observed in the die surface for fresh samples as well as completed AC and TC test samples. On the other hand, slide delamination is observed in the flag area of the fresh samples which is increased about 50% to 100% during AC and TC tests. Such failure is accepted by ON Semiconductor.

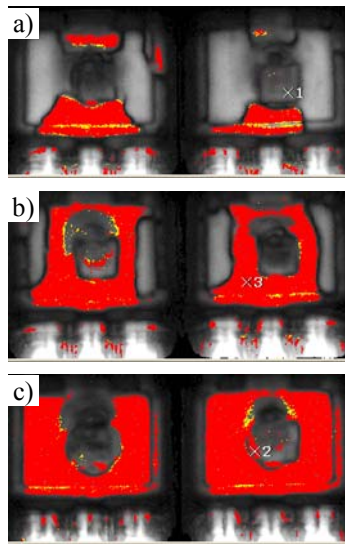


Figure 4.63 SAM images of molded die attach samples soldered with SAC-Cu epoxy: a) fresh samples; b) after AC test; and c) after 1000 TC test.

4.4.4 Summary

From this analysis, die attach was found successful with SAC-Cu-epoxy solder. Excluding trapped polymer area, about 55% solder can be converted in to Cu-Sn IMCs with 5% unconverted Cu particles after reflow and post oven cure. About 40% SAC solder remain unconverted due to lack of Cu particles. The IMCs conversion can be improved by adding more Cu particles with finer size. The minimum die shear strength was found 14.7 MPa which is within acceptable limit (acceptable limit: 12.5 MPa) for the die size used for this analysis. Reliability test results were also found acceptable with zero failure. But crack was developed almost entire area of the bulk solder during TC test which may affect in the reliability for long term use. It is to be noted that most of the time crack propagates through unconverted SAC alloy which is the weakest part in the bulk solder. Crack also developed in the trapped polymer. This situation can be improved by reducing polymer contents in the solder and adding more Cu particles with finer size such that almost entire SAC alloy can be converted in to Cu-Sn IMCs. From SAM test, no delamination was observed in the die surface. Though delamination was found in the flag area during AC and TC test, it can be accepted by the electronic industry. Therefore, SAC-Cu-epoxy shows promises as a high-temperature die attach

material which can be accepted by industry as alternative of high-Pb solder. The main concerns of SAC-Cu-epoxy as a high-temperature die attach material is that it requires longer time for die attachment due to 5 minutes reflow and 1 hour post cure operation in oven for conversion of IMCs. It will also increase the capital expenses for the reflow and post cure ovens that will be required for each of the die attach machine.

4.5 Summary Overall

It is found from the above studies that Bi-Ag-Cu, Bi-Ag-Cu-In and Zn-Al-Ge solders are not suitable for high-temperature Pb-free solder for Si die attachment due to poor wetting and voids under the present experimental conditions. Zn-Al-Mg-Ga solder was found suitable for die attachment on bare and Ni metallized Cu lead-frame at 380°C based on wetting, void and die shear strength. Cumulative void was found less than 10%. Die shear strength was found 24.2 MPa and 20.5 MPa for die attach samples at 380°C on bare and Ni metallized Cu lead-frame respectively. SAC-Cu-epoxy solder was also found suitable for die attachment on bare Cu lead-frame. Die shear strength for this solder was found 14.7 MPa. Reliability test results of Zn-Al-Mg-Ga and SAC-Cu-epoxy solder were also found satisfactory with zero electrical test failure out of 80 samples. But crack was developed at Zn-Cu IMCs for Zn-Al-Mg-Ga solder and at bulk for Zn-Al-Mg-Ga and SAC-Cu-epoxy solder after 1000 thermal cycles. No delamination was found in die attachment for both the solders. Therefore, Zn-Al-Mg-Ga and SAC-Cu-epoxy solder shows promises as a high-temperature Pb-free solder for Si die attachment.

CHAPTER 5 CONCLUSIONS AND FUTURE WORK

5.1 Conclusions

This thesis is devoted to the research and development of high-temperature Pb-free solder for Si die attachment applications. Following conclusions are made from this work.

- Bi-Ag-Cu and Bi-Ag-Cu-In solders are not suitable as high-temperature die attach material under present experimental conditions because of poor wetting on Cu lead-frame and excessive voids in the die attach joint. Die displacement was observed during wire bonding process due to poor bonding strength with lead-frame.
- Die shear strength of Zn-Al-Ge soldered samples at 390°C was found 22.3 MPa which is within acceptable limit but it is close to the maximum allowable temperature of the Si die. Cumulative void was found more than 10% and wetting on Cu lead-frame was not as good as standard Pb-5Sn solder. Therefore, under present experimental conditions this solder is not suitable for Si die attachment.
- Zn-Al-Mg-Ga solder was found suitable for Si die attachment both on bare and Ni metallized Cu lead-frame at temperature of 380°C. Die shear strength was found 24.2 MPa and 20.5 MPa for die attach samples at 380°C on bare and Ni metallized Cu lead-frame respectively.
- Reliability test of Zn-Al-Mg-Ga soldered samples on bare Cu lead-frame was found satisfactory. However, crack was found in the IMC layers at lead-frame/solder interface as well as in the bulk solder after 1000 thermal cycles

which may effect on the reliability during long term use. No delamination was observed at die surface after PC test.

- Shear failure mode of Zn-Al-Mg-Ga soldered samples was found different from that of the standard Pb-5Sn soldered samples. Shear failure of Zn-Al-Mg-Ga soldered samples on bare Cu lead-frame occurred by the cracking of Si die. For Ni metallized Cu lead-frame, it was occurred at the lead-frame/solder interface. Failure of standard Pb-5Sn soldered samples was occurred at bulk solder. Failure of Zn-Al-Mg-Ga soldered samples on bare Cu started just above the Ti layer at the die back metallization and completed by breaking of entire Si die.
- Total IMC layers thickness of Zn-Al-Mg-Ga soldered samples at lead-frame/solder interface was increased up to 20.1 μm during TC and HTOL test. Initial thickness of IMC layers was measured and found in the range of about 2.8-5.1 μm .
- SAC-Cu-epoxy solder was also found suitable for Si die attachment on bare Cu lead-frame. Die shear strength was found 14.7 MPa.
- Reliability test of SAC-Cu-epoxy soldered samples on bare Cu lead-frame was found satisfactory. However, crack was found in the bulk solder after 1000 thermal cycles which may effect on the reliability during long term use. No delamination was observed at die surface after AC and TC test.
- After 5 minutes reflow at 245°C and post oven cure at 175°C for 1 hour of SAC-Cu-epoxy soldered samples, it was found that 55% solder converted to Cu-Sn IMCs, 5% unconverted Cu particles and about 40% SAC solder remain unconverted due to lack of Cu particles.

5.2 Future Work

- Reliability of Zn-Al-Mg-Ga soldered samples on Ni metallized Cu lead-frame need to be analyzed.
- Factors that are responsible for crack initiation at Cu-Zn IMCs and bulk solder of Zn-Al-Mg-Ga soldered samples during TC test need to be identified.
- For SAC-Cu-epoxy solder, further study is necessary on reflow profile, post oven cure, and proportion of SAC alloy & Cu particles such that maximum Cu-Sn IMCs conversion can be achieved.
- In SAC-Cu-epoxy solder, epoxy can be replaced by other medium since 25% area of die attach joint occupied by trapped epoxy after post oven cure.
- Factors that are responsible for the crack development in the bulk solder of die attach samples using SAC-Cu-epoxy solder during TC test need to be investigated.

APPENDIX-A DIE SHEAR STRENGTH DATA

Table A1 Minimum Die Shear Strength in MPa.
(According to ON Semiconductor standard)

x y	Die size in mm									
	0-0.37	0.38-0.63	0.64-0.88	0.89-1.13	1.14-1.39	1.4-1.64	1.65-1.9	1.91-2.15	2.16-2.4	2.41-2.65
0-0.37	5.73	6.73	7.23	7.51	7.63	7.76	7.81	7.89	7.95	8.00
0.38-0.63	6.73	7.91	8.49	8.82	8.96	9.11	9.18	9.27	9.34	9.40
0.64-0.88	7.23	8.49	9.12	9.47	9.62	9.79	9.86	9.96	10.03	10.10
0.89-1.13	7.51	8.82	9.47	9.83	9.99	10.16	10.23	10.34	10.42	10.48
1.14-1.39	7.63	8.96	9.62	9.99	10.15	10.33	10.40	10.50	10.59	10.65
1.4-1.64	7.76	9.11	9.79	10.16	10.33	10.50	10.58	10.68	10.77	10.83
1.65-1.9	7.81	9.18	9.86	10.23	10.40	10.58	10.65	10.76	10.76	9.74
1.91-2.15	7.89	9.27	9.96	10.34	10.50	10.68	10.76	10.61	9.51	8.61
2.16-2.4	7.95	9.34	10.03	10.42	10.59	10.77	10.76	9.51	8.52	7.71
2.41-2.65	8.00	9.40	10.10	10.48	10.65	10.83	9.74	8.61	7.71	6.98

APPENDIX-B PUBLICATIONS

Journal

1. **Haque, A.**, Lim, B. H., Haseeb, A. S. M. A., & Masjuki, H. H. (2011). Die Attach Properties of Zn-Al-Mg-Ga High-Temperature Lead-Free Solder on Cu Lead-Frame. *Journal of Materials Science: Materials in Electronics*. DOI: 10.1007/s10854-011-0511-x.

Conference

2. **Haque, A.**, Won, Y. S., Haseeb, A. S. M. A., & Masjuki, H. H. (2010). Investigations on Zn-Al-Ge Alloys as High-Temperature die attach material. Paper presented at the Electronics System-Integration Technology Conference (ESTC 2010), 13-16 September 2010, Berlin, Germany. DOI: 10.1109/ESTC.2010.5643009.
3. **Haque, A.**, Won, Y. S., Lim, B. H., Haseeb, A. S. M. A., and Masjuki, H. H. (2010). Effect of Ni Metallization on Interfacial Reactions and Die Attach Properties of Zn-Al-Mg-Ga High Temperature Lead-free Solder. Paper presented at the 34th International Electronics Manufacturing Technology Conference (IEMT 2010), 30 November-2 December 2010, Melaka, Malaysia, (Received best paper award).

REFERENCES

- Abtew, M., & Selvaduray, G. (2000). Lead-free Solders in Microelectronics. *Materials Science and Engineering: R: Reports*, 27(5-6), 95-141.
- Anderson, I. E. (2007). Development of Sn–Ag–Cu and Sn–Ag–Cu–X alloys for Pb-free electronic solder applications. *Journal of Materials Science: Materials in Electronics*, 18(1-3), 55-76.
- Baliga, B. J. (1989). Power semiconductor device figure of merit for high-frequency applications. *Electron Device Letters, IEEE*, 10(10), 455-457.
- Çay, F., & Can Kurnaz, S. (2005). Hot tensile and fatigue behaviour of zinc-aluminum alloys produced by gravity and squeeze casting. *Materials & Design*, 26(6), 479-485.
- Chin, H. S., Cheong, K. Y., & Ismail, A. B. (2010). A review on die attach materials for SiC-based high temperature power devices. *Metallurgical and Materials Transactions B*, 41(4), 824-832.
- Chuang, R. W., & Lee, C. C. (2002). Silver-indium joints produced at low temperature for high temperature devices. *Components and Packaging Technologies, IEEE Transactions on*, 25(3), 453-458.
- Coppola, L., Huff, D., Wang, F., Burgos, R., & Boroyevich, D. (2007). *Survey on High-Temperature Packaging Materials for SiC-based Power Electronics Modules*. Paper presented at the Power Electronics Specialists Conference, IEEE, (pp. 2234-2240). Orlando, FL, USA.
- Coquery, G., Lefranc, G., Licht, T., Lallemand, R., Seliger, N., & Berg, H. (2003). High temperature reliability on automotive power modules verified by power cycling tests up to 150°C. *Microelectronics Reliability*, 43(9-11), 1871-1876.
- Cressler, J. D. (2005). On the Potential of SiGe HBTs for Extreme Environment Electronics. *Proceedings of IEEE*, 93(9), 1559-1582.
- Dennis, R. O., & Howard, M. B. (1979). Properties of die bond alloys relating to thermal fatigue. *IEEE transactions on Components, Hybrids, and Manufacturing Technology, CHMT-2(2)*, 257-263.
- Directive 2002/95/EC of the European Parliament (2003, 27 January). The restriction of the use of certain hazardous substances in electrical and electronic equipment. Eur-Lex: Official Journal of the European Union online, L37, 19-23.

- Gervais, E., Barnhurst, R. J., & Loong, C. A. (1985). An analysis of selected properties of ZA alloys. *Journal of Metals*, 37(11), 43-47.
- Glazer, J. (1995). Metallurgy of Low Temperature Pb – Free Solders for Electronic Assembly. *International Materials Reviews*, 40(2), 65-93.
- Hermida, E. B., Melo, D. G., Aguiar, J. C., & Lopez, D. E. (2000). Temperature Dependence of the Viscoelastic Response of In, Sn and In–Sn Alloys. *Journal of Alloys and Compounds*, 310(1-2), 91-96.
- Ishikawa, M., Nonaka, S., Sasaki, H., Kohinata, M., Mishima, A., & Yoshida, H. (2004). Paper presented at the 10th Symp. on Microjoining and Assembly Technology in Electronics, 5-6 February 2004. Yokohama, Japan.
- Jang, J. W., Ramanathan, L. N., Lin, J. K., & Frear, D. R. (2004). Spalling of Cu₃Sn intermetallics in high-lead 95Pb-5Sn solder bumps on Cu under bump metallization during solid-state annealing. *Journal of Applied Physics*, 95(12), 8286-8289.
- Jiang, H. (2008). *Synthesis of Tin, Silver and Their Alloy Nanoparticles for Lead-Free Interconnect Applications*. Unpublished doctoral dissertation, Georgia Institute of Technology.
- Johnson, R. W., Cai, W., Yi, L., & Scofield, J. D. (2007). Power Device Packaging Technologies for Extreme Environments. *Electronics Packaging Manufacturing, IEEE Transactions on*, 30(3), 182-193.
- Kang, N., Na, H. S., Kim, S. J., & Kang, C. Y. (2009). Alloy design of Zn-Al-Cu solder for ultra high temperatures. *Journal of Alloys and Compounds*, 467(1-2), 246-250.
- Kassner, M. E., & Perez-Prado, M. T. (2004). *Fundamentals of Creep in Metals and Alloys*: ELSEVIER.
- National Aeronautics and Space Administration (1996). GaAs MMIC Reliability Assurance Guideline for Space Applications. (JPL publication 96-25). California Institute of Technology, Pasadena, California, USA.
- Kim, K. S., Huh, S. H., & Sukanuma, K. (2003). Effects of fourth alloying additive on microstructures and tensile properties of Sn-Ag-Cu alloy and joints with Cu. *Microelectronics Reliability*, 43(2), 259-267.

- Kim, S., Kim, K.-S., Kim, S.-S., Suganuma, K., & Goro, I. (2009). Improving the Reliability of Si Die Attachment with Zn-Sn-Based High-Temperature Pb-Free Solder Using a TiN Diffusion Barrier. *Journal of Electronic Materials*, 38(12), 2668-2675.
- Kim, S., & Ledbetter, H. M. (1998). Low Temperature Elastic Coefficients of Polycrystalline Indium. *Material science and Engineering*, 252, 139-143.
- Kim, S. J., Kim, K. S., Kim, S. S., Kang, C. Y., & Suganuma, K. (2008). Characteristics of Zn-Al-Cu Alloys for High Temperature Solder Application. *Materials Transactions*, 49(7), 1531-1536
- Kirschman, R. K., Sokolowski, W. M., & Kolawa, E. A. (2001). Die Attachment for -120C to +20C Thermal Cycling of Microelectronics for Future Mars Rovers – An Overview. *Journal of Electronic Packaging, ASME*, 123(2), 105-111.
- Lalena, J., Dean, N., & Weiser, M. (2002). Experimental investigation of Ge-doped Bi-11Ag as a new Pb-free solder alloy for power die attachment. *Journal of Electronic Materials*, 31(11), 1244-1249.
- Lee, J. E., Kim, K. S., Suganuma, K., Inoue, M., & Izuta, G. (2007). Thermal Properties and Phase Stability of Zn-Sn and Zn-In Alloys as High Temperature Lead-Free Solder. *Materials Transactions*, 48(3), 584-593.
- Lee, J. E., Kim, K. S., Suganuma, K., Takenaka, J., & Hagio, K. (2005). Interfacial Properties of Zn--Sn Alloys as High Temperature Lead-Free Solder on Cu Substrate. *Materials Transactions*, 46(11), 2413-2418.
- Leicht, L., & Skipor, A. (2000). Mechanical Cycling Fatigue of PBGA Package Interconnects. *Microelectronics Reliability*, 40, 1129-1133.
- Mannan, S. H., & Clode, M. P. (2004). Materials and processes for implementing high-temperature liquid interconnects. *Advanced Packaging, IEEE Transactions on*, 27(3), 508-514.
- Matijasevic, G., Wang, C., & Lee, C. (1990). Void-free bonding of large silicon dice using gold-tin alloy. *IEEE transactions on Components, Hybrids, and Manufacturing Technology*, 13(4), 1128-1134.
- Mazda, F. (1997). *Power Electronics Handbook* (Vol. 3rd Edition): Newnes.
- Muralidharan, G., & Tiegs, T. N. (2006). *Composite Die-Attach Materials for High-Temperature Packaging Applications*. Paper presented at the High Temperature Electronics Conference, Santa Fe, New Mexico, USA.

- Nimmo, K. (1999). *SnAgCu alloy: Patent and Phase Diagram*. Paper presented at the SOLDERTEC GROUP MEETING.
- Nobumasa, M., & Shuichi, N. (2006). Japan patent No. 2006-320913, Japan.
- Okamoto, H. (1995). Al-Zn (aluminum-zinc) *Journal of Phase Equilibria*, 16(3), 281-282.
- Pidaparti, R. M. V., & Song, X. (1996). Fatigue Crack Propagation Life Analysis of Solder Joints under Thermal Cyclic Loading. *Theoretical and Applied Fracture Mechanics* 24, 157-164.
- Rettenmayr, M., Lambracht, P., Kempf, B., & Tschudin, C. (2002). Zn-Al based alloys as Pb-free solders for die attach *Journal of Electronic Materials*, 31(4), 278-285.
- RoHS Regulations (UK) Government Guidance Notes*. (2011, February), URN 10/590.
- Rusanen, O., & Lenkkeri, J. (1995). Reliability Issues of Replacing Solder With Conductive Adhesives in Power Modules. *IEEE Transaction on Components, Packaging, and Manufacturing Technology*, 18(2), 320-325.
- SGTE Alloy Phase Diagrams. (2004). Retrieved 20-09-2010, from http://www.crct.polymtl.ca/fact/documentation/SGTE/SGTE_Figs.htm
- Shammas, N. Y. A. (2003). Present problems of power module packaging technology. *Microelectronics Reliability*, 43, 519-527.
- Shang, J. K., Zheng, Q. L., Zhang, L., & Zhu, Q. S. (2007). Mechanical Fatigue of Sn-rich and Pb-free Solder Alloys. *Journal of Material Science: Materials in Electronics*, 18, 211-227.
- Shetty, S., Lehtinen, V., Dasgupta, A., & Halkola, V. (2001). Fatigue of Chip Scale Package Interconnects Due to Cyclic Bending. *Journal of Electronic Packaging*, 123(3), 302-308.
- Shetty, S., & Reinikainen, T. (2003). Three and Four-Point Bend Testing for Electronic Packages. *Journal of Electronic Packaging, Transaction of ASME*, 125(4), 556-561.
- Shimizu, T., Ishikawa, H., Ohnuma, I., & Ishida, K. (1999). Zn-Al-Mg-Ga alloys as Pb-free solder for die-attaching use *Journal of Electronic Materials*, 28(11), 1172-1175.

- Singer, A., Echeverria, G., Chouta, P., Stafstrom, E., & McLenaghan, A. J. (2003). *The Effect of Via-in-Pad Via-Fill on Solder Joint Void Formation*. Annual meeting, Minneapolis, October 2003. S06-6-1 – S06-6-11.
- Soga, T., Ishida, T., Miura, K., Hata, H., Okamoto, M., & Nakatsuka, T. (2003). United States Patent No. US 6563225, USA.
- Song, H., Ahn, J., & Morris, J. (2001). The microstructure of eutectic Au-Sn solder bumps on Cu/electroless Ni/Au. *Journal of Electronic Materials*, 30(9), 1083-1087.
- Song, J. M., Chuang, H. Y., & Wu, Z. M. (2006). Interfacial reactions between Bi-Ag high-temperature solders and metallic substrates. *Journal of Electronic Materials*, 35(5), 1041-1049.
- Suganuma, K. (2001). Advances in lead-free electronics soldering. *Current Opinion in Solid State and Materials Science*, 5(1), 55-64.
- Suganuma, K. (2004). Japan Patent No. 2004-237375 (26 August 2004), Japan.
- Suganuma, K., Kim, S. J., & Kim, K. S. (2009). High-Temperature Lead-Free Solders: Properties and Possibilities. *Journal of Metals*, 61(1), 64-71.
- Takaku, Y., Felicia, L., Ohnuma, I., Kainuma, R., & Ishida, K. (2008). Interfacial Reaction Between Cu Substrates and Zn-Al Base High-Temperature Pb-Free Solders. *Journal of Electronic Materials*, 37(3), 314-323.
- Takaku, Y., Makino, K., Watanabe, K., Ohnuma, I., Kainuma, R., Yamada, Y., et al. (2009). Interfacial Reaction between Zn-Al-Based High-Temperature Solders and Ni Substrate. *Journal of Electronic Materials*, 38(1), 54-60.
- Takao, I., & Aoyama, S. (2005). Fluxless Fabrications of Sn-Au Solder Microbumps by a Hydrogen Plasma Reflow Technique. *Journal of Electronic Materials*, 34(5), 630-634.
- Thomas, M. (2007, April). Die-attach Materials and Processes: A Lead-free Solution for Power and High-power Applications. *Advanced Packaging*, 16, 32-36.
- Tsai, J. Y., Chang, C. W., Ho, C. E., Lin, Y. L., & Kao, C. R. (2006). Microstructure Evolution of Gold-Tin Eutectic Solder on Cu and Ni Substrates. *Journal of Electronic Materials*, 35(1), 65-71.

- Tsai, J. Y., Chang, C. W., Shieh, Y. C., Hu, Y. C., & Kao, C. R. (2005). Controlling the microstructure from the gold-tin reaction. *Journal of Electronic Materials*, 34(2), 182-187.
- Tschudin, C., Hutin, O., Arsalane, S., Bartels, F., Lambracht, P., & Rettenmayr, M. (2002). *Lead Free Soft Solder Die Attach Process for Power Semiconductor Packaging*. Paper presented at the SEMICON China, 26-27 March 2002.
- Tu, K. N., Gusak, A. M., & Li, M. (2003). Physics and materials challenges for lead-free solders. *Journal of Applied Physics*, 93(3), 1335-1853
- Tuhus, T., & Bjorneklett, A. (1993). *Thermal Cycling Reliability of Die Bonding Adhesives*. Paper presented at the IEEE Annual International Reliability Physics Symposium Digest (pp. 208), 23-25 March 1993.
- Tummala, R. (2001). *Fundamentals of microsystems packaging*. New York: McGraw-Hill, Inc.
- Yamada, Y., Takaku, Y., Yagi, Y., Nishibe, Y., Ohnuma, I., Sutou, Y., et al. (2006). Pb-free high temperature solders for power device packaging. *Microelectronics and Reliability*, 46(9-11), 1932-1937.
- Zhang, Z., & Guo-Quan, L. (2002). Pressure-assisted low-temperature sintering of silver paste as an alternative die-attach solution to solder reflow. *Electronics Packaging Manufacturing, IEEE Transactions on*, 25(4), 279-283.
- Zhao, J., Mutoh, Y., Miyashita, Y., & Wang, L. (2003). Fatigue Crack Growth Behavior of Sn-Pb and Sn-based lead-free Solders. *Engineering Fracture Mechanics* 70, 2187-2197.
- Zheng, Y. (2005). *Effect of Surface Finishes and Intermetallics on the Reliability of SnAgCu Interconnects*. University of Maryland.
- Zinov'ev, & Vladislav, E. (1989). *Thermophysical Properties of Metals at High Temperature*: Nova Sci. Pub. Inc.